

Doctoral thesis

Doctoral theses at NTNU, 2021:22

Vilde Elisabeth Mikkelsen

Human Glioblastomas: Histopathology, Tumor Growth, and *MGMT* Status

NTNU
Norwegian University of Science and Technology
Thesis for the Degree of
Philosophiae Doctor
Faculty of Medicine and Health Sciences
Department of Clinical and Molecular Medicine



NTNU

Norwegian University of
Science and Technology

Vilde Elisabeth Mikkelsen

Human Glioblastomas: Histopathology, Tumor Growth, and *MGMT* Status

Thesis for the Degree of Philosophiae Doctor

Trondheim, January 2021

Norwegian University of Science and Technology
Faculty of Medicine and Health Sciences
Department of Clinical and Molecular Medicine



NTNU

Norwegian University of
Science and Technology

NTNU

Norwegian University of Science and Technology

Thesis for the Degree of Philosophiae Doctor

Faculty of Medicine and Health Sciences

Department of Clinical and Molecular Medicine

© Vilde Elisabeth Mikkelsen

ISBN 978-82-471-9774-5 (printed ver.)

ISBN 978-82-471-9449-2 (electronic ver.)

ISSN 1503-8181 (printed ver.)

ISSN 2703-8084 (online ver.)

Doctoral theses at NTNU, 2021:22

Printed by NTNU Grafisk senter

Humane Glioblastomer: Histopatologi, Tumorvekst og MGMT Status

Studier på glioblastomers naturlige biologi med fokus på vekstmekanismer og MGMT status

Glioblastomer er den vanligste og mest aggressive typen hjernesvulst som oppstår i hjernen hos voksne. Glioblastomene har en meget aggressiv og kompleks biologi, som medfører en dårlig prognose på omtrent 10 måneder etter diagnose. Svulstcellene infiltrerer også hjernevevet diffust, som gjør det umulig å fjerne hele svulsten under operasjon. Sammen med den aggressive biologien bidrar dette til at så godt som alle får tilbakefall etter behandling. Til tross for omfattende forskning har hverken overlevelsen eller standardbehandlingen endret seg i noen særlig grad de siste 15 årene. Likevel er det et håp om at bedre innsikt i tumorbiologien kan føre til bedre håndtering av pasientene gjennom identifisering av biologiske trekk som kan si noe om prognose, effekt av behandling, eller hva som kan være mulige angrepsmål for målrettet kreftbehandling.

I denne doktorgradsavhandlingen har det overordnede målet vært å få bedre innsikt i den naturlige tumorbiologien i glioblastomer. Den naturlige biologien vil si at biologien er upåvirket av behandling. Dette har vi forsket på ved å undersøke biologiske mekanismer i vevspreparater og på MR-bilder som var tatt før pasientene fikk stråle- og/eller cellegiftbehandling. I alle de tre studiene i denne doktorgraden undersøkte vi en gruppe på 106 glioblastompasienter. Disse pasientene var valgt ut basert på om tumorveksthastigheten kunne beregnes utfra målinger av tumorvolum fra to MR bilder tatt før operasjon og tidsintervallet mellom dem.

I Studie I og II var målet å se om det var sammenhenger mellom mikroskopiske vevsstrukturer sett i vevsprøver (histopatologiske trekk) og tumorveksthastighet beregnet fra MR bildene. Glioblastomene ble delt inn i to grupper basert på veksthastigheten: de som vokste raskere enn forventet og de som vokste saktere enn forventet. I Studie I undersøkte vi om tilstedeværelse av 27 ulike biologiske vevsstrukturer kunne si noe om veksthastighet, mens i Studie II så vi på om tetthet av kar i vevspreparatene hadde noen sammenheng med veksten. I begge studiene fant vi at tumorer med høy celletetthet og tumorer med blodpropper i tumorkar hadde en høyere sannsynlighet for å vokse raskere. Funnene våre tyder på at blodpropper i tumorkar kan utløse en mer aggressiv tumorbiologi ved at det blir et lavere oksygennivå i tumorvevet. I Studie II fant vi at kartetthet ikke var relatert til veksthastighet, som tyder på tumorvekst ikke nødvendigvis er avhengig av økt nydannelse av kar (angiogenese).

I Studie III endret vi fokus til *MGMT* status, eller *MGMT* promoter metylerings status, som er en viktig genetisk markør som sier noe om hvor effektiv cellegiftbehandling vil være hos glioblastompasienter. *MGMT* (O6-metylguanin-DNA metyltransferase) er et enzym som opphever effekten av cellegift når det er til stede i vevet (umetylert), mens når genet for *MGMT* er metylert, hindres dannelsen av enzymet og cellegift har bedre effekt. Målet i Studie III var å se om den naturlige biologien var forskjellig mellom *MGMT* metylerte og *MGMT* umetylerte glioblastomer. De biologiske trekkene vi undersøkte var 24 ulike mikroskopiske vevsstrukturer, 4 strukturer på MR-bilder og tumorveksthastigheten. Vi fant ingen forskjeller i fordelingen av disse trekkene mellom de *MGMT* metylerte og de *MGMT* umetylerte glioblastomerne. Funnene våre tyder på at den økte overlevelsen hos *MGMT* metylerte pasienter ikke kan forklares av en mindre aggressiv tumorbiologi. Videre tilsier funnene at det ikke er ulikheter i biologien annet enn *MGMT* status som forklarer den ulike responsen på cellegift. Disse funnene tyder også på at man ikke kan bruke utseendet på MR-bilder tatt før operasjon til å forutsi *MGMT* status.

Samlet sett har studiene i denne doktorgraden bidratt til økt innsikt i den naturlige tumorbiologien i glioblastomer hos pasienter. Likevel, så må funnene bekreftes i fremtidige studier før vi kan trekke endelige konklusjoner.

Navn kandidat: Vilde Elisabeth Mikkelsen

Institutt: Institutt for klinisk og molekylærmedisin (IKOM)

Hovedveileder: Sverre Helge Torp

Biveileder: Ole Solheim

Finansieringskilde: Norges teknisk-naturvitenskapelige universitet (NTNU)

*Ovennevnte avhandling er funnet verdig til å forsvares offentlig
for graden ph.d. i medisin og helsevitenskap.*

Disputas finner sted fredag 22. januar 2021 kl.12.15 på digital plattform

Contents

1 Acknowledgements vii

2 List of papersix

3 Abbreviationsxi

4 Summary xiii

5 Introduction 1

5.1 Glioblastoma..... 1

5.1.1 Classification 1

5.1.2 Epidemiology 2

5.1.3 Clinical presentation..... 3

5.1.4 Treatment 3

5.1.5 Magnetic resonance imaging 4

5.1.6 Molecular pathology 6

5.1.7 Prognostic and predictive markers 6

5.1.8 *MGMT* promoter methylation status 7

5.2 Tumor growth 9

5.2.1 Tumor growth biology 9

5.2.2 Tumor growth models 10

5.2.3 Glioblastoma growth dynamics..... 11

5.2.4 Glioblastoma growth biology 12

5.2.5 Experimental models of glioblastoma growth 13

5.3 Histopathological features 14

5.3.1 General histopathology 14

5.3.2 Histopathological features of glioblastoma 14

5.4 Neovascularization 15

5.4.1 Tumor neovascularization 15

5.4.2 Neovascularization in diffuse astrocytic tumors 17

5.4.3 Angiogenesis and growth of glioblastomas 17

5.5 Immunohistochemistry 18

5.5.1 General immunohistochemistry 18

5.5.2 GFAP 19

5.5.3 IDH1 19

5.5.4 vWF 19

5.5.5 CD105 20

5.5.6	Ki-67/MIB-1.....	20
6	Aims.....	21
7	Material and methods.....	23
7.1	Patient selection.....	23
7.2	Estimation of tumor growth.....	24
7.3	Histopathological features	28
7.4	Immunohistochemistry	38
7.4.1	Microvessel density measurements	39
7.4.2	Proliferative activity.....	41
7.5	Molecular techniques.....	41
7.5.1	Methylation specific PCR	41
7.5.2	Sanger sequencing of <i>IDH</i> mutation status	44
7.6	Clinical variables	44
7.7	Statistical analyses.....	44
7.8	Ethics	46
8	Summary of papers	47
8.1	Paper I.....	47
8.2	Paper II	48
8.3	Paper III	49
9	Discussion	51
9.1	Main findings.....	51
9.1.1	Biology and tumor growth	51
9.1.2	Biology and <i>MGMT</i> status	52
9.2	Clinical considerations	53
9.3	Biological considerations	55
9.4	Prognostic and predictive markers	57
9.5	Methodological considerations.....	58
9.5.1	External validity	58
9.5.2	Growth estimates.....	59
9.5.3	Histopathological features.....	60
9.5.4	Microvessel density.....	61
9.5.5	Proliferation assessments	62
9.5.6	Immunohistochemistry.....	62
9.5.7	Methylation specific PCR	63

9.5.8	Statistics	63
10	Main conclusions.....	65
11	Future perspectives.....	67
12	Errata	69
13	References	71
14	Publications	83

1 Acknowledgements

The work behind this thesis was made possible through the Medical Student Research Programme and the subsequent PhD funding provided by the Department of Clinical and Molecular Medicine (IKOM) at the Faculty of Medicine and Health Sciences at the Norwegian University of Science and Technology (NTNU). I am very grateful for the opportunity to pursue my research interest at such an early time point and to collaborate with so many inspirational people.

First of all, I want to thank Sverre H. Torp for being an extraordinary main supervisor. With his contagious enthusiasm and inspirational knowledge, he has encouraged me to be curious and follow my own ideas. The open-door policy, interesting conversations, and a dose of humor have made the whole process very enjoyable. Also, a big thank you to my co-supervisor, Ole Solheim, for the interesting discussions and the constructive feedbacks during these years.

This project would not have been possible without the help from my collaborators Anne Line Stensjøen, Hong Yan Dai, Erik Magnus Berntsen, Øyvind Salvesen, and Ivar Skjåk Nordrum. I also want to thank the bioengineers at the Cellular and Molecular Imaging Core Facility (CMIC), Unn S. Granli, Kathrin G. Torset, Ingunn Nervik, Camilla B. Setsaas, and Borgny Ytterhus for their important work and help. An extra thank you to Unn S. Granli, who put substantial work into the immunostains in Paper II and for educating me about immunohistochemistry. Also thank you to the bioengineers that conducted the methylation specific PCR analyses at the Department of Pathology at St. Olavs Hospital. In addition, I want to thank the Department of Pathology for making the tumor tissue available.

A huge thank you goes to all my amazing friends. A lot of love goes to ‘the Office’ Magnus B. Arnli, Rosilin K. Varughese, Bente E. Opsjøn, Maria R. Kraby, Magnus Kvisten, Elias Koppen, Rahmina Meta, and Sofie E. Tollefsen, for filling these years with interesting discussions and hilarious distractions and for making up a workplace I always wanted to go to. A huge thank you to my best friend, Iris A. Kummen, for the substantial help with language editing in Paper I. I also would like to thank Sonja Sarah Porter for contributing with her design talent in this thesis.

Finally, I want to express my gratitude to my lovely family, especially my parents and my brother, for the continuous support and encouragement.

2 List of papers

Paper I: Histopathologic features in relation to pretreatment tumor growth in patients with glioblastoma

Mikkelsen VE, Stensjoen AL, Berntsen EM, Nordrum IS, Salvesen O, Solheim O, Torp SH.
World Neurosurgery, 109, e50-e58, 2018

Paper II: Angiogenesis and radiological tumor growth in patients with glioblastoma

Mikkelsen VE, Stensjøen AL, Granli US, Berntsen EM, Salvesen Ø, Solheim O, Torp SH.
BMC Cancer, 18, 862, 2018

Paper III: *MGMT* promoter methylation status is not related to histological or radiological features in *IDH* wild-type glioblastomas

Mikkelsen VM, Dai HY, Stensjøen AL, Berntsen EM, Salvesen Ø, Solheim O, Torp SH.
Journal of Neuropathology & Experimental Neurology, 79, 855-862, 2020

3 Abbreviations

ADC	Apparent diffusion coefficient
AI	Artificial intelligence
BRAF	Proto-oncogene B-Raf
CBF	Cerebral blood flow
CBV	Cerebral blood volume
CD	Cluster of differentiation
CDK	Cyclin-dependent kinase
CI	Confidence interval
CpG	Cytosine-phosphate-guanine
CSF	Cerebrospinal fluid
ctDNA	Circulating tumor DNA
DAB	3,3'-diaminobenzidine
DCE	Dynamic contrast enhanced
DNA	Deoxyribonucleic acid
DSC	Dynamic susceptibility contrast
DWI	Diffusion-weighted imaging
EANO	European Association of Neuro-oncology
EGFR	Epidermal growth factor receptor
FFPE	Formalin-fixed paraffin-embedded
FLAIR	Fluid-attenuated inversion recovery
GFAP	Glial fibrillary acidic protein
GTR	Gross total resection
Gy	Gray
HE	Hematoxylin-eosin
HIER	Heat induced epitope retrieval
HIF-1 α	Hypoxia inducible factor 1 α
HPF	High power field
HRP	Horseradish peroxidase
IDH	Isocitrate dehydrogenase
IHC	Immunohistochemistry

KPS	Karnofsky performance status
LSAB	Labeled Streptavidin Biotin
MGMT	O ⁶ -methylguanine-DNA-transferase
MIB-1	Molecular immunology borstel-1
MRI	Magnetic resonance imaging
mRNA	Messenger ribonucleic acid
MRS	Magnetic resonance spectroscopy
MSP	Methylation specific PCR
mt	Mutant
MVD	Microvessel density
NF1	Neurofibromin 1
OR	Odds ratio
PCR	Polymerase chain reaction
PDGFR	Platelet-derived growth factor receptor
PET	Positron emission tomography
PTEN	Phosphatase and tensin homolog
PI	Proliferative index
PI3K	Phosphoinositide 3-kinase
RCT	Randomized controlled trial
REMARK	Reporting recommendation for tumor MARKer prognostic studies
RTK	Receptor tyrosine kinase
T	Tesla
TERT	Telomerase reverse transcriptase
TF	Tissue factor
TGFβ	Transforming growth factor β
TP53	Tumor protein 53
VEGF	Vascular endothelial growth factor
vWF	von Willebrand factor
WHO	World Health Organization
wt	Wildtype

4 Summary

Glioblastomas are the commonest and most malignant of the primary brain tumors found in adults. They are highly aggressive tumors with a dismal prognosis of only 10-14 months. Virtually all tumors recur, which is due to the diffuse infiltration of tumor cells and the extensively heterogenous biology. Despite extensive research, the patient outcomes have not been significantly improved, and the standard treatment has not been altered the past 15 years. The hope is that an increased understanding of tumor biology could lead to better patient outcomes through the identification of biological markers that associate with different risks or responses to therapies. Insights into the natural biology (i.e. unaffected by therapies) of human glioblastomas could potentially lead to the discovery of new biomarkers that are important for tumor aggressiveness and could be potential targets of therapies. When studying the natural tumor biology instead of links to overall survival, we avoid the confounding effects of clinical features that affect survival but not tumor biology.

The general aim of this thesis was to increase the understanding of the natural tumor biology of human glioblastomas. This was investigated by exploring if phenotypical biological features seen in glioblastoma tissue samples or at magnetic resonance imaging (MRI) scans were associated with radiological speed of tumor growth or with O⁶-methylguanine-DNA-transferase (*MGMT*) promoter methylation status. *MGMT* status is an important predictive marker of response to chemotherapy in glioblastomas. The tissue samples and the MRI scans were retrieved before radiochemotherapy treatment, which enabled investigations of inherent biology of human glioblastomas.

All the papers in this thesis were based on a selected population of 106 glioblastoma patients, where all had at least two preoperative MRI scans taken with at least 14 days apart in order to estimate radiological speed of tumor growth. Tumor growth was estimated from segmented tumor volumes on the two MRI scans and the time interval between them. Patients were dichotomized as having either ‘fast-growing’ or ‘slow-growing’ tumors, based on if the tumor had a larger or smaller volume increase than expected from a fitted Gompertzian growth curve. The fitted growth curve was calculated based on the volume data from all the included tumors. The second MRI scans were also assessed for several morphological characteristics. Tissue sections were microscopically assessed for 27 histopathological features and immunohistochemical

quantifications of the degree of angiogenesis quantified as microvessel densities (MVDs) using two endothelial markers (vWF and CD105). The proliferative index (PI) of Ki-67/MIB-1 was also quantified. In addition, the tissue was assessed for *MGMT* status using methylation-specific PCR.

In Paper I and II, we investigated biological mechanisms behind preoperative tumor growth. We assessed possible associations between radiological tumor growth and 27 histological features (Paper I) and immunohistochemical MVDs (Paper II). The results showed that high cellular density and thromboses were significant independent predictors of faster tumor growth in both papers. Mitotic count and CD105-MVD were significant in the univariable analyses in Paper I and II, respectively, but neither were significant in the multivariable models. Our results suggest high cellular density might be a better measure of high proliferative activity than mitotic counts. Our findings are also in line with hypotheses describing thrombosis as an important inductor of hypoxia, which triggers more aggressive tumor biology. Also, the degree of angiogenesis was inadequate as a marker of faster tumor growth, which suggests angiogenesis-independent mechanisms, most likely facilitated by hypoxia, contribute to faster glioblastoma growth.

In Paper III, we explored if *MGMT* status was associated with pretreatment tumor biology. In 85 isocitrate dehydrogenase (*IDH*) wildtype glioblastomas, *MGMT* status was assessed for associations with 22 histopathological features, CD105-MVD, Ki-67/MIB-1 PI, MRI characteristics, and radiological tumor growth. None of the above features were significantly associated with *MGMT* status, which suggests that the survival benefit of *MGMT* methylated glioblastomas is not due to an inherently less aggressive tumor biology. This further suggests methylated *MGMT* status is not in part a prognostic factor but merely a predictive marker. The results also indicate that the increased response to chemotherapy in *MGMT* methylated glioblastomas is not due to pretreatment differences in phenotypical tumor biology. The lack of pretreatment biological differences between *MGMT* methylated and unmethylated tumors, further suggests that *MGMT* status cannot be non-invasively predicted from MRI scans.

The findings of our papers have increased the knowledge of the natural tumor biology of glioblastomas. However, the studies were explorative, and the findings need to be validated in future studies before firm conclusions can be drawn.

5 Introduction

5.1 Glioblastoma

5.1.1 Classification

Glioblastomas are the most aggressive and most common of the primary malignant brain tumors found in adults (1). The tumor cells of glioblastomas diffusely infiltrate the surrounding brain tissue (Figure 1), which makes complete surgical resection impossible. They are classified according to the World Health Organization's (WHO) Classification of Tumors of the Central Nervous System (2), based on histopathological and molecular examinations of surgically excised tumor material.

Histopathologically, glioblastomas are classified as diffusely infiltrating astrocytic gliomas (i.e. astrocytomas) WHO grade IV, which is the highest malignancy grade (2). The tumor cells of diffuse gliomas resemble glial cells (i.e. the supporting cells of the neurons). In glioblastomas, the tumor cells are predominantly of astrocytic differentiation (2), and the cell of origin is thought to be a neuroglial stem cell or progenitor cell (3, 4). Diffuse astrocytic tumors are graded based on the presence of the histopathological features nuclear atypia, high cellularity, high mitotic activity, necrosis, and microvascular proliferation (2). The presence of either necrosis or microvascular proliferation is mandatory for the grade IV (2) (Figure 1). The grading features portray biological mechanisms of aggressiveness, as they have been shown to associate with prognosis in diffuse astrocytic tumors (2). Glioblastomas are among the most histopathologically heterogeneous tumors in humans (2), which reflects the extensive molecular heterogeneity of these tumors (5, 6).

In the most recent 2016 WHO Classification, glioblastomas are diagnostically stratified into isocitrate dehydrogenase (*IDH*) mutant (mt) and *IDH* wildtype (wt) glioblastomas (2). *IDH* wt status is more commonly found in *de novo* glioblastomas (previously known as primary glioblastomas) (7-9), which typically originates in older patients (7, 8). On the other hand, *IDH* mt glioblastomas clinicopathologically correspond to tumors that have evolved from lower-grade diffuse astrocytomas (WHO grade II) or anaplastic astrocytomas (WHO grade III) (previously known as secondary glioblastomas) (9), which are more common in younger patients (8). Another important molecular marker is O⁶-methylguanine DNA methyltransferase (*MGMT*) promoter methylation status, because methylated *MGMT* status is a predictive marker of increased sensitivity to temozolomide – the chemotherapy of choice in glioblastomas (10-15).

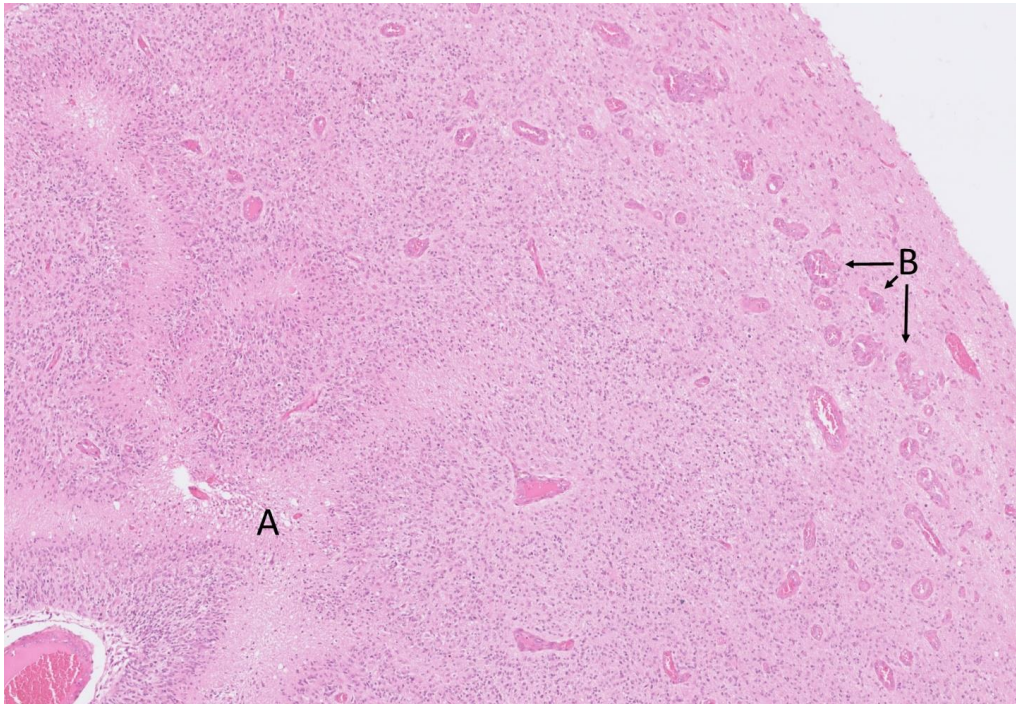


Figure 1. Glioblastoma histopathology, hallmark features, HE stain at x50 magnification. The diffuse infiltration of tumor cells is illustrated by the gradual decrease in cellular density from the lower left to the upper right corner. **A** Micronecrosis with surrounding palisades (i.e. aggregated cells at the edge of the necroses, forming serpiginous structures). **B** Microvascular proliferation. Arrows indicate microvascular proliferation in the infiltration zone, where tumor cells are diffusely dispersed within normal brain tissue. Photo: Vilde E. Mikkelsen.

5.1.2 Epidemiology

Glioblastomas account for 14.6% of the primary brain tumors, which is the third most common tumor type (1). However, they are the commonest of the primary malignant brain tumors (48.3%) (1). Approximately 12% of all glioblastomas are *IDH* mt (16).

Glioblastomas have the highest incidence rate of the primary malignant brain tumors (3.22 per 100 000 population). The incidence increases with age and the median age at diagnosis is 65 years (1). It is less common in children, where it accounts for only 3.0% of the primary brain tumors (1). Moreover, it is slightly more common in males (1.58 times) and in whites compared to blacks (1.95 times) (1). The Cancer Registry of Norway reports around 200 new cases of glioblastoma each year (17, 18).

The prognosis is dismal, and only 6.8% of glioblastoma patients are alive 5 years after diagnosis (1). The median overall survival is 10.1 months for unselected patients in Norway and may be increased to 14-16 months for patients undergoing standard treatment of surgical resection and radiochemotherapy (18, 19).

5.1.3 Clinical presentation

As glioblastomas grow rapid preoperatively (20, 21), symptoms may develop during weeks or months (17). In some cases, symptoms can present more abruptly and may be confused with strokes (22). Symptoms can be cognitive difficulties, personality changes, and focal neurological deficits, such as aphasia, hemiparesis, and visual field defects, depending on the location of the tumor (22). Also, 50% of patients have headaches at diagnosis and 20-40% have seizures as the presenting manifestation (22).

5.1.4 Treatment

To date, there are no curable treatment, and the standard treatment protocol has not been altered the past 15 years (3). Virtually all tumors recur, and the median time to recurrence is 7 months (3, 19). The standard treatment is maximum safe resection and adjuvant concomitant radiation and chemotherapy (i.e. the Stupp protocol) (19, 22, 23). Surgery relieves mass effect, leads to cytoreduction, and is necessary for adequate diagnosis (2, 22). During surgery, a preliminary pathological diagnosis is often performed on frozen sections to guide surgical decision-making (17). The aim of the surgery is to achieve gross total resection (GTR), which is defined as removal of the contrast-enhancing compartment of the tumor on magnetic resonance imaging (MRI) scans (Figure 2A, page 5) (3, 24). Also, a smaller volume of the residual contrast-enhancing mass after surgery has been shown to associate with improved survival (25). However, the extent of resection must be balanced against preservation of neurologic functions (i.e. maximum safe resection) (3, 26), as acquired deficits due to surgery are negatively associated with survival (27, 28). In patients with tumors in eloquent brain areas and/or poor clinical conditions, biopsies are often preferred (3, 17, 23).

Because there will always be left infiltrating tumor cells after surgical resection (29-31), patients with glioblastomas are treated with aggressive adjuvant treatment. Patients receive radiotherapy at a total dose of 60 gray (Gy) fractioned into 30 treatments of 2 Gy (3, 17, 22, 23). Concomitantly and following radiotherapy, the patients are given temozolomide, a DNA alkylating cytostatic agent (22, 23). The addition of temozolomide has been shown to increase survival with

a few months and increase long term survival when compared to radiotherapy alone (19). As *MGMT* promoter methylation predicts an increased response to temozolomide (10, 11), temozolomide treatment can be withheld in selected *MGMT* unmethylated patients with a higher risk of toxicity, such as in elderly patients (3, 32). Hence, although *MGMT* status is not used to guide treatment decisions in younger patients, it can be used for clinical decision making in elderly patients (23). Interestingly, the antiangiogenic agent bevacizumab (anti-vascular endothelial growth factor A (VEGFA)) was initially regarded as a promising targeted therapy in glioblastomas, as studies found a prolongation of the progression-free survival (33, 34). However, subsequent randomized controlled trials (RCTs) showed no effect on overall survival (35-37). Moreover, symptomatic treatment with corticosteroids is recommended in patients with symptoms due to peritumoral edema, and antiepileptic agents are given to patients with seizures (3, 22).

5.1.5 Magnetic resonance imaging

In patients with suspected brain tumors, the diagnostic modality of choice is T1-weighted MRI with contrast (3, 38). In addition, T2-weighted, Fluid-attenuated inversion recovery (FLAIR), and diffusion weighted imaging (DWI) sequences are recommended as parts of the standard protocol during the diagnostic investigation (39). The radiological diagnosis of glioblastoma can often be achieved with confidence when combined with clinical history (3). MRI has also an essential role in response assessments and the follow-up of glioblastoma patients (38, 40, 41).

The morphology on the MRI scans reflect biological properties of the tumors. In glioblastomas, the morphology can be quite variable, but the typical look on postcontrast T1-weighted scans is a contrast-enhancing rim surrounding a hypointense, central necrotic compartment (Figure 2A) (41, 42). In addition, glioblastomas are usually surrounded by peritumoral edema seen as hypointensity on T1-weighted scans (Figure 2A) and as hyperintensity on T2-weighted/FLAIR scans (Figure 2B) (22). In more atypical cases, glioblastomas can be multifocal or show faint contrast enhancement. In cases of *IDH* mt glioblastomas, parts of the tumor typically lack contrast enhancement. In glioblastomas, the contrast-enhancing areas represent highly cellular and proliferative tumor tissue with extensive vascularity with a breached blood-brain-barrier (29, 43, 44). High grade features such as necrosis, microvascular proliferation, and increased mitotic activity are more likely to be found in these contrast-enhancing areas (43). On the other hand, the peripheral non-contrast-enhancing areas represent infiltrating tumor cells (43), which contribute to the surrounding edema.

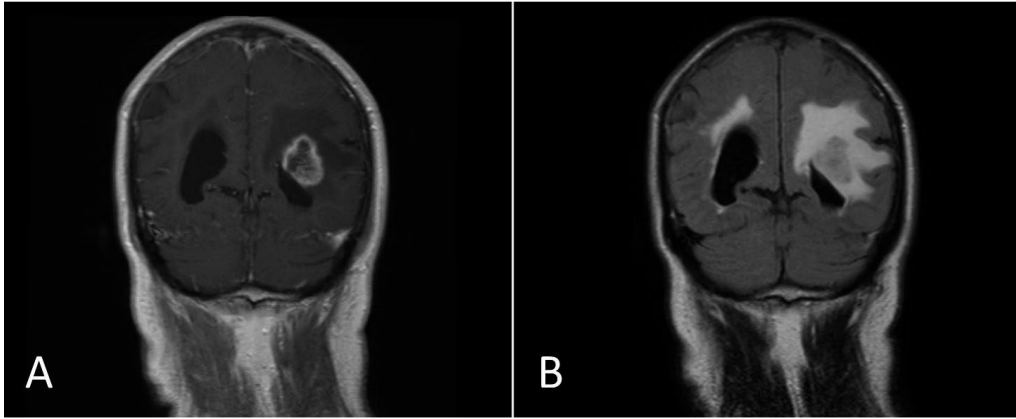


Figure 2. Typical glioblastoma morphology on MRI scans. **A** T1-weighted postcontrast scan with ring-enhancement, central necrosis and peritumoral edema. **B** FLAIR scan with hyperintense peritumoral edema. Picture courtesy of Anne Line Stensjøen.

Advanced MRI techniques can be used to more specifically quantify biological processes *in vivo*. For example, tumor vasculature can be assessed using dynamic contrast enhanced (DCE) MRI, which evaluates the diffusion of contrast through leaky blood vessels, and dynamic susceptibility contrast (DSC) MRI, which utilizes the spatial distribution of contrast agent to quantify the size of blood vessels (45). Perfusion-weighted imaging is based on the DSC technique, where serial imaging of the first passage of the contrast agent is used to generate maps of parameters such as the cerebral blood volume (CBV) and cerebral blood flow (CBF) (45). CBV has been shown to be a useful tool to differentiate glioblastoma from other tumor types and grades (3, 46, 47). DWI imaging does not require contrast agent, instead, it exploits the ability of water to diffuse within the tissue (45). From DWI imaging, apparent diffusion coefficient (ADC) maps can be calculated, where the ADC values inversely correlate with the cellular density (3, 45).

Recently, ‘radiogenomics’ has been established as the study of relationships between non-invasive radiological features and molecular alterations (48). For example, many studies have sought to non-invasively predict the *MGMT* status from MRI scans (48-59). However, the results have been conflicting and derived no expert consensus (53).

5.1.6 Molecular pathology

The last 30 years, the development of high-throughput molecular profiling techniques, such as microarray and next-generation sequencing methods, has led to the discovery of several molecular alterations in glioblastomas (7, 60-64). In *IDH* wt glioblastoma, the following alterations are commonly found: *TERT* promoter mutations (about 80%), homozygous deletion of *CDK2A/CDKN2B* (about 60%), loss of chromosome 10p (about 50%) and 10q (about 70%), *EGFR* alterations (about 50%), *PTEN* mutations/deletions (about 40%), *TP53* mutations (about 30%), and *PI3K* mutations (about 25%) (2, 7, 9, 60-62, 65, 66). However, among the molecular markers, only *IDH* status and *MGMT* status are established markers in the clinic (23).

Based on comprehensive studies using molecular profiling of somatic mutations, gene expression analyses, and methylation patterns, three molecular subclasses of *IDH* wt glioblastomas have been proposed (3). These molecular subtypes are (i) the proneural/receptor tyrosine kinase (RTK) I type characterized by *CDK4* and *PDGFRα* amplifications, which are typically found in younger patients; (ii) the classical type/RTK II, characterized by *EGFR* amplifications and *CDKN2A/B* loss; and (iii) the mesenchymal type characterized by *NF1* loss and increased macrophage infiltration (3, 63, 67-69). However, the clinical utility of the molecular subclasses remains unclear, and they are not implemented in the WHO Classification (2, 3). Moreover, it has been shown that several glioblastoma subtypes can be detected within the same tumor (6, 70), illustrating the extensive intratumoral heterogeneity of this disease. However, in brain tumor diagnostics, DNA methylation profiling has been shown to be promising tool (63, 71). A major advantage with this methodology is that it avoids the limitations of the subjective histopathological typing and grading causing observer variability (72, 73). Interestingly, DNA methylation profiling has been shown to lead to a change the diagnosis in 12% of brain tumors (63) with a substantial clinical benefit in some of the patients (74).

5.1.7 Prognostic and predictive markers

The most established clinical prognostic factors in glioblastoma patients are age at diagnosis, preoperative performance status, and GTR (2, 3, 75). Other important clinical prognostic factors are radio- and chemotherapy treatment (12, 76). Of the many histopathological features encountered in glioblastomas, only necrosis and giant cell glioblastomas have been shown to associate with prognosis (2) (necrosis with an unfavorable outcome (77-79), and giant cell glioblastoma with a favorable outcome (80-82)). Regarding the prognostic value of MRI

characteristics, compelling evidence suggests that a larger preoperative total tumor volume (defined by the contrast-enhancing rim on T1-weighted scans) is a negative prognostic factor in glioblastomas (38). Studies also suggest that a larger extent of necrosis and an increased degree of contrast enhancement are negative prognostic factors (76, 83). Among the genetic alterations in glioblastomas, only *IDH* mutation status and *MGMT* status are established as a prognostic and a predictive marker, respectively (12, 16, 84).

5.1.8 *MGMT* promoter methylation status

As previously mentioned, the favorable outcome of *MGMT* promoter methylated glioblastoma patients is linked to an increased sensitivity to temozolomide. Temozolomide causes DNA damage through the alkylation of guanine residues (85), whereas *MGMT* is a DNA repair enzyme that counteracts this effect through removal of the alkylated guanine residues (10). In this way, *MGMT* inhibits the cytostatic effect of temozolomide when expressed (10). Hypermethylation of the *MGMT* promoter inactivates the expression of the enzyme (10, 86), so that the effect of temozolomide is no longer counteracted (i.e. an increased effect) (Figure 3).

MGMT is methylated in 30-60% of newly diagnosed glioblastoma patients (10) and in as much as 74% of glioblastoma patients who survive more than 5 years (87). However, it is not established whether *MGMT* status is just a predictive marker or in part a prognostic marker, as previous studies have shown conflicting results regarding its association with survival among patients who were not treated with temozolomide (11, 13-15, 88-90) (see the Discussion, subsection ‘prognostic and predictive markers’, page 57-58). Although most data suggest that *MGMT* unmethylated patients have little benefit from the addition of temozolomide (11, 91), temozolomide is still a part of the standard treatment regime irrespective of *MGMT* status (23). This is due to the lack of effective treatment alternatives for *MGMT* unmethylated patients and that temozolomide generally has a favorable safety and tolerability profile (91, 92). Hence, as already mentioned, *MGMT* status can only be used to guide treatment decisions in elderly patients who cannot tolerate well the combined treatment (23). Also, a recent RCT showed a clinically meaningful effect (although not statistically significant) of the addition on temozolomide in *MGMT* unmethylated patients (15). However, some argue that the *MGMT* assay technique used in this study could explain the effect (93). This also illustrates how technical challenges regarding the testing of *MGMT* status are significant obstacles to the use of *MGMT* status for clinical decision making (69, 93-95).

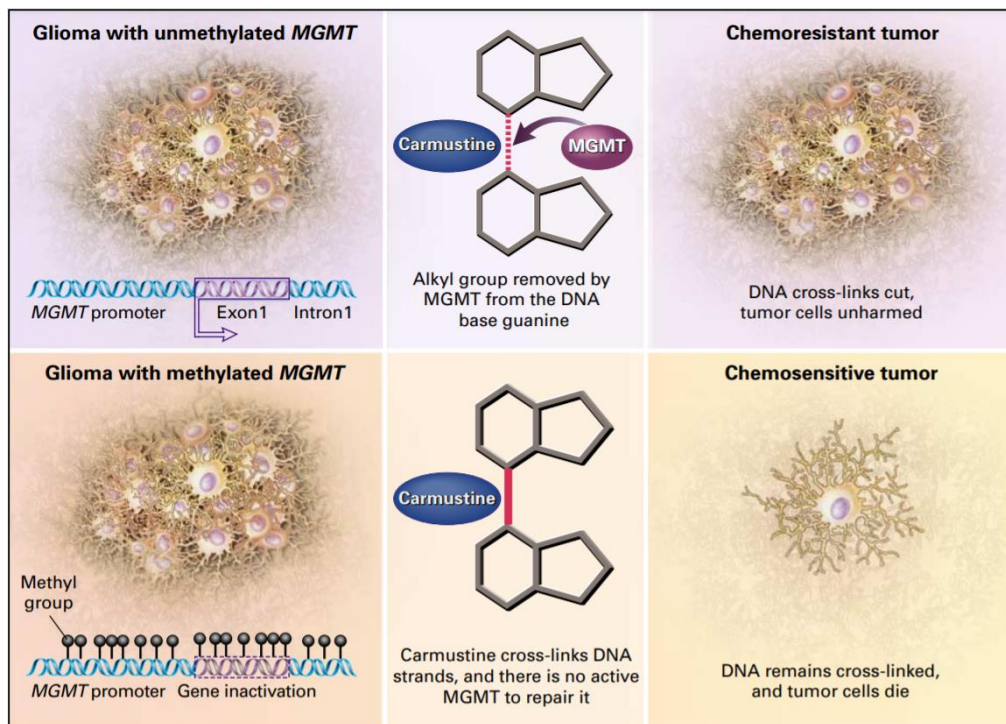


Figure 3. *MGMT* promoter methylation and chemosensitivity in response to alkylating agents. The action of carmustine illustrates that of temozolomide. Reprinted from N Engl J Med, 2000, Vol 343, Esteller et al., Inactivation of the DNA-repair gene *MGMT* and the clinical response of gliomas to alkylating agents. Figure 1 page no. 1351. Reproduced with permission from (96), Copyright Massachusetts Medical Society

The methylation status of the *MGMT* promoter can be assessed using several different techniques; however, no gold standard has been established (93, 95). Immunohistochemistry (IHC) and mRNA extraction techniques have shown unreliable results (84). Instead, techniques that interrogate the methylation status of the promoter region, such as methylation specific PCR (MSP) and pyrosequencing, are the recommended techniques (23). During methylation, methyl groups are covalently bound to cytosine, primarily in regions with a high content of cytosine-phosphate-guanine dinucleotides, known as CpG islands (10, 97, 98). CpG islands are often located in the gene promoters, where hypermethylation leads to inhibition of the gene expression (10, 97). The CpG island of *MGMT* promoter has 97 CpGs, which are all usually unmethylated in normal tissues (10, 94, 95). During *MGMT* methylation assays, the methylation statuses of only a few of the CpGs are interrogated to predict the activity of the *MGMT* enzyme (10).

Despite the clinical value of *MGMT* status, little is known about if it is linked to other biological processes in glioblastomas. It has been speculated that methylated *MGMT* status could potentially be a surrogate marker of undiscovered biological processes causing an inherently less aggressive tumor biology (88). The latter would also indicate that *MGMT* status is in part a true prognostic marker. Previous experimental *in vitro* studies have indicated that *MGMT* status could be linked to angiogenesis or hypoxia (99-102). However, such experimental models do not fully mimic the complex biology of human glioblastomas (103). Hence, it remains unclear if there are links between *MGMT* status and other biological process in human glioblastomas.

5.2 Tumor growth

5.2.1 Tumor growth biology

Tumor growth and the ability to metastasize are the major malignant factors contributing to the death of cancer patients (104). Tumor growth is a result of a complex interplay of several different biological hallmark processes of cancer, such as proliferation, evasion of cell death and growth suppression, infiltration, neovascularization, metabolic changes, and microenvironmental interactions (104) (Figure 4). The molecular biology behind these hallmarks and which of these processes that are the most important to the growth of different tumor types have been subjects of extensive research (104). The goal of this research has been to discover new mechanism-based targets of therapy to effectively impede tumor growth and progression (104).

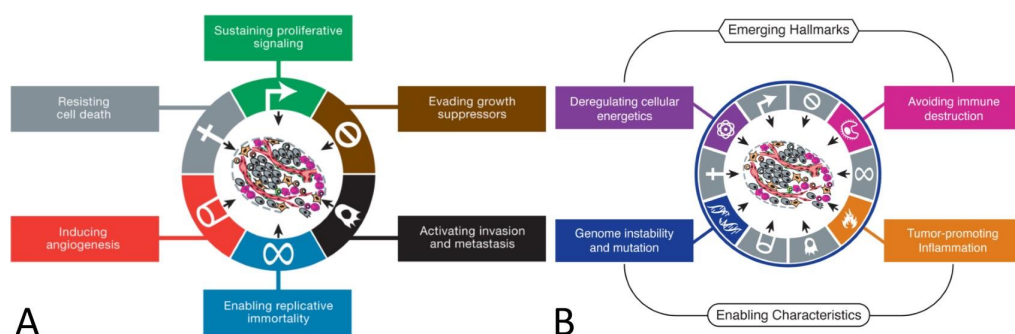


Figure 4. The Hallmarks of cancer. The complex interplay of these factors contributes to the growth and metastases of cancers. **A** The original hallmarks of cancer (from 2000). **B** Emerging hallmarks and enabling characteristics of cancer (added to the hallmarks in 2011). Reprinted from The Cell, 2011, Vol 144, Hanahan and Weinberg, Hallmarks of Cancer, The Next Generation (104), Figure 1 page no. 647 and Figure 3 page no. 658, with permission from Elsevier (licence no. 4904331277964)

The biology and dynamics behind tumor growth have been extensively studied in *in vitro* and *in vivo* animal models (103, 105-107). However, such models will never truly mimic the biology of *in vivo* human tumors (103). To adequately study the *in vivo* growth of human tumors, repeated, non-invasive, volumetric imaging assessments are necessary to estimate tumor growth rates. To estimate the tumor volumes, the borders of the tumors can be delineated on radiological imaging scans and volumes calculated from the delineated region of interest (108). This process is known as segmentation. In this way, growth rates can be estimated from segmented tumor volumes from \geq two imaging scans and the time interval between them. Also, to study the mechanisms behind the natural growth, the assessed tumors should be unexposed to therapies that could affect the biology and tumor size. However, with today's standard of care, patients are treated rapidly after diagnosis. Hence, the acquisition of repeated image analyses separated by sufficient time intervals prior to treatment is challenging. In all the papers in this thesis, the natural tumor growth of human glioblastomas was estimated from two preoperative MRI scans and was investigated for associations with different biological features.

5.2.2 Tumor growth models

In addition to reveal insights into tumor biology, tumor growth models assessed from imaging scans in patients can potentially be used to guide optimal treatment logistics and improve prognostication (20). Throughout history, several different growth patterns for human tumors have been suggested (Figure 5), with exponential and Gompertzian growth being the most commonly assumed patterns (109). Exponential growth is characterized by a constant growth rate (i.e. volume doubling time) (109) (Figure 5B), whereas Gompertzian growth is characterized by an initial exponential growth phase followed by a progressively decreasing growth rate and a final plateau phase (105, 109) (Figure 5C). However, despite being widely accepted, both models have been criticized (110, 111). Another suggested growth pattern is linear growth (Figure 5A), which is the simplest growth pattern. Here, the tumor volume increases with the same volume for each time interval (i.e. absolute growth per day) (Figure 5A). Furthermore, linear radial growth has been suggested for glioma growth (Figure 2D), which is characterized by a linear increase in the radius of the tumor measured as mm/year (112, 113).

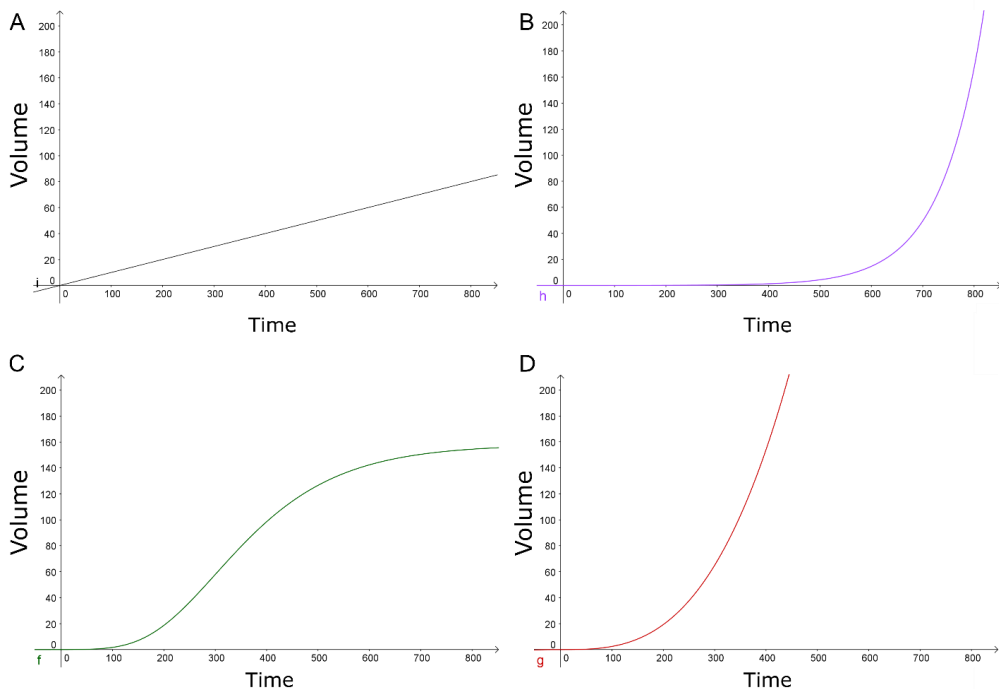


Figure 5. Examples of different growth patterns. **A** Linear growth. **B** Exponential growth. **C** Gompertzian growth. **D** Linear radial growth. Plots are made using GeoGebra by Anne Line Stensjøen, using arbitrary parameters.

5.2.3 Glioblastoma growth dynamics

In contrast to many other tumor entities, the growth dynamics of glioblastomas have been sparsely studied. This is mainly because of the difficulties of acquiring repeated imaging scans prior to treatment. To date, there are mainly three published studies that have explored the preoperative growth dynamics in a larger number of glioblastoma patients (20, 21, 114). A few smaller studies (10-32 patients) have also investigated the glioblastoma growth dynamics (113, 115-120); however, only one of them investigated the preoperative growth (113). In the three larger studies, Stensjøen et al. (106 patients) (20), Ellingson et al. (95 patients) (21) and Fan et al. (54 patients) (114) defined the tumor volumes as the combined volume of the contrast-enhancing rim and the necrotic core on contrast enhancing T1-weighted MRI scans (Figure 2A, page 5). All three studies showed that glioblastomas grew fast preoperatively, and that there was a large variability of growth rates among the patients. Stensjøen et al. (20) also explored the fitness of three different growth

patterns (exponential, Gompertzian, and linear radial growth (Figure 5)) with the observed volume changes. They found that exponential growth showed a poor fit, whereas Gompertzian and linear radial growth showed a good fit (20).

5.2.4 Glioblastoma growth biology

As previously mentioned, there are several biological hallmark processes that contribute to increased tumor growth and metastasis of tumors. Interestingly, glioblastomas rarely metastasize extracranially (121). Instead, the death of patients has been found to be mostly caused by mass effect, invasion of vital brain areas, subarachnoid and ventricular implantation, and/or complications to therapy (122, 123). Hence, it is mainly the local impacts that contribute to the death of glioblastoma patients (122, 123). Modeling of tumor growth in glioblastomas is therefore likely to have greater clinical implications than in extracranial tumors (124). Hence, a better understanding of the biology behind increased tumor growth in glioblastomas could potentially reveal new biomarkers or targets of therapies.

A major challenge in studying the biology of glioblastoma is the extensive genetic and histopathological heterogeneity observed both between and within tumors (125-127). Generally, glioblastomas are known for being highly proliferative (128), highly infiltrative (29, 30), highly angiogenic (129, 130), highly hypoxic (131, 132), and highly prothrombotic (133-135). However, due to the vast biological heterogeneity, there will always be cases of glioblastoma that are not in accordance with these characterizations.

Among the previous studies on growth rates in glioblastoma patients (20, 21, 113-120), only three investigated associations between tumor growth rates and biological factors (113, 114, 117). Blankenberg et al. (117) found a tendency of faster growth in aneuploid or multiclonal glioblastomas compared to diploid. However, they assessed only 7 patients that had received treatment. Wang et al. (113) used a biomathematical model that estimated the net proliferation and net invasion rates based on serial pretreatment MRI scans and the tumor growth rate (linear radial growth, Figure 5D) (112, 113, 136). They found that net proliferation and net proliferation/net invasion ratio independently predicted survival in the 32 included patients (113). Other studies using the same biomathematical model have shown promising results in predicting future growth and response to treatment for individual glioblastoma patients (136). Fan et al. (114) investigated associations between several molecular markers and the preoperative speed of tumor growth. They found that *TERT* promoter mutations and unmethylated *MGMT* status were significantly associated

with faster tumor growth in univariable analyses, but neither were significant in the multivariable analyses (114). They also found that in a subgroup of tumors with determined *IDH* and *MGMT* status (37 patients), *IDH1* wt and *MGMT* unmethylated tumors grew significantly faster (multivariable analysis) (114). Moreover, they also found that a low expression of Ki67 staining showed a marginally significant association with decreased tumor growth; however, this was only significant in the univariable analysis (114). Due to the limited number of previous studies with few included patients, a lot remains unclear about which biological processes that are the most important for the growth of human glioblastomas.

5.2.5 Experimental models of glioblastoma growth

The biology of glioblastoma growth has been extensively studied using *in vitro* and *in vivo* animal models. These experimental models enable detailed studies on molecular mechanisms and genetics behind the different biological processes (103, 104). Even though these processes can be modelled to some extent in *in vitro* models, only *in vivo* models account for tumor-host interactions (103). This is because the *in vivo* models include host components such as anatomical barriers, extracellular matrix, cytokines and growth factors, and the presence of endothelial cells and tissue-specific progenitor cells (103). However, the biology of these host factors and their interaction with the tumor cells (i.e. the micro-environment) differ between animals and humans (103). This causes dissimilar selection pressures and thus evolutionary advantages for different tumor clones (103). These dissimilarities are illustrated by a comprehensive genomic study that found considerable differences between the mRNA expression profiles and DNA methylation profiles between glioblastoma patient material and experimental *in vitro* and *in vivo* models derived from it (137). Hence, *in vitro* and *in vivo* animal models will never truly mimic the vastly complex biology of human glioblastomas (103).

Nevertheless, there are several advantages with these experimental models. In contrast to *in vivo* human studies on tumor growth, *in vivo* animal models enable more frequent measurements of tumor volumes, and thus more precise estimates of growth rates and growth patterns (138). *In vitro* and *in vivo* models have also revealed important insights into the molecular events contributing to brain tumor initiation and progression (103, 107). In addition, such models are frequently used for evaluation of new treatment strategies and investigations of resistance mechanisms (103, 107).

5.3 Histopathological features

5.3.1 General histopathology

Histopathology is the study of the microscopical structure of diseased or abnormal tissue. Hence, histopathological features represent biological processes within the assessed tissue material. The histopathology of excised tissue material is most commonly assessed on routine stained hematoxylin-eosin (HE) tissue sections from formalin-fixed paraffin-embedded (FFPE) tissue blocks. Since the early days of glioma research, the prognostic value of different histopathological features within diffuse astrocytic tumors have been extensively studied. This research eventually led to the histological grading scheme of today's WHO Classification (2), where the different grades predict prognosis and response to therapy (2, 75). This demonstrates how the hallmark features of glioblastomas, necrosis and microvascular proliferation, illustrate aggressive biological mechanisms in diffuse astrocytic tumors.

5.3.2 Histopathological features of glioblastoma

As previously mentioned, glioblastomas are one of the most histopathologically heterogeneous neoplasms seen in humans (2), and the histopathology can vary extensively both between and within tumors (125, 126). Neoplastic cells of astrocytic differentiation are often recognized (i.e. cells with angulated nuclei and irregular chromatin), but they can be difficult to identify in poorly differentiated glioblastomas (2). In addition to the grading features (necrosis, microvascular proliferation, cellular density, mitotic activity, and atypia), there are several other histopathological features that can be observed in glioblastomas (2, 139). These features are perinecrotic palisades (characteristically accumulated neoplastic cells at the edge of necrotic areas), apoptosis, hemorrhages (extravascular erythrocytes), thrombosed vessels (vessels occluded with fibrin), pseudorosettes (characteristic structures of circumferentially oriented neoplastic cells around vessels), different types of immune cells (lymphocytes, macrophages, neutrophilic granulocytes), desmoplasia (fibrovascular tissue), different patterns of invasion, and several different cellular patterns. The invasion patterns illustrate the preferred infiltration paths of tumor cells into normal brain tissue, which are known as the secondary structures of Scherer (140). These structures are perineuronal satellitosis (infiltration along neurons), angiocentric structures (infiltration in the perivascular space), and subependymal and subpial clustering (infiltration beneath the meninges). The different cellular patterns seen in glioblastomas are small cells, giant cells, gemistocytes (abundant eosinophilic cytoplasm and eccentric nuclei), sarcomatous cells (fusiform, bipolar cells

forming bundles), myxomatoid cells, oligodendroglioma-like cells (perinuclear haloes), primitive neuronal cells (undifferentiated cells), granular cells (abundant granulated cytoplasm), lipidized cells (foamy cytoplasm), and different types of metaplasia (adenoid, squamous, and mesenchymal). Pictures and more specific descriptions of the abovementioned histopathological features (except apoptosis, subependymal clustering, lipidized and granular cells, and epithelial metaplasia), can be found in the Material and methods section, subsection ‘Histopathological features’ (page 28-37) of this thesis.

In the 2016 WHO Classification, glioblastomas are subclassified into three variants that are different from classic glioblastoma in the dominant tissue pattern, outcome and/or clinical progression (2). These variants are gliosarcoma (biphasic pattern of mesenchymal and glial differentiation), giant cell glioblastoma, and epithelioid glioblastoma (epithelioid, rhabdoid and gemistocytic cells, associated with *BRAFV600E* mutations). In the 2007 Classification, epithelioid glioblastoma was not yet an established glioblastoma variant (141).

5.4 Neovascularization

5.4.1 Tumor neovascularization

Neovascularization – the ability to induce additional vascular supply – is a hallmark feature of cancer (Figure 4A, page 9) that is fundamental for sustaining the supply of nutrients and assure evacuation of metabolic waste products as tumors grow larger (104). The most important mechanism of tumor neovascularization is thought to be angiogenesis, which is the process where new capillaries sprout from already present vasculature (142). Angiogenesis is a highly complex process that involves a spectrum of events, from the breakdown of already occurring vessels, migration and proliferation of endothelial cells, and the recruitment of pericytes (142).

In 1971, Judah Folkman established the hypothesis that all tumor growth is dependent upon a gradual increase in new capillaries (i.e. angiogenesis-dependent) – today known as the Folkman hypothesis (143, 144). This hypothesis has led to many studies on pro-angiogenic molecules and angiogenic inhibitors (144), and it has been the rationale behind the development of antiangiogenic therapies (145). Although Folkman acknowledged that the initial tumor growth could be angiogenesis-independent (144), he stated that an “angiogenic switch” was necessary for tumor growth beyond a few mm³ (143, 144). In diffuse gliomas, this initial ‘prevascular’ phase has later been shown to rely on adoption of preexisting vasculature, known as vascular co-option (142, 146).

Vascular co-option can be seen as an accumulation of tumor cells around normal vasculature (corresponding to the previously mentioned perivascular accumulation) (Figure 6A and Figure 19B at page 33) (142). During the last 10-20 years, several neovascularization processes other than angiogenesis have been discovered, such as vasculogenesis (i.e. homing of circulating endothelial progenitor cells (147, 148)), vascular mimicry (i.e. tumor cells forming functional vascular networks (149, 150)), and tumor-to-endothelial cell transdifferentiation (i.e. tumor cells that transdifferentiate into an endothelial phenotype (151, 152)) (Figure 6). However, the contribution of these processes to the overall tumor vasculature and how they interact remains to be unveiled (142). Especially the role of tumor-to-endothelial cell transdifferentiation is debated (142, 153). Nevertheless, these other mechanisms of neovascularization represent exceptions to the Folkman hypothesis.

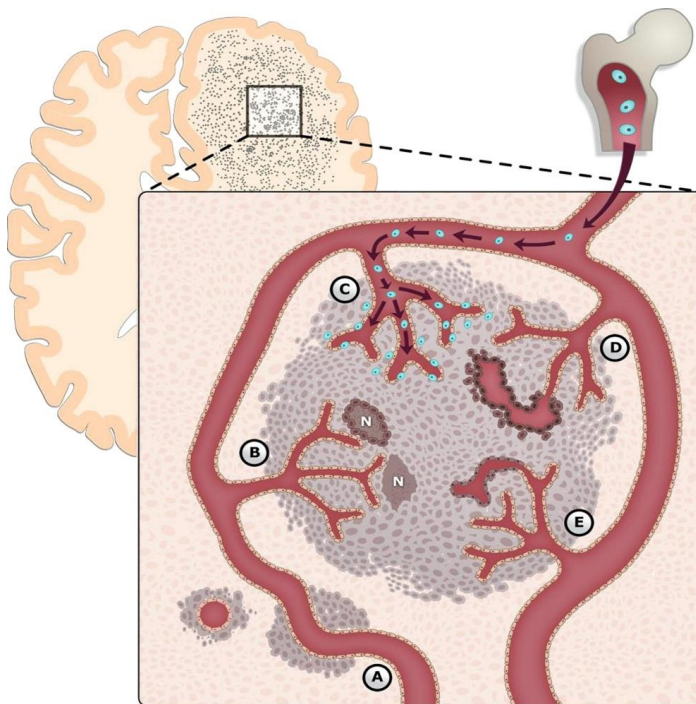


Figure 6. Mechanisms of glioma-associated neovascularization. **A** Vascular co-option. **B** Angiogenesis. **C** Vasculogenesis. **D** Vascular mimicry. **E** Glioblastoma-endothelial cell transdifferentiation. Reprinted from Am J Pathol, 2012, Vol 181, Hardee, M. E. and Zagzag, D., Mechanisms of glioma-associated neovascularization (142), Figure 6 page no. 1137, DOI: [10.1016/j.ajpath.2012.06.030](https://doi.org/10.1016/j.ajpath.2012.06.030), with permission from Elsevier, License: CC BY-NC-ND 4.0 <https://creativecommons.org/licenses/by-nc-nd/4.0/>.

5.4.2 Neovascularization in diffuse astrocytic tumors

High grade diffuse gliomas (WHO grade III and IV) have been shown to have among the highest degrees of vascularity of all solid tumors (2) and secrete high levels of pro-angiogenic factors (154). Moreover, the fact that microvascular proliferation is a hallmark feature of glioblastoma (2), illustrates the link between aberrant angiogenesis and a more aggressive tumor biology of diffuse astrocytic tumors. Microvascular proliferation is an exuberant form of angiogenesis characterized by multilayering of the vascular walls and occasional tufting (Figure 13, page 30) (155). In addition to microvascular proliferation, there is often a diffuse increase in the density of small capillaries in glioblastomas, which may be inconspicuous on routine HE sections (140). However, the microvessels can be visualized using IHC markers of endothelial cells (140) and quantified with microvessel density (MVD) measurements. Increasing MVDs of the endothelial marker von Willebrand factor (vWF) have been shown to associate with higher tumor grade and shorter survival in diffuse astrocytic tumors (156). Furthermore, the newly formed vasculature in glioblastomas has a defective blood-brain-barrier, which causes the excessive leakiness seen as contrast enhancement and peritumoral edema on MRI scans (Figure 2, page 5) (140, 142, 157, 158). The contrast enhancement on MRI scans is more frequent and intense in glioblastomas than in anaplastic astrocytomas (WHO grade III) (158, 159). In addition, these newly formed vessels are associated with an increased risk of intracerebral hemorrhages (160) and prothrombogenicity (133, 135).

5.4.3 Angiogenesis and growth of glioblastomas

Enhanced angiogenesis due to an increased secretion of VEGF has been shown to stimulate tumor growth in *in vivo* animal models of glioblastomas and gliomas (161-163). VEGF is a proangiogenic factor found in high concentrations in glioblastomas (130, 164), and it is believed to be the main proangiogenic factor secreted by these tumors (162, 163). A major trigger of angiogenesis is hypoxia (i.e. hypoxia-induced angiogenesis) (131, 142, 165). Hypoxia is thought to mainly induce angiogenesis through activation of the transcription factor hypoxia inducible factor 1 α (HIF-1 α), which mediates a metabolic adaptation to tumor hypoxia through increased expression of VEGF and glycolytic enzymes, among other effects (131, 153, 166, 167). HIF-1 α has been shown to increase angiogenesis and tumor growth in animal models (161, 167-170). In human glioblastomas, the expression of HIF-1 α and VEGF is enhanced in perinecrotic areas with or without palisades (131, 164, 165). The observed vicinity of microvascular proliferation and necrosis is therefore

believed to be caused by the paracrine secretion of VEGF due to hypoxia (155, 164, 171). Nevertheless, evidence suggests angiogenesis can also be stimulated by oncogenic mutations (i.e. hypoxia-independent angiogenesis) (142), such as the observed increased secretion of VEGF in tumors with *TP53* loss (169).

5.5 Immunohistochemistry

5.5.1 General immunohistochemistry

Immunohistochemistry (IHC) visualizes proteins (antigens) of interest in tissue sections by means of antibodies reactive against the protein. In general, IHC methods use antibodies that bind the protein of interest (primary antibodies) and use different detection techniques to visualize this binding (172). Two frequently used detection techniques are polymer-based detection (e.g. EnVision) and Labeled Streptavidin Biotin (LSAB) detection (Figure 7). In tissue sections from FFPE tissue blocks, antigen retrieval is first necessary to enable binding between the protein of interest and the primary antibody. During antigen retrieval, cross-links of the tissue antigens induced by formalin are broken to expose “masked” epitopes of the antigens (173). Antigen retrieval usually involves heating (heat induced epitope retrieval (HIER)) or application of proteolytic enzymes (173). Of the different detection techniques, the polymer-based technique is the most commonly used. Here, several secondary antibodies and horseradish peroxidase (HRP) enzymes are bound to a large dextran backbone (Figure 7A) (172). The secondary antibodies bind the primary antibodies, and subsequently added chromogene 3,3'-diaminobenzidine (DAB) is converted into color by HRP (172). In contrast to the polymer-based technique, the LSAB technique involves more steps, where a biotinylated secondary antibody is added first, and streptavidin bound to HRP is added later (Figure 7B) (172).

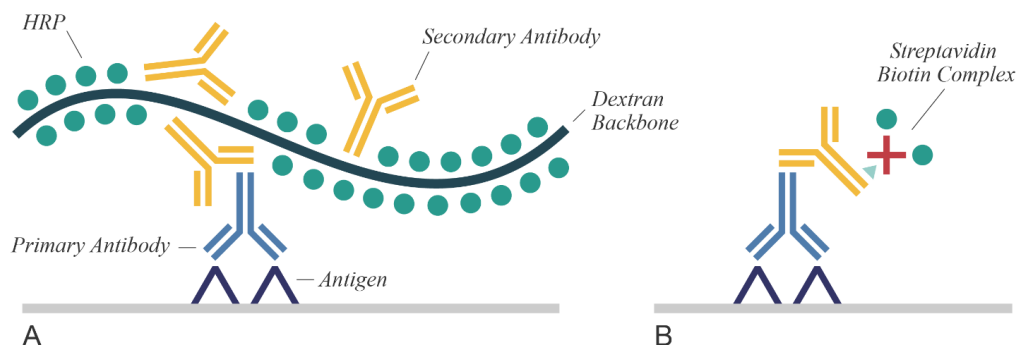


Figure 7. Immunohistochemical detection methods. **A** Polymer-based detection (e.g. EnVision). **B** LSAB detection. Illustration by Sonja Sarah Porter.

5.5.2 GFAP

Glial fibrillary acidic protein (GFAP) is the most specific marker of cells of the astrocytic origin. Hence, GFAP can be used in diagnostically challenging brain tumor cases, such as in distinguishing glioblastomas from metastatic tumors (174-177). GFAP is the principal intermediate filament of astrocytes (175, 178, 179). GFAP is therefore also expressed in normal astrocytes and gliosis (174-176). The expression can be less intense and found in fewer tumor cells in higher tumor grades due to dedifferentiation (174, 175, 179, 180).

5.5.3 IDH1

As previously mentioned, glioblastomas are divided into *IDH* wt and *IDH* mt in the 2016 WHO Classification, and about 90-95% of newly diagnosed glioblastomas are *IDH* wt (3). IDH is an enzyme of the Krebs cycle, which converts isocitrate to α -ketoglutarate (181). It exists in 3 isoforms, but only IDH1 and IDH2 have shown oncogenic mutations (8). Upon mutation, IDH produce D-2-hydroxyglutarate (8), which is an oncometabolite that induce epigenetic changes within the tumor (182). The mutation is believed to happen early in gliomagenesis, because it is detected in both diffuse astrocytomas (grade II) and oligodendrogliomas, and clinical and genetical findings have been shown to differ between *IDH* mt and *IDH* wt gliomas (8, 16).

As a part of the daily routine at most pathology departments, the *IDH* mutation status is assessed using IHC. However, IHC only detects the specific mutation *R132H* of the IDH1 enzyme. Hence, other *IDH1* mutations and *IDH2* mutations can only be detected using *IDH1/2* sequencing. Fortunately, more than 90% of *IDH* mt gliomas have the *IDH1 R132H* mutation (8), and other *IDH* mutations are very uncommon in older patients with newly diagnosed tumors, which makes additional sequencing excessive in these patients (2, 183). Still, there is no established age cut-off for when sequencing is necessary, but a cut-off of <55 years is commonly used in clinical practice (184).

5.5.4 vWF

von Willebrand factor (vWF, previously known as factor VIII-related antigen) is a plasma glycoprotein which is synthesized by endothelial cells and megakaryocytes (185, 186). vWF is stored in secretory vesicles of endothelial cells (186), and can therefore be used as an endothelial marker of both normal and neoplastic vasculature (i.e. a panendothelial marker) (185, 187). In addition, it stains megakaryocytes, platelets, and endothelial cells of lymphatic vessels (188). vWF acts by forming a bridge between platelets and exposed collagen of damaged vasculature, which

initiates the thrombus formation (186). The staining is cytoplasmic, and may show a discontinuous, granular staining of the endothelial cells (187) (Figure 24, page 40).

5.5.5 CD105

Endoglin (CD105) is a transmembrane glycoprotein of the transforming growth factor β (TGF β) receptor complex on endothelial cells (189). In contrast to vWF, CD105 has been found to predominantly stain proliferating (i.e. angiogenically active) endothelial cells (151, 189-197). As vWF, the CD105 staining is cytoplasmic (Figure 24, page 40).

5.5.6 Ki-67/MIB-1

Ki-67 is a DNA binding protein found in the nucleus which is expressed during all phases of the cell cycle (G1, S, G2 and mitosis), but not during quiescence (G0) (198). Hence, it is used as a marker of proliferating cells (Figure 25, page 41), which is widely used for the grading of tumors by quantifications of the proportion of dividing cells (i.e. the proliferative index (PI)) (199, 200). MIB-1 is the antibody that is most commonly used to detect Ki-67 (201). Recent discoveries indicate that Ki-67 have different functions during the cell cycle, where it is important for the structure of chromosomes and heterochromatin (200).

6 Aims

This thesis is based on the work by Stensjøen et al. (20) that examined the pretreatment tumor growth dynamics in glioblastoma patients. Our general aim was to investigate the natural tumor biology of human glioblastomas by exploring if phenotypical biological features were associated with speed of tumor growth or with *MGMT* promoter methylation status. In the long term, the hope is that a better understanding of the inherent biology of glioblastoma will pave the way for improved patient outcomes.

In Paper I and II, the general aim was to explore biological mechanisms behind the large variations in pretreatment speed of glioblastoma growth shown by Stensjøen et al. (20). The underlying hypothesis was that biological processes seen as histopathological or IHC features might explain the growth rate variability. This could increase our understanding of which biological mechanisms that are the most important for the natural growth of glioblastomas. Despite extensive research on growth mechanisms in experimental models, few studies have addressed this in human patients. This is mainly due to the difficulties in acquiring serial preoperative imaging scans to calculate the tumor growth rates. The aim of Paper II was based on the findings in Paper I where thromboses were found to independently predict faster growth. In Paper II we wanted to assess if the degree of angiogenesis was associated with growth, as it has been hypothesized that thromboses stimulate tumor growth through increased angiogenesis stimulated by hypoxia.

In Paper III we aimed to investigate if *MGMT* status could be a surrogate marker of the phenotypical tumor biology of glioblastomas before treatment. Methylated *MGMT* status is an important predictive marker of increased response to chemotherapy in glioblastomas, and it can be used to guide treatment decisions. The investigation of potential links between pretreatment biology and *MGMT* status could possibly disclose differences in aggressiveness, explain differences in response to chemotherapy, and reveal if *MGMT* status can be non-invasively predicted from MRI scans.

The specific aims of each paper were:

- I) To explore if the presence of 27 different histopathological features in glioblastomas could explain the observed variation in speed of preoperative tumor growth assessed from serial MRI scans.

- II) To investigate the association between degree of angiogenesis and speed of tumor growth. The degree of angiogenesis was assessed using microvessel density (MVD) counts by means of two endothelial IHC markers, vWF and CD105.
- III) To explore if *MGMT* status was associated with phenotypical tumor biology, assessed by 22 histopathological features, immunohistochemical proliferative index (PI) and MVD measurements, conventional MRI characteristics, or preoperative speed of tumor growth.

7 Material and methods

7.1 Patient selection

Patients were retrospectively selected from all patients ≥ 18 years with newly diagnosed (i.e. *de novo*) glioblastomas operated at St Olavs University Hospital in Trondheim between January 2004 and May 2014 (262 patients) (20). The selection was mainly based on if the pretreatment growth dynamics could be estimated from the preoperative MRI scans of the tumors (Figure 8). The included patients needed to have \geq two preoperative contrast-enhancing T1-weighted MRI scans taken ≥ 14 days apart. The interval of ≥ 14 days was established to reduce the uncertainty of the growth estimates (202). Patients with non-contrast-enhancing tumors and gliomatosis cerebri according to radiologic criteria (203) were excluded, because such tumors are inherently challenging to segment for tumor volumes.

Before inclusion, the patients were histopathologically revised by V.E.M. and S.H.T. according to the 2007 WHO Classification (141). One case was excluded due the lack of necrosis and microvascular proliferation. Altogether, 106 patients (40.8%) were included in Paper I, where all patients had sufficient tumor material for evaluation of histopathological features. In Paper II, four additional patients were excluded due to insufficient morphology and amount of material for the MVD assessments, which left 102 patients eligible for inclusion (Figure 8).

In Paper III, the 106 patients from Paper I were investigated for *MGMT* promoter methylation status. However, 18 cases (17%) were excluded due to inconclusive results on the *MGMT* assay. The material was also updated to be in accordance with the 2016 WHO Classification (2). Therefore, all patients < 55 years that were negative on the IHC analysis of *IDH1* status (*IDH1 R132H*) were additionally sequenced for *IDH1/2* mutation status using Sanger sequencing. In one case, we found a rare mutation in *IDH2* (c.434G>A, p.G145E). We excluded the three *IDH* mt patients from Paper III due the differences in tumor biology between *IDH* mt and wt glioblastomas (204). This left 85 patients to be included. In five of these patients, *IDH2* was not conclusive on sequencing but all were wildtype on the *IDH1* sequencing. Due to the very low frequency of *IDH2* mutations in glioblastomas (8, 60), these were categorized as *IDH* wt and included.

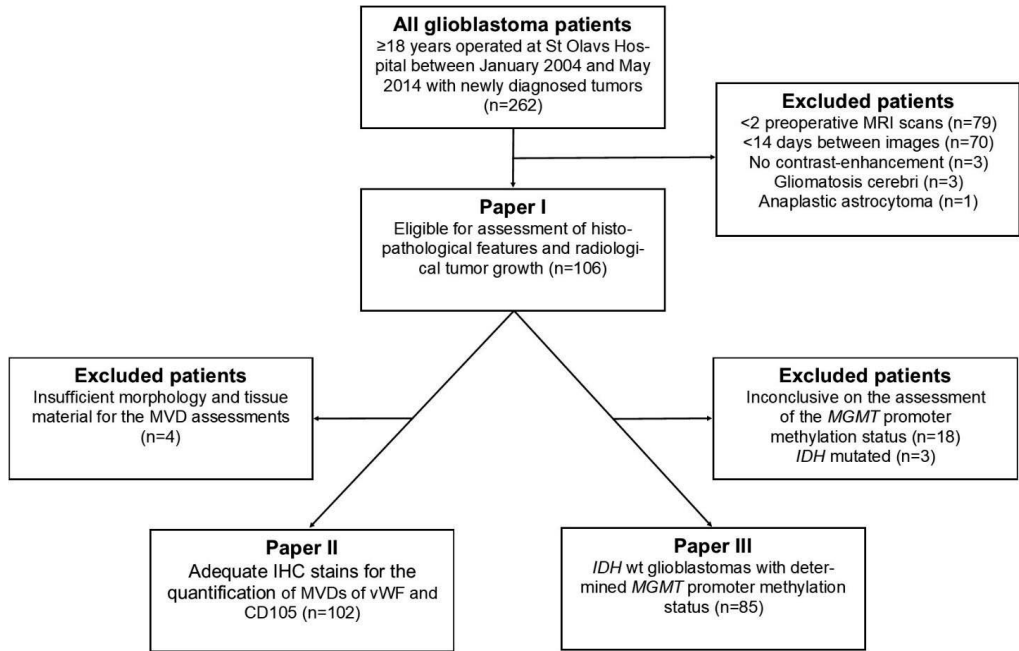


Figure 8: Flowchart of the selection of patients

7.2 Estimation of tumor growth

As already mentioned, the speed of tumor growth was estimated from two preoperative tumor volumes and the time interval between them. We also had to assume an underlying growth pattern to be able to compute the growth rates.

Tumor volume segmentation

In each patient, the tumor volumes were manually segmented on the two preoperative contrast-enhancing T1-weighted MRI scans taken ≥ 14 days apart. The tumor volumes from the first scans were from the MRIs taken for the diagnostic work-up, and the volumes from the second scans were from MRIs taken before surgery for intraoperative imaging. Tumor volume was defined as the combined volume of the contrast-enhancing rim and non-contrast-enhancing parts enclosed by it (Figure 9). In cases showing multifocal contrast enhancement, all enhancing lesions were segmented and added to the total volume. Contrast enhancement from adjacent blood vessels and meninges were not segmented.

The tumor volume segmentations were performed by A.L.S. and verified by E.M.B. using the software BrainVoyager QX, version 1.2.6 (Brain Innovation, Maastricht, the Netherlands) in a previous study (20). The segmentations were performed manually with help from a used-defined range-algorithm. The algorithm was first applied to enclose the contrast-enhancing compartment, which was then manually adjusted. The volume of the contrast-enhancing region was merged with the manually delineated volume of the non-contrast-enhancing compartment (i.e. necrosis) (Figure 9). When the tumor borders in all MRI planes were delineated, the tumor volume was computed from the following formula: Tumor volume = number of voxels segmented \times voxel area \times (slice thickness + gap thickness). The voxels are the 3D pixels of MRI scans, which dimensions are given by the voxel area and the slice thickness. In higher resolution scans (higher Tesla (T)), the area of each voxel is smaller (i.e. a higher in-plane resolution), slice thickness thinner, and gap thickness smaller. The diagnostic scans were taken from 15 different radiology clinics with MRI scanners of different resolutions (8 from 1T, 85 from 1.5T, and 13 from 3T). All preoperative scans except one were taken at St Olavs Hospital using 1.5T or 3T scanners.

In Paper III, characteristics on the second MRI scans were used for analyses. Here, the MRI characteristics were the total tumor volumes, volumes of the contrast-enhancing compartment and the non-contrast-enhancing compartment, and the percentage of necrosis (i.e. volume of the non-contrast-enhancing volume divided by the total tumor volume).

Growth pattern

As already mentioned, we must assume an underlying growth pattern to be able to compute growth estimates from the two tumor volumes and the time interval between them. Stensjøen et al. (20) explored the fitness of three different growth patterns (exponential, Gompertzian, and linear radial growth (Figure 5, page 11)) with the observed volume changes in the 106 included patients. They found that exponential growth showed a poor fit, whereas Gompertzian and linear radial growth showed a good fit (20). They also found that larger tumors grew significantly slower than smaller and that the volume of the necrotic core grew relatively faster in larger tumors (20). These findings were in accordance with the Gompertzian growth pattern, which is characterized by a progressively decreasing growth rate and a final plateau phase due to a lack of nutrition as the tumor grows larger (Figure 10 and 5C at page 11) (20, 21). The final plateau phase is also in line with the confined space in the human cranium. The Gompertzian growth pattern was therefore concluded as the most biologically plausible pattern (20).

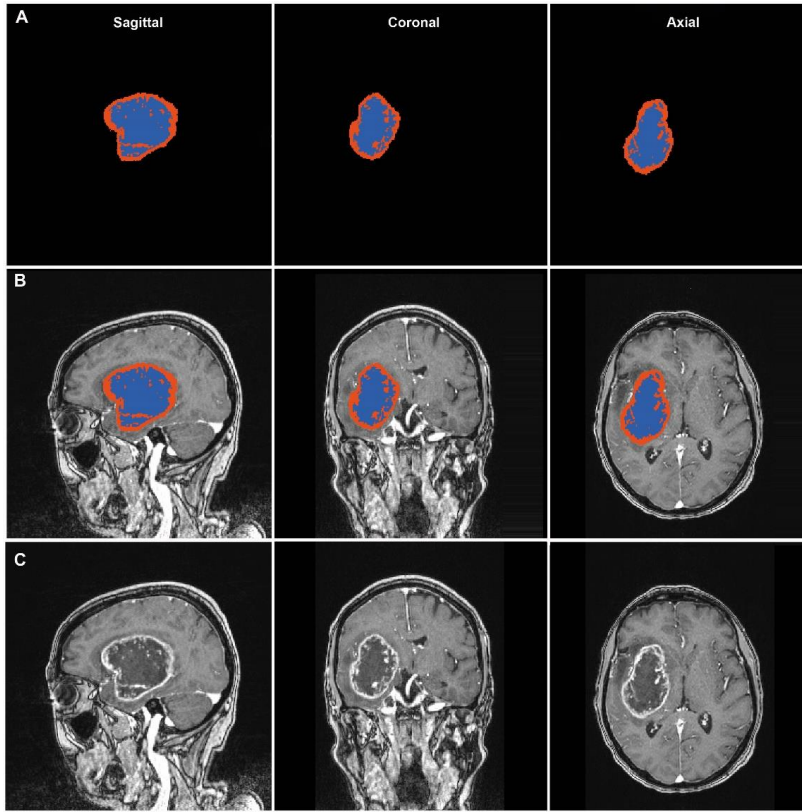


Figure 9. Manual segmentation of tumor volumes using the software BrainVoyager QX. The segmented contrast-enhancing compartment is marked in red, and the non-contrast-enhancing compartment (i.e. necrosis) in blue. Total tumor volume was the combined volume of both compartments. **Panel A** The segmented tumor area in all 3D planes. **Panel B** Segmented areas together with the original image. **Panel C** Original T1-weighted contrast-enhancing images. Picture courtesy of Anne Line Stensj en

Growth estimates

The Gompertzian growth pattern was therefore assumed to be the underlying pattern for all the tumors in the papers of this thesis. However, the establishment of growth estimates based on a Gompertzian growth pattern is challenging, because it assumes that the growth rate is progressively decreasing as the tumors grow larger. Hence, a point estimate of growth (such as volume doubling time) would be a wrong representation of tumor biology. This is because the same point estimate would not be comparable in tumors of different sizes. For instance, in two tumors with the same growth rate (volume doubling time) but of different sizes, the Gompertzian model implies that the largest tumor grows more aggressively than the smallest. To account for this issue, we calculated

an expected Gompertzian growth curve based on the volume data and time intervals from the 106 included patients (Figure 10). This fitted growth curve shows how the volume is expected to increase throughout the average glioblastoma's life. The observed volumes at the second MRI scans are also plotted relative to the curve. Their positions on the x-axis are determined by the volume of the first MRI scan and the time interval to the second MRI scan. In this way, the tumors with an observed volume increase that is larger than expected from the curve (i.e. a positive residual) were categorized as 'fast-growing', and tumors with a smaller increase than expected (i.e. a negative residual) were categorized as 'slow-growing' (Figure 10). This dichotomization into 'fast-growing' and 'slow-growing' tumors was used for analyses in all the papers of this thesis. The mathematical formula used for calculation of expected growth curve was developed by Chignola et al. (138). Moreover, we have previously investigated associations between the growth groups and clinical parameters (205). In the same study, we found that slower growth was a significant independent predictor of improved survival beyond 12 months of follow-up.

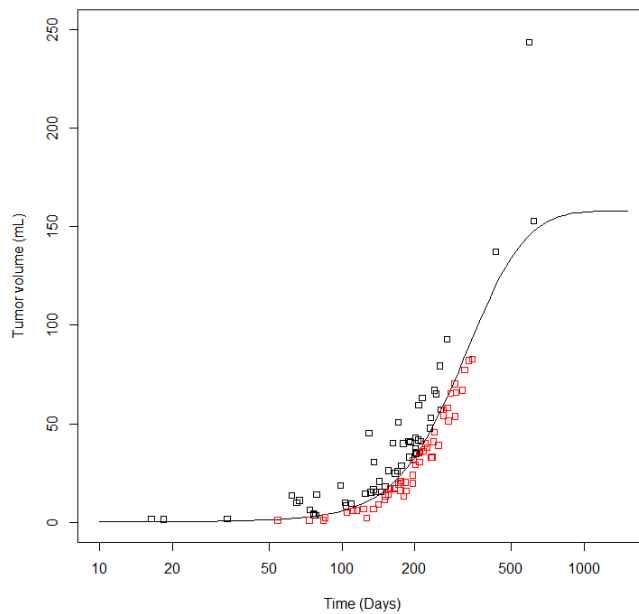


Figure 10: The expected Gompertzian growth curve based on the volume data and interval between the MRI scans from the 106 glioblastoma patients. The curve illustrates how the tumor volume is expected to increase throughout the average tumor's life span. The curve can be used to predict the future expected volume in tumors with one known volume. The squares are the observed tumor volumes from the second scans. The black squares are tumors with a larger volume increase than expected from the volume on the first scan (i.e. 'fast-growing'), while the red have smaller volume increases than expected (i.e. 'slow-growing'). The curve was drawn from an arbitrary volume of 0.135 mL at day 0. Illustration by Anne Line Stensj en

7.3 Histopathological features

In Paper I, we assembled all available HE sections in each patient from surgical resections (89 patients) and biopsies (17 patients) for the evaluation of histopathological features. We controlled that the sections were retrieved from the first surgical intervention. HE slides from both routine FFPE tissue and previously frozen FFPE tissue were collected. However, one patient had no sections from routine FFPE tissue, and 9 patients had no sections from FFPE frozen tissue.

The presence or degree of 27 different histopathological features were recorded in each case. The features were defined according to the 2007 WHO Classification (206) and Greenfield's Neuropathology (9th edition) (139). The features were first assessed by V.E.M. and controlled by S.H.T., and only conspicuous features were recorded to reduce observer variability. During the evaluation, the tissue material from each case was assessed for the presence of central tumor areas (i.e. solid tumor tissue and/or necrosis without the presence of any normal brain tissue), peripheral tumor (i.e. tumor cells intermingled with normal brain tissue), infiltration into grey matter (i.e. peripheral tumor tissue with neurons), and areas of infiltration into gray matter with present outer brain surface (i.e. present leptomeninges or, alternatively, cases containing \geq two of the following features: molecular cortical layer, corpora amylacea, or glia limitans) (Figure 11). In the following text, the 27 features and their definitions are presented.

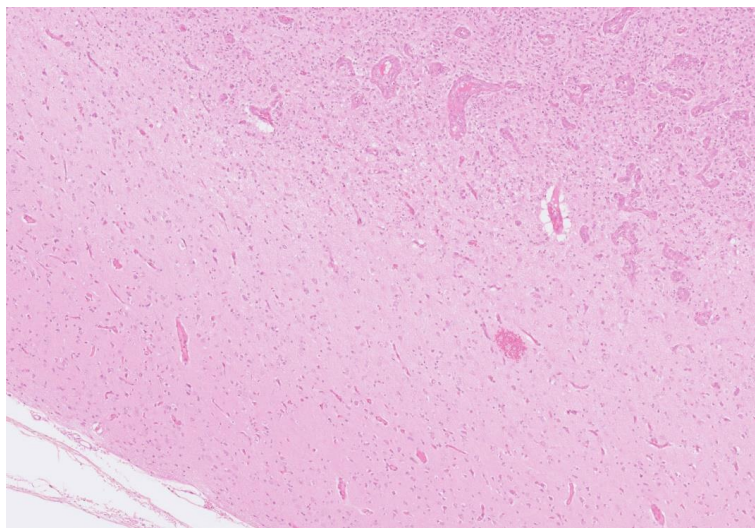


Figure 11. Infiltration zone into gray matter with outer brain surface. HE stain at x50 magnification. A gradual decrease in the cellular density illustrates the diffuse infiltration from a more central tumor area. Leptomeninges are seen in the lower left corner. Photo: Vilde E. Mikkelsen.

Necroses and perinecrotic palisades

Necrosis was defined as areas of cellular debris with absent or faded nuclei, often with remaining thrombotic and necrotic vessels (Figure 12). Necrotic areas were categorized as either large necrosis (ischemic tumor necrosis) (Figure 12A) or micronecrosis (small foci of necrosis, often with perinecrotic palisades) (Figure 12B). Palisades were defined as radially oriented, densely packed, small, fusiform glioma cell present at the rim of either large necroses or micronecroses (Figure 12B). Palisades were only assessed in in tumors with central tumor morphology.

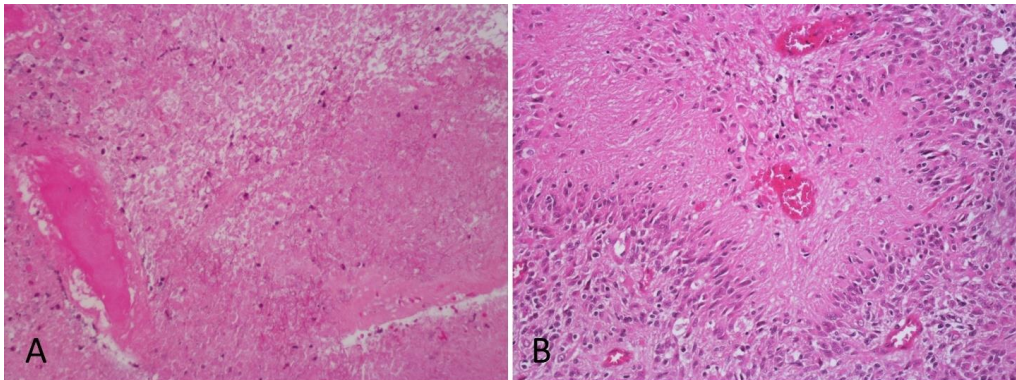


Figure 12. Necroses, HE stains at x200 magnification. **A** Large, ischemic necrosis with coagulative necrosis, cellular debris and faded nuclei. In the lower left-hand corner, a necrotic, dilated vessel occluded by a thrombus. **B** Micronecrosis with surrounding palisades. Radially oriented, accumulated cells form a serpiginous palisade around a small necrotic focus. Photos: Vilde E. Mikkelsen

Microvascular proliferation

Microvascular proliferation was defined as vascular structures with more than two layers of cells in the vascular wall (Figure 13). Vascular structures with connective tissue in the vascular walls were not registered. Glomeruloid tufts were also registered as microvascular proliferation. Moreover, microvascular proliferation was recorded as being present in either central tumor areas (Figure 13A) or in the infiltration zones into grey or white matter (Figure 13B).

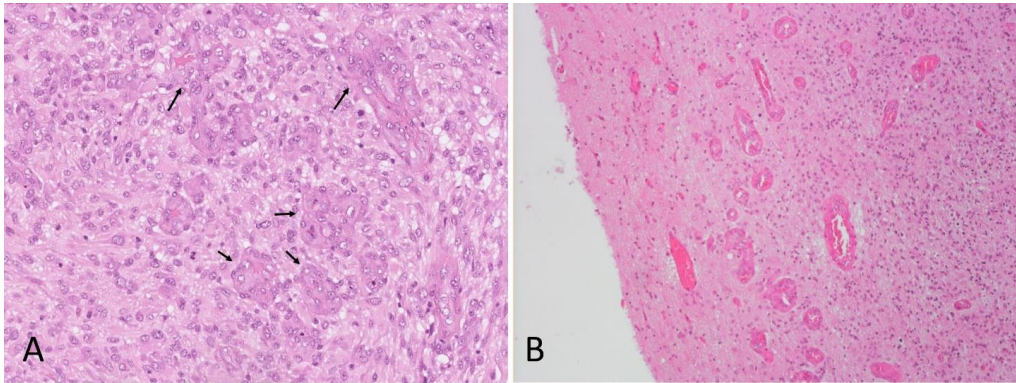


Figure 13. Microvascular proliferation. **A** Central microvascular proliferation. HE stain at x200 magnification. Arrows indicate microvascular proliferation structures in a central tumor area, which show a conspicuous multilayering of the vascular walls necessary for the categorization microvascular proliferation. **B** Peripheral microvascular proliferation. HE stain at x100 magnification. Microvascular proliferation seen in an infiltration zone. Photos: Vilde E. Mikkelsen

Cellular density

Cellular density was subjectively categorized as low, intermediate, or high (Figure 14). The categorization was based on the observed number of cells per area based on all viable tumor material. Cellular density was assessed in central tumor areas when present.

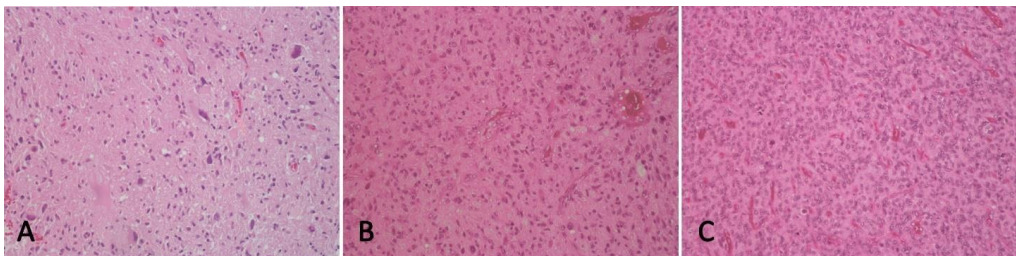


Figure 14. Cellular density, HE stains at x200 magnification. **A** Low cellular density. **B** Moderate cellular density. **C** High cellular density. Photos: Vilde E. Mikkelsen

Atypia

Atypia was subjectively categorized as mild, moderate, or severe (Figure 15). The categorization was based on the degree of variability of cellular and nuclear shapes and sizes.

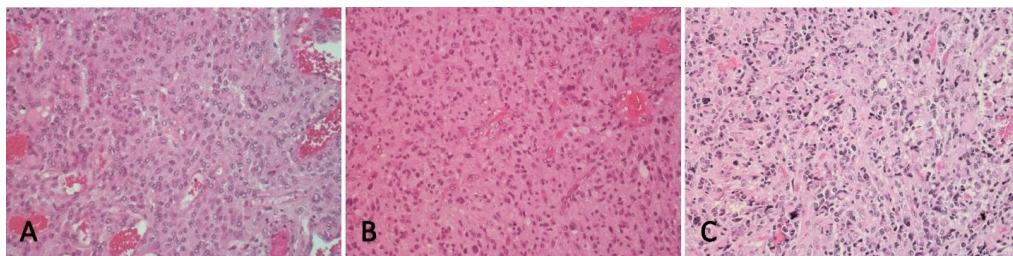


Figure 15. Atypia, HE stains at x200 magnification. **A** Mild atypia. **B** Moderate atypia. **C** Severe atypia. Photos: Vilde E. Mikkelsen

Mitotic count

Mitotic figures were counted using a Nikon DS-Fi2 microscope in 10 high power fields (HPFs) at x400 magnification in areas of the highest density of mitotic figures (i.e. hotspots) (Figure 16A). Hotspots were typically found in HPFs in central tumor tissue with higher cellular densities. Mitotic figures of vascular cells and leukocytes were not counted. The counting was preferably performed in sections from FFPE tissue that had not previously been frozen. In addition, cases with low quality of the nuclear morphology were not assessed.

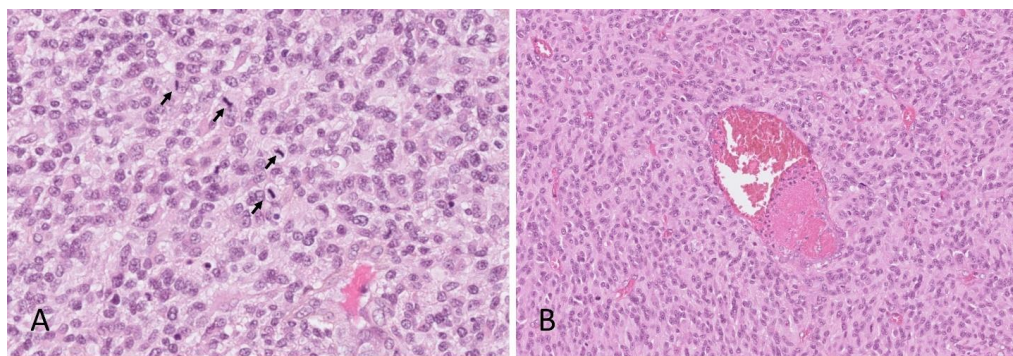


Figure 16. **A** Mitotic figures. HE stain at x400 magnification. Arrows highlight mitotic figures in an area with small cell differentiation. Most of the mitotic figures are in the metaphase of the mitosis. **B** Thrombosis. HE stain at x200 magnification. A partly occluded vessel with fibrin and adhered leukocytes. Photos: Vilde E. Mikkelsen

Thromboses

Thromboses were defined as vascular structures having their lumen partly or completely occluded with fibrin that adhered to the vascular wall (Figure 16B). Thromboses in both viable and necrotic areas were recorded.

Hemorrhages

Hemorrhages were defined as the presence of abundant extravascular erythrocytes and fibrin, often with perivascular neutrophils, damaged vascular walls, or cellular debris (Figure 17A). The mere presence of hemosiderin-containing macrophages was also sufficient for the categorization. The presence of extravascular erythrocytes alone did not satisfy the criteria, as their presence could have been caused by the surgical intervention.

Pseudorosettes

Pseudorosettes were defined as the presence of ordered perivascular tumor cells surrounding smaller vessels with sparse amount of vascular connective tissue with a distinct anucleate perivascular area (Figure 17B). Pseudorosettes could only be assessed in viable, central tumor areas, and not in sections from FFPE frozen tissue.

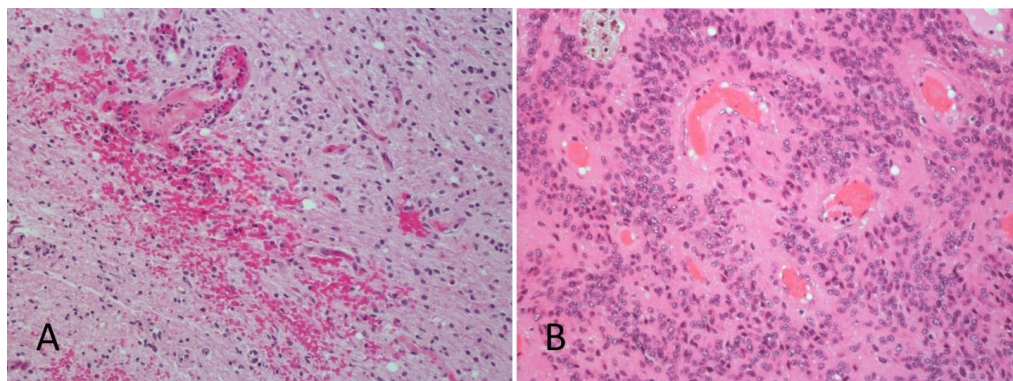


Figure 17. Vascular features, HE stains at x200 magnification. **A** Hemorrhage. Extravascular erythrocytes and neutrophilic granulocytes suggest a non-iatrogenic hemorrhage. **B** Pseudorosettes. Characteristic pseudorosettes with perivascular anucleated areas, a typical feature seen in ependymomas (2). Photos: Vilde E. Mikkelsen

Vascular density

The vascular density was subjectively categorized as low, intermediate, or high (Figure 18). The categorization was based on the mean distances between separate blood vessels in all the viable tumor material.

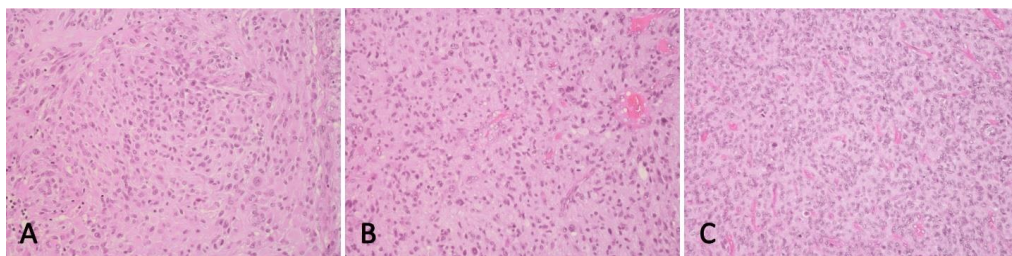


Figure 18. Vascular density, HE stains at x200 magnification. **A** Low vascular density. **B** Moderate vascular density. **C** High vascular density. Photos: Vilde E. Mikkelsen

Secondary structures of Scherer

The secondary structures of Scherer were only assessed in cases containing infiltration zones into gray matter. Perineuronal satellitosis was recorded when distinct tumor cells surrounded neurons (Figure 19A). Angiocentric structures were defined as neoplastic cells located adjacent to capillaries or smaller vessels (Figure 19B). Subpial clustering was only assessed in cases with present outer brain surface in the infiltration zone, and it was defined as densely packed neoplastic cells just below the meninges (Figure 19C).

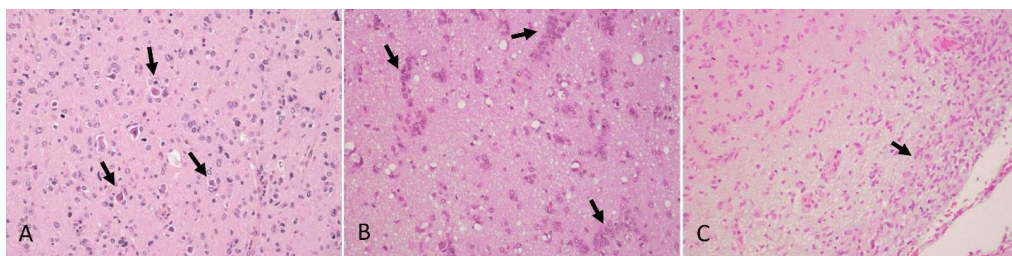


Figure 19. Secondary structures of Scherer, HE stains at x200 magnification. **A** Perineuronal satellitosis. Arrows indicate tumor cells surrounding neurons in an infiltration zone into grey matter. **B** Angiocentric structures. Arrows indicate perivascular accumulation of neoplastic cells in an infiltration zone into grey matter. **C** Subpial clustering. Accumulated neoplastic cells are seen beneath the leptomeningeal layer in the lower right-hand corner. The higher cellularity beneath the leptomeninges relative to the deeper parts of the cortex illustrates the preferred subpial path of neoplastic migration. Photos: Sverre H. Torp (A) and Vilde E. Mikkelsen

Desmoplasia

Desmoplasia was defined as distinct fibrovascular tissue and collagen deposits (Figure 20). Desmoplasia was distinguished from vascular structures with abundant connective tissue walls and leptomeningeal infiltration (i.e. it was not recorded in the presence of leptomeninges).

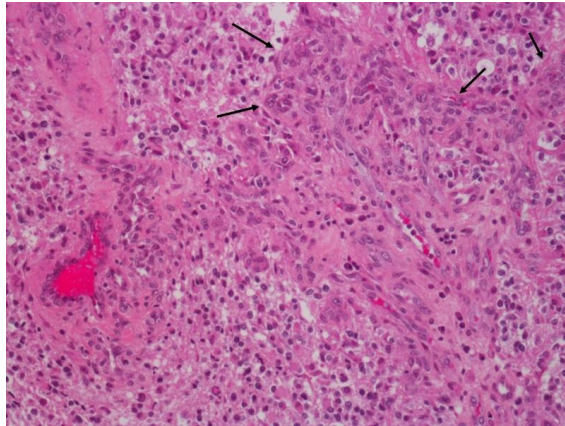


Figure 20. Desmoplasia. HE stain at x200 magnification. Arrows indicate vascular proliferations associated with a typical fibrovascular structure. Photo: Vilde E. Mikkelsen

Leukocytes

Two types of leukocytes were recorded: macrophages and lymphocytes. Macrophages were defined as large cells with a round contour, eccentric nuclei, and a spongy and sharply demarcated cytoplasm (Figure 21A). Sometimes, they were filled with hemosiderin from previous hemorrhages. Macrophages were often observed in the periphery of large necrotic areas. Lymphocytes were defined as the accumulation of small cells with a high nucleocytoplasmic ratio and a hyperchromatic and sometimes angular nuclei (Figure 21B). Lymphocytes were only recorded when found as larger infiltrates in viable tumor tissue or as perivascular infiltrates.

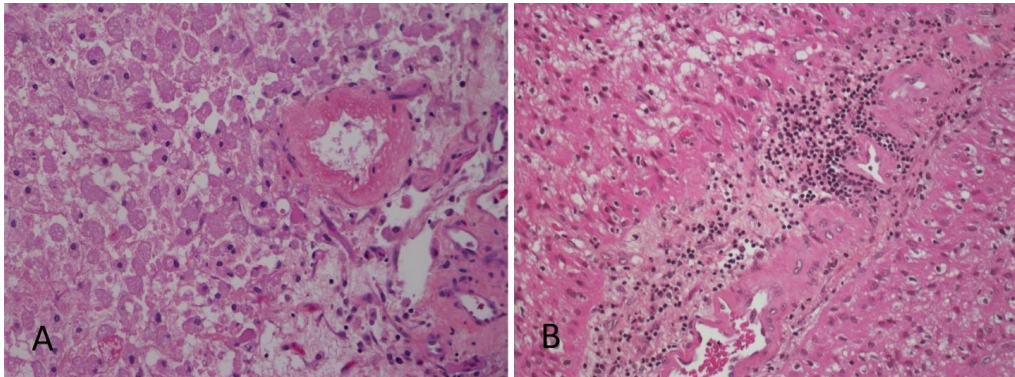


Figure 21. Leukocytes, HE stains at x200 magnification. **A** Macrophages. Multiple spongy macrophages with large, sharply demarcated cytoplasm and eccentric nuclei, seen in a necrotic area. **B** Perivascular lymphocytes. Small, hyperchromatic lymphocytes accumulated around vessels in a fibrovascular structure. Photos: Sverre H. Torp (A) and Vilde E. Mikkelsen (B)

Glioblastoma subtypes

In the 2007 WHO Classification, two established glioblastoma variants were defined: giant cell glioblastomas and gliosarcomas (141). Giant cell glioblastomas were defined as tumors dominated by multinucleated, bizarre giant cells (Figure 22A). Gliosarcomas were defined as tumors showing a biphasic pattern with a sarcomatous and a gliomatous component; the sarcomatous component was composed of neoplastic spindle cells (Figure 23D) and was clearly demarcated from the glial component (Figure 22B) and negatively stained for GFAP. Although not an established variant in the WHO Classifications, small cell glioblastoma is a well-recognized subset of glioblastoma with predominant small cells (2, 141). In this study, small cell glioblastomas were defined as tumors where the viable tumor tissue contained >75% small cells (round to slightly elongated monomorphic cells with high nucleocytoplasmic ratios, mildly hyperchromatic nuclei, often with frequent mitotic figures) (Figure 23A).

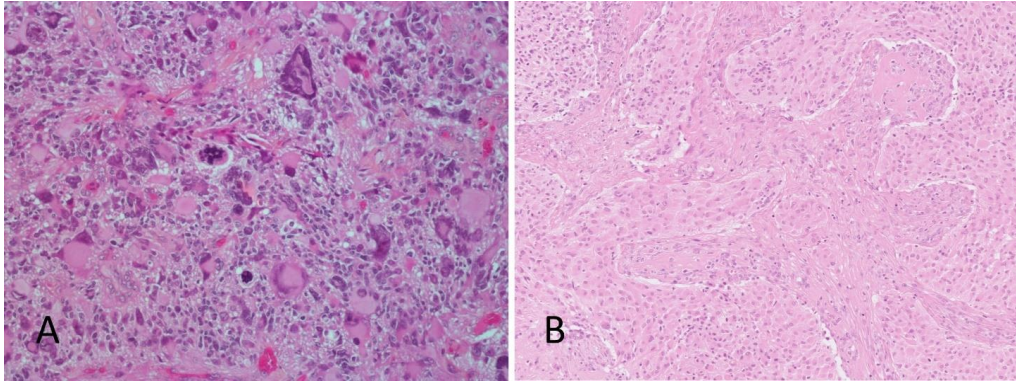


Figure 22. Glioblastoma subtypes. **A** Giant cell glioblastoma. HE stain at x200 magnification. Multiple bizarre and multinucleated giant cells. **B** Gliosarcoma. HE stain at x100 magnification. The characteristic, sharply demarcated biphasic pattern of gliosarcoma, with a gliomatous and sarcomatous component. Photos: Vilde E. Mikkelsen

Cellular patterns

Seven different cellular patterns recognized in glioblastoma were recorded. Small cells were defined as above (Figure 23A), and the presence of <75% small cells was defined as a cellular pattern. Gemistocytes were defined as tumor cells with large, glassy eosinophilic cytoplasm and eccentric nuclei (Figure 23B). Tumors with myxomatoid components showed a loosely woven tissue with elongated cells surrounded by a mucinous extracellular substance (Figure 23C). Sarcomatous cells were defined as the spindle shaped cells, sometimes with nuclear atypia (Figure 23D), as seen in gliosarcomas. Giant cells were defined as described for giant cell glioblastomas (Figure 22A); however, when focally present, they were recorded as cellular pattern. Tumors with primitive neuronal components showed sharply demarcated, densely packed small, hyperchromatic cells with high nucleocytoplasmic ratio that lack distinctive architectural or cytological features (undifferentiated) (Figure 23E). Tumors with oligodendroglial components displayed small, monotonous, hyperchromatic cells with perinuclear haloes, often with associated chicken wire vasculature and/or microcalcifications (Figure 23F).

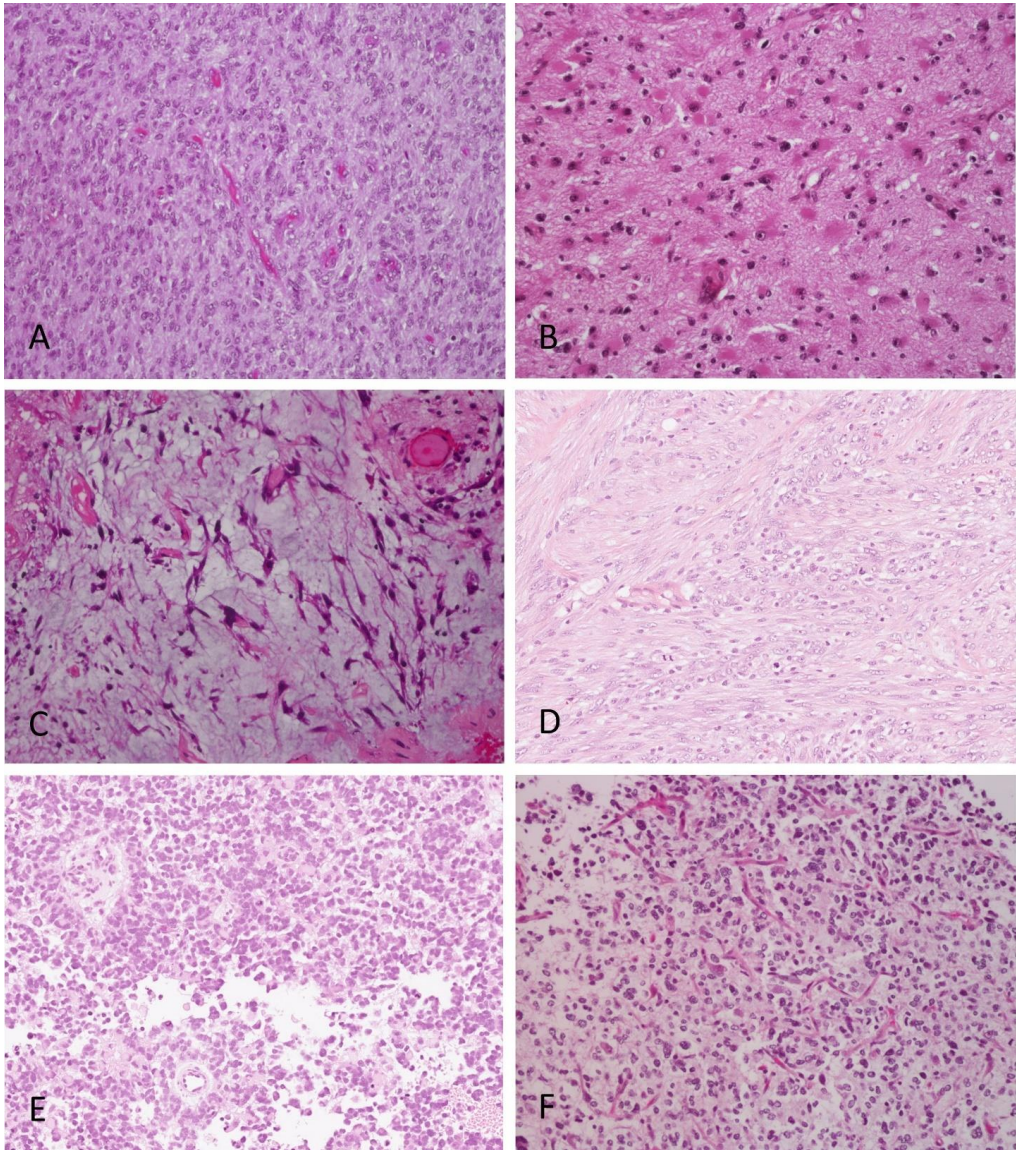


Figure 23. Cellular patterns, HE stains at x200 magnification. **A** Small cells. Typical small cells with round to oval, mildly hyperchromatic nuclei and high nucleocytoplasmic ratios. **B** Gemistocytes. Large, eosinophilic cytoplasm, eccentric nuclei. **C** Myxomatoid component. Loosely woven tissue with elongated cells and extensive mucinous extracellular substance. **D** Sarcomatous cells. Neoplastic spindle cells forming bundles. **E** Primitive neuronal component. Undifferentiated, densely packed small, hyperchromatic cells, with high nucleocytoplasmic ratios. **F** Oligodendroglial component. Small, monotonous, oligodendroglial cells with high nucleocytoplasmic ratios and perinuclear haloes. Characteristic chickenwire vasculature can also be seen. Photos Vilde E. Mikkelsen and Sverre H. Torp (C)

7.4 Immunohistochemistry

The most representative FFPE tissue block was selected for IHC analyses based on an assessment of all available HE slides in each patient. The most representative HE section should preferably show both central tumor areas and infiltration zones. In cases showing only one of these areas, the tissue block with central tumor was selected. In cases of multiple sections with representative morphology, tissue blocks with less hemorrhages and less blood cell infiltrates were preferred. All cases were checked up in the pathology database SymPathy (Tieto, Sweden) and results from previous IHC analyses retrieved. In cases with previously performed IHC, the previously used FFPE block was preferred. In some cases, the preferred FFPE tissue block was unavailable due to overlapping research projects. In such cases, FFPE from frozen tissue was often used for IHC instead. Altogether, 12 cases (11%) had IHC analyses performed on sections from FFPE blocks of previously frozen tissue. The selected FFPE tissue blocks were cut at 4µm, pretreated, and stained according to Table 1.

All immunohistochemical analyses except for CD105 were carried out on a Dako Autostainer (Dako Denmark AS, Glostrup, Denmark). For GFAP, IDH1, and Ki-67/MIB-1, the IHC analyses were previously performed in 40 cases (38%), 18 cases (17%), and 44 cases (42%), respectively. The antibodies used for the previously performed IHC stains were the same as reported in Table 1. The only difference was the dilution of 1:10000 and 1:800 for the cases previously stained for GFAP and Ki-67/MIB-1, respectively. In Paper II, all cases were stained for vWF and CD105 as described in Table 1. For the endothelial markers, a glioblastoma FFPE tissue block with extensive vascularity, present necrosis and hemorrhages was used for titration of the optimal antibody dilutions. In all the IHC analyses, both positive and negative controls were included. In the negative controls, we used the same tissue as for the positive controls but with omitted primary antibodies (Table 1).

Table 1. Antibodies and IHC procedures

Antibodies	GFAP	IDH1	vWF	CD105	Ki-67/MIB-1
Type	Rabbit, polyclonal	Mouse, monoclonal	Rabbit, polyclonal	Mouse, monoclonal	Mouse, monoclonal
Source and code number	Dako, Glostrup, Denmark Z0334	Dianova, Hamburg, Germany R123H/DIA- H09	Dako, Glostrup, Denmark A0082	Dako, Glostrup, Denmark M3527	Dako, Glostrup, Denmark M7240
Clone		H09		SN6h	MIB-1
Pretreatment in PT Link*	pH 9	pH 9	pH 6	None	pH 6
Additional pretreatment	None	None	None	Proteinase K	None
Dilution	1:2000	1:100	1:2000	1:50	1:50
Antibody incubation time	40 min room temperature	40 min room temperature	40 min room temperature	Overnight incubation 4°C	40 min room temperature
Detection system	EnVision Rabbit-HRP	EnVision Mouse-HRP	EnVision Rabbit-HRP	LSAB-HRP	EnVision Rabbit-HRP
Chromogene	DAB	DAB	DAB	DAB	DAB
Positive control	Medulloblast oma and gliosis	Oligodendro glioma WHO grade II	Glioblastoma and tonsil	Glioblastoma	Medulloblast oma

*PT Link is a pretreatment module for tissue specimens which allows the pretreatment processes of deparaffination, rehydration, and heat induced antigen retrieval (HIER). DAB 3,3'-Diaminobenzidine, HRP Horseradish peroxidase, LSAB Labeled Streptavidin Biotin. Table courtesy of Unn Sophie Granli

7.4.1 Microvessel density measurements

In Paper II, the degree of vascularity on vWF and CD105 stained sections was assessed using microvessel density (MVD) measurements (Figure 24). V.E.M. performed the MVD assessments without knowledge of the growth data. MVD was assessed according to the method described by

Weidner et al. (207) with modifications. MVD was quantified as the mean number of vascular units in hotspots for three HPFs at x400 magnification using an ocular grid (Nikon CFI 10x/22) and a Nikon Eclipse 80i microscope (area within the grid equal to 0.059mm²). A vascular unit was defined as any individually stained endothelial cell or vessel within or in contact with the grid. Only positive cells with an endothelial morphology were counted. In cases of long, branched vessels and glomeruloid tufts, each lumen was counted as described by Kraby et al. (208). In addition, separate units of \geq two staining endothelial cells within the same vascular structure were counted as one vascular unit. Areas with glomeruloid tufting were rarely regarded as hotspots.

Hotspots were identified using x40 and x100 magnification on vWF sections, and corresponding hotspots were identified on CD105 sections. Only HPFs with >50% of viable tumor tissue were selected and tissue edges were avoided. HE sections were assessed to control that the selected hotspots were not in necrotic, desmoplastic, or infiltrating tumor areas. However, HPFs close to necrosis and in infiltration zones dominated by tumor cells were counted if it was the only hotspot. In cases with higher background staining, the morphological requirements for what was regarded a vascular unit were stricter. In cases with sparse amount of viable tumor tissue, three HPFs were counted regardless of the degree of vascularity, but no overlapping HPFs were counted. Of the 102 assessed cases, one case was not assessed for vWF-MVD due to a high background staining, and another case was not evaluated for CD105-MVD due to non-existent antigenicity.

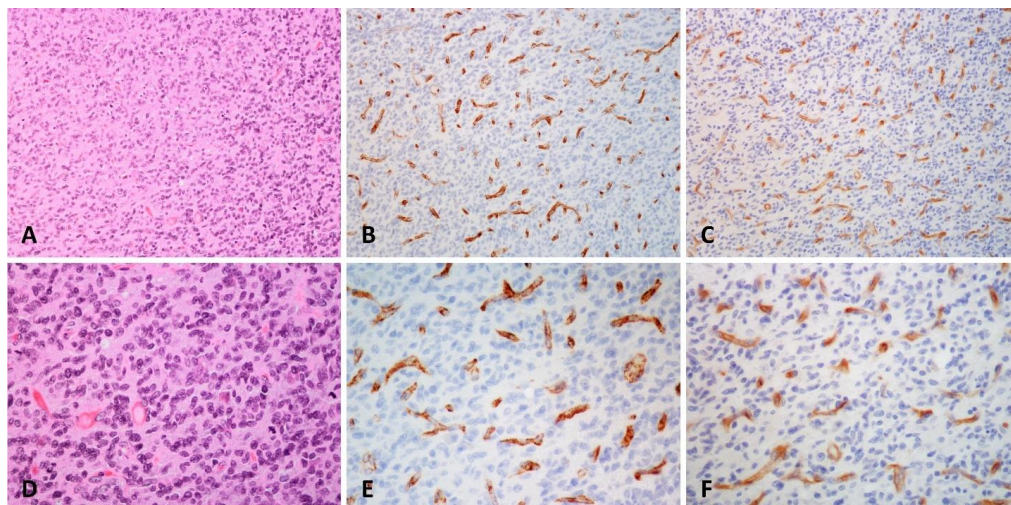


Figure 24. Endothelial immunohistochemical markers. Pictures taken from the same tumor in corresponding areas. **A-C** x200 magnification. **D-E** x400 magnification. **A and D** HE stain. **B and E** vWF. **C and F** CD105. Photos: Vilde E. Mikkelsen

7.4.2 Proliferative activity

The Ki-67/MIB-1 proliferative index (PI) had previously been quantified as a part of our paper investigating radiological growth and survival (205). The PI data was included in Paper III. The Ki-67/MIB-1 PI was calculated as a percentage of distinct immune-positive tumor cell nuclei for three HPFs (x400 magnification) in hotspots using an eye-piece grid (Figure 25). Cells resembling endothelial cells, lymphocytes, macrophages, or fibroblasts were not counted. Tissue edges were avoided due to the risk of unspecific staining.

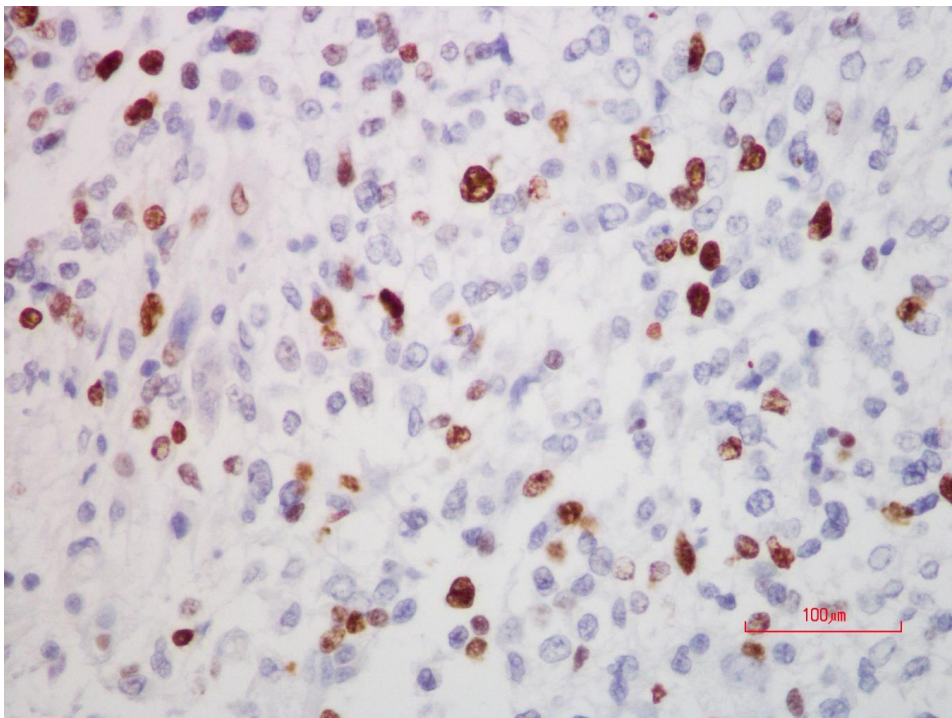


Figure 25. Immunohistochemical Ki-67/MIB-1 staining in a glioblastoma at x400 magnification. Nuclear staining of proliferating cells. The PI of this tumor was 15.4 %, which is considered to be moderate. Photo: Vilde E. Mikkelsen

7.5 Molecular techniques

7.5.1 Methylation specific PCR

In Paper III, all 106 patients from Paper I were assessed for *MGMT* promoter methylation status using methylation specific PCR (MSP). We used the conventional gel-based MSP technique based on the methods described by Esteller et al. (96).

DNA extraction

To analyze the methylation status of the CpGs of the *MGMT* promoter, tumor DNA was first isolated from the FFPE tissue blocks. Representative HE sections from FFPE blocks were analyzed under the microscope by V.E.M., and areas with visually 100% tumor cell content were manually marked on the tissue slide and selected for DNA isolation. Necrotic areas, hemorrhages, and infiltration zones were avoided. However, it was not always possible to avoid small necrotic foci, and incipient necrosis can be hard to determine on HE slides. Moreover, in 4 cases, DNA was isolated from infiltration zones due to sparse amounts of material. In these cases, the tumor cell content was visually estimated to be 40% for one case, 60% for two cases, and 70% for one case. In 16 cases, DNA was isolated from FFPE blocks from previously frozen tissue. Moreover, the marked areas on the HE slides were manually dissected from the FFPE blocks, and the DNA was isolated using the QIAamp DNA FFPE Tissue Kit (Qiagen, Hilden, Germany). A QIAcube (Qiagen) device was used for automated DNA purification. After the DNA isolation, the DNA concentrations were measured using a Qubit Fluorometer (Invitrogen).

Bisulfite conversion

The isolated DNA was treated with the EpiTect Fast Bisulfite Conversion kit (Qiagen) to convert unmethylated cytosines to uracil. The conversion enables the discrimination of methylated from unmethylated DNA. If the DNA concentration was <40 ng/mL, two samples from each case were treated with bisulfite. In addition, a known *MGMT* methylated sample (i.e. a positive control) was treated with bisulfite and included in the following steps. The bisulfite solution and a DNA protect buffer with a pH indicator were added before thermal cycling to optimize cytosine conversion. The product was purified in a series of steps to reduce bisulfite salts and chemicals that might inhibit the PCR. DNA concentrations were measured after the bisulfite treatment.

PCR

The next step was to amplify the bisulfite treated DNA with PCR. We used a 25µL PCR protocol with *MGMT* methylated and unmethylated specific primers (CpG sites 74-78) as used by Esteller et al. (96). The primers covered the *MGMT* promoter and exon 1 region and had the following sequences: methylated primers (81bp) 5'-TTTCGACGTTTCGTAGGTTTTTCGC-3' and 5'-GCACTCTTCCGAAAACGAAACG-3', and unmethylated primers (93bp) 5'-TTTGTGTTTTTGATGTTTGTAGGTTTTTGT-3' and 5'-AACTCCACACTCTTCCAAAAACAAAACA-3'. Two samples

from each patient were therefore run through the PCR: one with the methylated primers and one with the unmethylated primers. In addition to the positive control from the bisulfite treatment, an extra positive control sample (which was methylated on the previous PCR run), a negative control (unmethylated), and a blind control (water sample) were included in the PCR and the following gel-electrophoresis (Figure 26).

Gel-electrophoresis

For detection on the gel-electrophoresis, 10 μ L PCR product was loaded onto E-gel 4% agarose gel (Invitrogen) for 20 minutes. An experienced molecular biologist (H.Y.D.), who was blinded to the clinical data, interpreted the gel-electrophoresis and determined the *MGMT* methylation status. Cases with both methylated and unmethylated bands were categorized as *MGMT* methylated, because normal cells are mostly unmethylated (10, 94, 95). Cases with only an unmethylated band were determined as *MGMT* unmethylated. Cases showing only a weak unmethylated band were categorized as inconclusive and were repeated.



Figure 26. Detection of the *MGMT* status using gel-electrophoresis during the MSP analyses. There were two samples from each patient or control: one sample with methylated primers (M) and the other sample with unmethylated (UM) primers. All samples show an unmethylated band because there will always be some normal cells in the sample. Hence, it is the presence of a methylated band that determines if a sample is methylated or not. In this example, case 1, 2, and 5 were *MGMT* methylated, and case 3 and 4 were *MGMT* unmethylated. 'pos 1' was the positive control from the bisulfite treatment, and 'pos 2' was the positive control from a previous PCR and gel-run, 'NEG' was the unmethylated control, and 'Blank' was a water sample to control for unspecific binding.

7.5.2 Sanger sequencing of *IDH* mutation status

Of the 106 patients included in Paper I, 21 were <55 years and immunonegative on IHC for the *IDH1* R132H mutation. In Paper III, these 21 patients were therefore additionally sequenced using Sanger sequencing for the mutation status of codon 132 of *IDH1* and codon 172 of *IDH2*. DNA isolation was performed in the same manner as described for the MSP assay. A 25µL PCR protocol was also used, with the primers for *IDH1* ex4 (129bp) 5'-CGGTCTTCAGAGAAGCCATT-3' and 5'-GCAAAATCACATTATTGCCAAC-3', and for *IDH2* ex6 (236bp) 5'-GCTGCAGTGGGACC ACTATT-3' and 5'-GTGCCCAGGTCAGTGGAT-3'. Also, a universal primer pair 5'-CACGAC GTTGTAACACGAC-3' and 5'-CAGGAAACAGCTATGACC- 3' was attached to the *IDH1* and *IDH2* primers, respectively. For sequencing, the BigDye Terminator v3.1 cycle sequencing kit and the 3130 genetic analyzer (Applied Biosystems, Foster City, CA) were used. The sequence chromatogram was interpreted by H.Y.D. who was blinded to other data.

7.6 Clinical variables

The clinical variables age, sex, performance status, treatment, and overall survival were collected in our previous publication (205). The data were mostly recorded from a prospectively collected research database. However, in 25 patients, the Karnofsky performance status (KPS) was estimated after retrospective review of hospital records. Patients were categorized as having a GTR (i.e. complete resection) when the residual volume was calculated to be <0.175mL on the postoperative MRI control (using an ellipsoid formula) (209). Patients that were categorized as temozolomide treated had received temozolomide within the first 6 months after surgery, and radiotherapy treated had received radiotherapy in any regime during follow-up. Patients who received corticosteroids before surgery were categorized as corticosteroid treated. Overall survival was defined as the time from the first operation to death of the patient. The end of follow up was 24.5 months after the surgery of the last included patient (June 2016). Patients alive at the end of follow-up were censored.

7.7 Statistical analyses

The computation of the expected Gompertzian growth curve was performed by A.L.S. and Ø.S. using R version 2.13.1 (R Foundation for Statistical Computing, Vienna, Austria). The remaining statistical analyses were performed using IBM SPSS Statistics version 21 (Paper I) and version 24 (Paper II) (IBM Corp., Armonk, New Jersey, USA), and in Paper III using Stata (version 16,

StataCorp LLC, College Station, TX). The significance limit was set to $p < 0.05$ without corrections for multiple testing in any of the papers.

In Paper I, the presence of the 27 histopathological features was assessed for associations with faster tumor growth using univariable and multivariable binary logistic regression analyses. Before conduction of the statistical analyses, the three ordinal variables (cellular density, atypia, and vascular density) were dichotomized by merging the two lowest categories, because few cases were assigned to the lowest of these. The histopathological features that were significantly associated in the univariable analyses were included in the multivariable analysis. The multivariable model with the highest number of significant independent predictors was selected. We also examined associations between the features that were significantly associated in the univariable analyses using Chi Square (categorical vs categorical variables) and Mann-Whitney U (continuous vs categorical variables) tests.

In Paper II, we first assessed the correlation between vWF-MVD and CD105-MVD using the Spearman rank correlation test. Then, we assessed associations between both MVDs and histopathological features using Mann-Whitney U tests (categorical vs continuous variables) and Spearman rank correlation tests (continuous vs continuous variables). The included histopathological features in Paper II were the features in Paper I that significantly associated with growth in the univariable analyses and the subjectively assessed vascular densities on HE slides. Furthermore, vWF-MVD and CD105-MVD were investigated for univariable associations with fast-growing tumors using Mann-Whitney U tests. The significantly associated MVD in the univariable analyses was further included in a multivariable binary logistic regression analysis with the significantly associated histopathological features in the univariable analyses from Paper I. However, mitotic count was not included in the multivariable model due to significant associations with all other features included.

In Paper III, *MGMT* status was assessed for associations with 22 histopathological features, CD105-MVD, Ki-67/MIB-1 PI, MRI characteristics at the second scan, speed of tumor growth, overall survival, and clinical factors. Associations between *MGMT* status and categorical variables were assessed using Chi square/Fisher's exact tests, and associations with continuous variables were assessed using Mann-Whitney U analyses. For the survival analyses, we used a Kaplan-Meier plot and the Log-Rank test for the univariable analysis and a Cox proportional hazard model for the multivariable analysis. The selection of variables in the multivariable model has previously

been accounted for (205). The proportional hazard assumption was tested using Schoenfeld residuals.

7.8 Ethics

The study was approved by the Regional Ethics Committee (Central) as part of a larger project (references 2011/974 and 2013/1348) and adhered with the Declaration of Helsinki. Most patients had provided informed consent to be included in a related glioma outcome study (reference 2011/974). The regional ethics committee waived informed consent for retrospective evaluation of patient data for the remaining patients.

8 Summary of papers

8.1 Paper I

Histopathologic Features in Relation to Pretreatment Tumor Growth in Patients with Glioblastoma

Mikkelsen VE, Stensjøen AL, Erik Magnus Berntsen EM, Nordrum IS, Salvesen Ø, Solheim O, Torp SH.

World Neurosurgery, 109, e50-e58, 2018

The aim of the study was to explore if the presence of 27 histopathological features could explain the observed variation in speed of preoperative tumor growth in glioblastoma patients.

In the 106 included patients, speed tumor growth was estimated from segmented tumor volumes at two preoperative MRI scans and the interval between them. A fitted Gompertzian growth curve based on the volume data was used to dichotomize the tumors into two groups: faster or slower tumor growth than expected from the initial volume. These two groups were assessed for associations with the presence of the histopathological features using univariable and multivariable logistic regression analyses.

In the univariable analyses, high cellular density (odds ratio (OR) 3.05, $p=0.013$), thromboses (OR 4.40, $p=0.015$), and mitotic count (OR 1.03, $p=0.026$) were significantly associated with faster than expected tumor growth. In the multivariable model, both high cellular density (OR 2.98, 95% confidence interval (CI) 1.2-7.4, $p=0.018$) and thromboses (OR 4.3, 95% CI 1.3-14.5, $p=0.019$) were significant independent predictors of faster tumor growth when corrected for each other. Mitotic count was not significant in the multivariable models and was not included in the final multivariable model.

To investigate why mitotic counts did not reach statistical significance in the multivariable models, we examined associations between the three significant features in the univariable analyses. Thromboses and cellular density were not significantly associated (Chi-square test, $p=0.419$). However, increasing mitotic counts were significantly associated with both high cellular density (Mann-Whitney U test, $p<0.001$) and with the presence of thromboses (Mann-Whitney U test, $p=0.006$).

8.2 Paper II

Angiogenesis and radiological tumor growth in patients with glioblastoma

Mikkelsen VM, Stensjøen AL, Granli US, Berntsen EM, Salvesen Ø, Solheim O, Torp SH.

BMC Cancer, 18, 862, 2018

In this paper, we aimed to assess if the degree of angiogenesis was associated with preoperative radiological speed of tumor growth.

Radiological tumor growth was estimated in the same manner as in Paper I, using the Gompertzian growth curve to dichotomize the patients into ‘fast-growing’ and ‘slow-growing’ tumors. In the 102 included patients, MVD counts of the IHC markers vWF (a pan-endothelial marker) and CD105 (marker of proliferating endothelial cells) were assessed. The MVDs were assessed for univariable and multivariable associations with ‘fast-growing’ tumors using Mann-Whitney U tests and a binary logistic regression analysis, respectively.

In the descriptive analyses, the median vWF-MVD was 15.5 per field (range, 0.7-62.0) and median CD105-MVD was 12.7 (range, 0.7-50.0). vWF-MVD and CD105-MVD were significantly correlated ($\rho=0.92$, $p<0.001$). Before the analyses of the MVDs in relation to growth, both MVDs were assessed for associations with high cellular density, thromboses, mitotic count, and high vascular density. Here, higher mitotic counts and high vascular density were significantly associated with both MVDs (CD105-MVD $p=0.001$ and $p=0.004$, respectively; vWF-MVD $p=0.004$ and $p=0.016$, respectively). Despite being non-significant associations, there was a tendency towards higher CD105-MVDs in cases with present thromboses or high cellular density. A similar tendency was observed for vWF-MVD and thromboses.

Only CD105-MVD was significantly associated with faster growth in the univariable analyses ($p=0.049$), but it explained only 3% of the variance in speed of growth. CD105-MVD was no longer significant when corrected for the presence of thromboses and high cellular density in a multivariable model. In this model, thromboses (OR 4.2, 95% CI 1.2-14.3, $p=0.021$) and high cellular density (OR 2.6, 95% CI 1.0-6.5, $p=0.048$) were significant independent predictors of faster growth.

8.3 Paper III

MGMT Promoter Methylation Status Is Not Related to Histological or Radiological Features in IDH Wild-type Glioblastomas

Mikkelsen VM, Dai HY, Stensj en AL, Berntsen EM, Salvesen  , Solheim O, Torp SH.

J Neuropathol Exp Neurol, 79, 855-862, 2020

The aim of this paper was to investigate if *MGMT* promoter methylation status was associated with pretreatment phenotypic tumor biology of human *IDH* wt glioblastomas.

The *MGMT* status was determined by methylation-specific PCR in 85 *IDH* wt glioblastomas. The *MGMT* status was assessed for associations with the following biological features: 22 histopathological features, Ki-67/MIB-1 PI, CD105-MVD, conventional MRI characteristics, and preoperative speed of tumor growth (Chi square/Fisher's exact tests and Mann-Whitney U analyses). *MGMT* status was also assessed for associations with clinical factors and overall survival.

None of the investigated histological or radiological features were significantly associated with *MGMT* status. Methylated *MGMT* status was significantly associated with survival in the univariable analysis ($p=0.048$, Log-Rank test). Methylated *MGMT* status was also a significant independent predictor of improved overall survival (hazard ratio 0.60, 95% CI 0.37-0.97, $p=0.038$, Cox proportional hazard model) when adjusted for age, KPS, preoperative tumor volume, complete resection, chemotherapy, and radiation. *MGMT* status was not significantly associated with any of the clinical variables.

9 Discussion

Glioblastomas are known for being highly malignant, extremely heterogenous, and fast-growing tumors. Interestingly, despite extensive research on tumor biology and experimental treatments, the patient outcomes have not been significantly improved and the standard treatment-regime has not been altered the past 15 years (3). However, there is still hope that insights into the biology can improve patient care through the use of biomarkers to guide clinical management or the discovery of new targets of therapy. In this thesis, we have aimed to increase the understanding of the natural biology of human glioblastomas by investigating if biological features in tumor tissue and at MRI scans acquired before treatment were related to tumor growth or *MGMT* status.

9.1 Main findings

9.1.1 Biology and tumor growth

Paper I and II are among few studies that have examined relationships between biological features and pretreatment tumor growth rates of human glioblastomas. The sparse amount of studies is probably due to the challenges in obtaining sufficient preoperative imaging scans to estimate tumor growth rates. Of the previously mentioned studies on glioblastoma growth dynamics (see the ‘Introduction’, page 11-13), only two investigated the biology behind the preoperative tumor growth (113, 114). However, these studies included few glioblastoma patients (32-50 patients) (113, 114) and focused on molecular markers (114). Still, both studies indicated a role of increased proliferation in faster tumor growth (113, 114), which is in line with our findings that high cellular density was associated with faster tumor growth.

In Paper I and II, high cellular density and the presence of thromboses were significant independent predictors of faster tumor growth in the multivariable analyses. In Paper I, these features were corrected for each other, and in Paper II they were also corrected for CD105-MVD (which was not significant). We speculated high cellular density might be a better marker of high proliferative activity than mitotic counts and PIs, because of the limitations of these proliferative quantifications (see ‘Methodological considerations’, page 62). The cellularity is also affected by both cell cycle time and cell loss, which are factors that are not captured by mitotic count and PI (109, 210). In this way, the link between high cellularity and aggressiveness supports high cellular density as an important feature in glioma grading.

The results in Paper I led to the speculation that thromboses promoted tumor growth through the induction of hypoxia (155, 211). Interestingly, thrombosis has previously been suggested as a diagnostic criterion of glioblastoma (135, 212, 213). This is supported by our findings, which indicates that thrombosis is related to a more aggressive tumor biology. Thrombosis has also been linked to *IDH* wt status in diffuse astrocytic tumors (212), which further substantiates the link with an aggressive tumor biology. Unruh et al. (212) further speculated that thrombosis could be a surrogate marker of *IDH* wt status (212). Moreover, mechanisms associated with thrombus formation have been suggested as a potential target of therapy in glioblastomas (214).

In Paper II, the finding that CD105-MVD was not associated with faster growth when corrected for thrombosis and high cellular density, indicates that thromboses facilitate faster growth through angiogenesis-independent processes. Such angiogenesis-independent growth might happen through the other mechanisms of glioma-associated vascularization (i.e. co-option, vasculogenesis, vascular mimicry, and glioblastoma-endothelial cell transdifferentiation (142, 153), see the ‘Introduction’, page 15-16 and Figure 6), enhanced proliferation (215, 216), and increased invasion (215, 216). These hypoxia-induced mechanisms are some of the proposed mechanisms for resistance to anti-angiogenic therapy in glioblastomas (106, 153, 216-218), which can explain why bevacizumab (anti-VEGF treatment) has not been shown to improve survival in RCTs (35-37). The inadequacy of CD105-MVD as a marker of glioblastoma growth was also illustrated by the wide ranges of CD105-MVD counts within both growth groups and that CD105-MVD explained very little of the variance in growth. This could also potentially be explained by methodological limitations (see ‘Methodological considerations’, page 61-62) and/or the compensatory mechanisms mentioned above. In summary, our findings are not in accordance with the Folkman hypothesis (144), which states that tumor growth is angiogenesis-dependent (see the ‘Introduction’, page 15-16).

9.1.2 Biology and *MGMT* status

Despite extensive research on the predictive marker *MGMT* promoter methylation status, there are few studies that have investigated if *MGMT* status is linked to the pretreatment biology of human glioblastomas. However, many studies have been conducted with the aim to predict *MGMT* status non-invasively from MRI scans, but the results have been conflicting and derived no expert consensus (53).

In Paper III, *MGMT* status was not significantly associated with any of the biological features assessed as 22 histopathological features, Ki-67/MIB-1 PI, CD105-MVD, conventional MRI characteristics, and preoperative speed of tumor growth. These findings seen together with previous studies (see a more detailed discussion in Paper III), suggest the survival benefit of *MGMT* methylated glioblastomas is not due to an inherently less aggressive tumor biology. This further suggests that methylated *MGMT* status is not in part a prognostic factor, but merely a predictive marker (see the ‘Prognostic and predictive markers’ subsection for definitions, page 57-58).

The lack of pretreatment biological differences further suggests that *MGMT* status cannot be non-invasively predicted from MRI scans. There has been huge research interest into the non-invasive prediction of *MGMT* status (48-59, 219-221). Interestingly, the rationale behind such radiological studies is that there are pretreatment biological differences between *MGMT* methylated and unmethylated patients that can be measured on MRI scans. However, it is our impression that many of these studies might not have considered that *MGMT* status quite possibly is not a prognostic marker in itself. This would mean that the difference in biological aggressiveness between *MGMT* methylated and unmethylated tumors mainly occur after treatment. The latter also suggests that the increased response to chemotherapy in *MGMT* methylated glioblastomas is not due to other pretreatment biological differences than the *MGMT* status.

In contrast to our findings, the study by Fan et al (114) found that *IDH1* wt and *MGMT* unmethylated tumors were significantly associated with a faster preoperative tumor growth when corrected for WHO grade, *TERT* mutations, and Ki-67 expression. However, this was investigated in a subgroup of tumors with determined *IDH* and *MGMT* status (only 37 patients) (114). Although this study included 109 high grade tumors, only 50 were glioblastomas and only 19 were *IDH* wt glioblastomas. Interestingly, most *IDH* mt diffuse gliomas are *MGMT* methylated and *MGMT* status is only a prognostic and not a predictive marker in these tumors (69, 222). Hence, the inclusion of only *IDH* wt glioblastomas is a strength of Paper III.

9.2 Clinical considerations

Research is the cornerstone of medical practice, where the goal is ultimately to improve patient outcomes. Evidence-based medicine has been proposed as a paradigm shift in modern medicine, where the aim is to enable better identification of the best available research evidence to improve clinical practice (223). Scales of evidence levels based on the type of study design have been proposed as guides to assess the quality and validity of medical studies, such as the one proposed

by the Cochrane collaboration (Figure 27A) (223). Pathology, however, has been a latecomer in evidence-based medicine, but the interest in evidence-based pathology has increased the last years (223). As the RCT design is inappropriate for pathological studies, alternative evidence levels for pathological studies have been suggested (Figure 27B) (223).

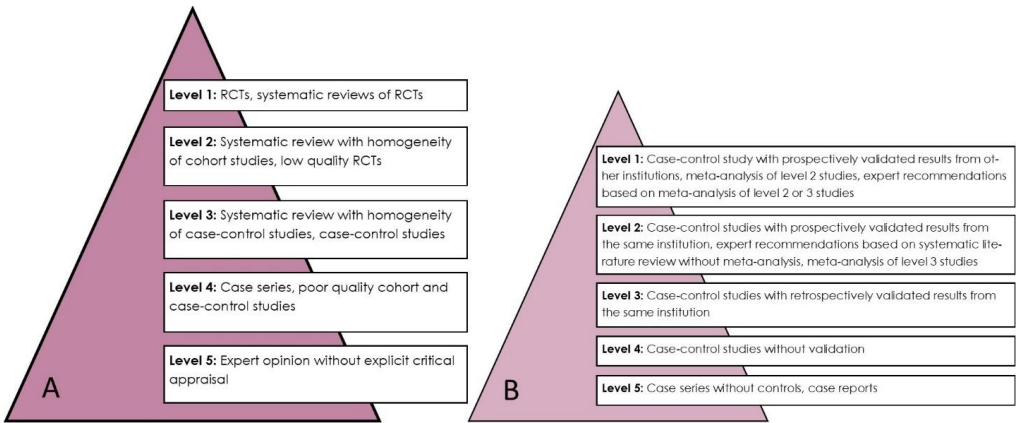


Figure 27. Evidence levels. **A** Evidence levels as proposed by the Cochrane collaboration, modified by Marchevsky et al. (223). **B** Evidence levels for evaluation of pathology literature. Inspired by evidence levels presented by Marchevsky et al. (223). RCT: Randomized controlled trial.

Considering the evidence levels suggested for pathology literature (Figure 27B), the papers in this thesis represent Level 4 evidence (i.e. case-control studies without validation). The low evidence levels indicate that few clinical implications can be drawn from the studies, and that the findings need to be validated. The retrospective design is a major limitation of our studies. However, a strength is that most of the clinical data were prospectively collected. In a prospective setting, a standardization of the MRI protocol for all patients (39) could have led to the inclusion of more patients, and it would probably have decreased the variability of the growth estimates. Also, prospective tissue sampling would probably have led to the collection of more tissue, which would have decreased the risk of sampling errors. Validation of the results in Paper III should be feasible. However, the validation of the results in Paper I and II is more difficult due to the challenges of acquiring preoperative tumor volumes to compute the growth data. Also, shorter time intervals between the preoperative MRI scans would lead to more uncertain growth estimates. In addition, other institutions would probably be reluctant to publish data showing long time intervals before surgery. However, Ellingson et al. (21) found that that only 6% of the patients had decreasing or

stable growth when patients with as short as 7-day intervals between the preoperative MRI scans were included. This suggests that shorter time intervals could be used in future studies.

As a part of evidence-based pathology, the Reporting recommendation for tumor MARKer prognostic studies (REMARK) guideline (224) was published to encourage transparent and complete reporting. Although the papers in this thesis are not prognostic studies (except the survival analysis in Paper III), the studies adhered to most of the guidelines. However, we realize that more attention should have been given to sample size and power (see ‘Methodological considerations’, page 63-64), and an effect size for the univariable associations between MVDs and tumor growth in Paper II should have been reported.

Despite the lack of direct clinical consequences of the findings of the papers in this thesis, the knowledge of the pretreatment tumor biology of glioblastomas has been increased. The use of biological markers to identify patients with different risks and responses to therapies is an important aspect of ‘personalized medicine’ (225). The goal is that more precise stratifications of patients based on biological characteristics could in turn guide a more informed and effective clinical management (225). Hence, ‘personalized medicine’ aims to bridge the gap from biological insights to clinical practice (i.e. ‘translational research’) (225). As an example, our finding that thrombosis predicted faster glioblastoma growth, might suggest that thrombosis could be a promising marker to identify patients in need of more aggressive treatment, or it could be a potential target of therapy. Although further research is needed and the findings in our papers must be validated, our studies complement previous research and could serve as fundamentals for future research. The hope is that better understanding of the tumor biology of glioblastomas will eventually lead to improved patient outcomes.

9.3 Biological considerations

In this work, we studied the phenotypical tumor biology of human glioblastomas by means of histopathological features seen in HE and IHC stained tissue sections and MRI characteristics on T1-weighted contrast-enhancing scans. An advantage with MRI is that it portrays the whole tumor *in vivo*. Histology, on the other hand, enables a more detailed assessment of the biology; however, only parts of the tumors are assessed, and it requires surgery. Even though experimental *in vitro* and *in vivo* models enable even more detailed studies of biological mechanisms (103), such models will never fully represent the vast intratumoral genetic and phenotypic heterogeneity of human glioblastomas (103) (see the subsection ‘Experimental models of glioblastoma growth’, page 13).

In the papers of this thesis, the histology sections represent the biology at the time of the second MRI scans (i.e. the scans taken right before surgery). The analyzed tissue was retrieved from the first surgical intervention in these patients, which means that the biology was unaffected by radiochemotherapy. Hence, the tissue sections and MRI scans reflected the natural biology of human glioblastomas. Unfortunately, we cannot entirely exclude an effect of preoperative corticosteroid treatment on the biology, as about 80% of the patients received such treatment. Still, in a previous analysis of the same patients, the steroid treatment was not significantly associated with growth when adjusted for the diagnostic tumor volume (20). Moreover, both histology and MRI are limited by that they only assess the biology at one time point, whereas tumor biology is a dynamic process in constant evolution (103, 226). Radiological tumor growth, on the other hand, is probably a biological marker that better reflects the net result of the different biological mechanisms over time.

Tumor growth was the end point in Paper I and II. Although we believe tumor growth more precisely reflects the underlying tumor biology than overall survival, it is an auxiliary end point and not a hard clinical end point. Overall survival is considered “the gold standard” end point (227) because associations with overall survival reflect a clinically meaningful effect. However, when the aim is to study tumor biology, overall survival is confounded by clinical factors that do not reflect tumor biology (44). Such clinical factors are for example the patient’s overall health, extent of resection, given treatments, and second-line therapies. Hence, these confounding factors may hide the effect of potential biomarkers when overall survival is the end point. Therefore, the use of tumor growth as the end point has the potential to discover new biomarkers associated with the aggressiveness of glioblastomas. Tumor growth as the endpoint is further supported by the fact that it is mainly the local impacts that lead to the death of glioblastoma patients (122, 123). In a previous study, we found that slower preoperative tumor growth was associated with improved survival 12 months after follow-up (205). The finding might indicate that other clinical factors affect survival more than tumor biology during the first 12 months, whereas the inherent biology is important for survival beyond 12 months.

As part of ‘personalized medicine’, extensive research interest has been devoted to the discovery of new treatment targets and the conduction of clinical trials on the effects of such targeted therapies. However, because glioblastomas are highly heterogenous and that tumor biology is in constant evolution, it has been speculated that compensatory mechanisms virtually

always will lead to treatment resistance of targeted therapies (228, 229). In glioblastomas, the lack of effect of targeted therapies is thought to be caused by the vast tumor heterogeneity, decreased penetration of the blood-brain barrier, and dose-limiting toxicities (3, 69). As seen with the bevacizumab-trials, compensatory mechanisms for the lack of angiogenesis are induced and drive treatment resistance (153). Hence, it has been suggested that combined drug treatment is needed to reduce drug resistance, but such treatment has been associated with an increased risk of toxicity (3, 228). An intriguing speculation is that it might be more effective to target more abundant cellular pathways, such as the proteasome (e.g. marizomib (230)). This is because the inhibition of more common cellular pathways is more likely to limit compensatory mechanisms that cause treatment resistance.

9.4 Prognostic and predictive markers

As previously mentioned, the finding that *MGMT* status was not associated with the pretreatment phenotypical tumor biology in Paper III, suggests that it is purely a predictive marker and not in part prognostic. *MGMT* status is often referred to as a prognostic marker, because it has been associated with overall survival in several studies (11, 12, 231). However, it is often confusing what the authors actually mean when they call a tumor marker prognostic, as the terms ‘prognostic’ and ‘predictive’ are sometimes used interchangeably (232). A prognostic marker is defined as a biomarker of the natural history of the disease that is associated with outcome (232). This means that its association with outcome is regardless of the therapy given, and that it reflects the inherent aggressiveness of the disease. In glioblastomas, it is not established if the prolonged survival in *MGMT* methylated patients is only due to the predictive effect of increased chemosensitivity, or if the marker is also in part prognostic. The best way to study if a marker is purely prognostic, is in cohorts where the patients do not receive any treatment (i.e. ‘pure’ prognostic studies) (224). However, this is seldom realistic for glioblastoma patients, and the closest we get is to study the survival effect of *MGMT* status in patients that have only received radiotherapy. The results from such analyses have been conflicting (11, 13-15, 88-90). However, as mentioned above, overall survival is also affected by second-line therapies. Second-line treatment with temozolomide is believed to have caused the seemingly prognostic effect in the radiotherapy-only treated patients in the Stupp-trial (11, 233). This is further substantiated by the lack of difference in progression-free survival in the same study (11). A predictive marker, on the other hand, implies a different benefit from treatment depending on the status of the biomarker (232). To confirm the predictive

significance of a biomarker, the RCT study design is necessary, because a control group is needed to confirm a statistical interaction between the treatment effect and the biomarker (232). The predictive value of *MGMT* status has been substantiated by many previous publications (11, 13-15, 91, 233). Interestingly, none of the RCTs were able to show a significant interaction between *MGMT* status and treatment, however, trends were established and the lack of significance is believed to be caused by underpowering (11, 13, 14).

The descriptions above emphasize that the design of the survival analysis in Paper III is inadequate to determine if *MGMT* status is either a true prognostic or true predictive marker. This is because the independent association between *MGMT* status and overall survival is still potentially affected by second-line treatment with temozolomide. This is because we only corrected for chemotherapy treatment that was received 6 months after surgery in the multivariable model. Nevertheless, the aim of the survival analysis was to check the external validity of our material. Instead, we used phenotypical pretreatment biology as a surrogate end point of a true prognostic value, because a true prognostic factor should theoretically reflect the inherent aggressiveness of the tumor.

9.5 Methodological considerations

9.5.1 External validity

A considerable strength of work is that the included patients were selected from all patients operated for glioblastoma at the same neurosurgical center within the given time interval (262 patients). All patients with suspected brain tumors within the central health region in Norway are referred to this neurosurgical center, which means the original population of 262 patients probably had a minimal amount of selection biases. However, there might still be some fragile patients that were not referred to surgical evaluation. Most of the excluded patients were due to inadequate imaging data: 79 patients had <two preoperative scans and 70 had <14 days between the scans (Figure 8, page 24). Still, the distributions of sex and age of the included patients were not significantly different from the excluded, and the mean age was comparable to glioblastoma patients in Norway (20). Also, the median overall survival of the 106 included patients (12.6 months) (205) was comparable to 10.1 months for unselected patients in Norway (18). In addition, the range and median of the KPS scores (205) were comparable to population-based studies (234, 235). The patients included were diagnosed between 2004 and 2014, which means that some of the patients diagnosed around 2004 did not receive the Stupp-protocol, as this protocol was introduced

around 2005 (19). However, this only affects the generalizability of the survival analysis in Paper III.

Before inclusion in Paper I, all tumors were histopathologically reviewed for diagnosis according to the 2007 WHO Classification (141) and the *IDH1 R132H* status determined using IHC. However, due to the subjective nature of pathology, we cannot entirely exclude the occurrence of differential diagnoses in our material (73). This potential bias is illustrated in a central review of the 360 glioblastoma patients from the Stupp-trial (19, 236), where 15 cases (4%) did not fulfill the criteria for glioblastoma. These cases were mostly re-diagnosed as lower-grade diffuse gliomas, but also re-diagnosed as other tumor types (236). However, because the diagnostic revision and the presence of contrast enhancement were requirements for inclusion in our papers, we believe the proportion of potentially misdiagnosed cases is probably quite low. Still, an independent assessment by another expert pathologist would have further increased the diagnostic validity. In 2016, the WHO Classification was updated, and the glioblastomas were diagnostically stratified into *IDH* mt and wt. As *IDH1* status was only determined with IHC, we had to preform additional *IDH1/2* sequencing to be in accordance with the 2016 Classification in Paper III. Also, the epithelioid glioblastoma subtype and diffuse midline glioma could have been considered more closely, as these were new types in the 2016 Classification. However, as both types are rare and occur predominately in children and young adults (237, 238), it is unlikely that they would have affected on the results. The finding of 3% *IDH* mt in our material, is in accordance with the frequency of 5% found in primary (i.e. *de novo*) glioblastomas (8). Due to the differences in biological behavior between *IDH* wt and mt tumors (184, 204), we excluded the *IDH* mt patients from Paper III.

9.5.2 Growth estimates

The precision of the growth estimates is affected by the quality of the volume segmentations. Substantial strengths of this project were that all volume segmentations were controlled by an experienced neuroradiologist (E.M.B.), the agreement of the volume segmentations were shown to be quite good (20), and the interobserver agreement was found to be acceptable (239). Still, the amount of contrast enhancement might have been affected by the timing and administration of the contrast agent and other factors such as infarctions (40). Importantly, there will always be diffusely infiltrating tumor cells beyond the contrast-enhancing rim of glioblastomas (29, 30). Therefore, it was only the bulk tumor growth that was estimated in this project. Hence, tumors with a more

diffuse growth pattern would not be captured as tumor growth, unless there occurs a subsequent induction of angiogenesis that breaches the blood-brain barrier (217, 226). A more diffuse growth pattern could have been measured using T2-weighted or FLAIR sequences. However, these sequences are also affected by corticosteroid treatment (41). In our previous study, we could not observe any significant growth of the T2/FLAIR compartments without co-occurring growth of the contrast-enhancing compartments (measured by visual inspection) (205).

Tumor growth was estimated as faster and slower growth than expected, based on the assumption that all tumors followed a Gompertzian growth pattern. This contrasts to most previous studies that have used volume doubling times (i.e. they assumed exponential growth). However, as described previously, exponential growth showed a poor fit, whereas Gompertzian growth and linear radial growth pattern showed a good fit with the volume data (20). However, there were not enough data on larger tumors to determine whether a final plateau phase took place (i.e. Gompertzian growth) or not (i.e. radial linear growth) (20). Nevertheless, in our previous study, the assumption of linear radial growth instead of Gompertzian growth led to the same conclusions (205). Individual growth curves from each patient could not be estimated, as this would require more than two preoperative tumor volumes.

9.5.3 Histopathological features

The assessment of histopathological features is limited by its subjective nature causing interobserver variability (73). This is especially challenging for features that are gradual processes, such as the degree of cellular density and atypia (73). To reduce observer variability, we strived to establish clear cut definitions and only record conspicuous features. The definitions of the features were in accordance with established literature (139, 141). However, in retrospect, we have realized that some of the definitions should have been more clearly defined beforehand, and some of the features had to be revised due to altered definitions (such as thrombosis and mitotic count). The assessments of the histopathological features by the two observers were not entirely independent, and interobserver agreement could therefore not be investigated. Still, we attempted to keep the second observer blinded when possible. The addition on an external observer, preferably an experienced pathologist, would have increased the reliability of the histopathological assessment and enabled computation of interobserver agreement.

Whereas high interobserver variability will lead to reduced reliability, sampling errors due to small tissue samples will lead to reduced validity of the assessments. Studies have found a that

glioblastomas can be undergraded on stereotactic biopsies (240-248). It is especially the histopathological features with large regional heterogeneity, such as mitotic figures (249), that are more prone to sampling errors.

9.5.4 Microvessel density

MVD measurements are also hampered by sampling errors and interobserver variability, and the latter has been shown to be high for MVD assessments in glioblastomas (250). Like the histopathological assessment, the reliability of the MVD assessment would have increased if we had included another independent observer.

Most previous studies have used the methods according to Weidner et al. (207) with modifications. Such modifications can be differences in the choice of endothelial antibodies, the definition of immunoreactive blood vessels, the use of eye-piece grids, which objective used, which magnification used, the number of HPFs counted, the definition of representative areas for counting, and the handling of glomeruloid tufts and longer vessels (156, 195, 196, 208, 251-256). Most studies define single positive cells as one vascular unit and avoid areas of sclerosis, necrosis, and non-neoplastic tissue. Yet, few have specified their handling of glomeruloid tufts and longer vessels. We believe as Leon et al. (156) that counting such tufts as one vascular unit will underestimate the angiogenic potential of glioblastomas. We have therefore as Kraby et al. (208) counted the lumens of these structures. Regarding the number of HPFs and the magnification, a study on MVDs in breast cancer showed that an increased field area led to a dilution of MVD counts and loss of prognostic informativeness (257). However, they recommended a field area that was twice as large as the area we assessed in Paper II (257). The differences in methodology between studies cause decreased validity of the findings and make results less comparable. In this respect, we realize that we should have been more restrictive with modifications of the methodology. Also, the counts should have been divided by the field area to increase comparability. Due to the different methodologies, a consensus guideline was published in 2002 (258). In this guideline, the Chalkley method with the CD34 antibody was recommended. However, the guideline has been criticized (259), and a new guideline has not been published since. Today, MVD is the most frequently used method and new antibodies and technologies have emerged.

There are several pan-endothelial antibodies to choose from, such as CD31, CD34, and vWF. We chose vWF as the pan-endothelial marker, because CD31 and CD34 have been found to stain different inflammatory cells (260). However, Wang et al. (197) has shown that vWF

sometimes does not stain microvessels. Although CD105 has predominately been found to stain proliferative endothelial cells (151, 189-197, 260), a few studies have shown that it can be positive in non-proliferating endothelial cells as well (261, 262). Hence, this marker needs to be further validated. The finding that vWF-MVD was not significantly associated with tumor growth in the univariable analysis of Paper II could perhaps be explained by its additional staining of pre-existing, not angiogenically active vasculature (263).

9.5.5 Proliferation assessments

As previously mentioned, there are several limitations to mitotic count and Ki-67/MIB-1 proliferative index (PI) assessments. Such limitations are heterogeneity of mitotic figures and positively stained cells both between and within glioblastomas (140, 177, 249, 264), sampling errors (177, 249, 264, 265), differences in fixation (249) and staining methodology (177, 249, 264), and the large interobserver variability (266). Such methodological errors are thought to be some of the reasons why Ki-67/MIB-1 PI has shown conflicting results as a prognostic marker in glioblastomas (2, 177, 265, 267, 268).

9.5.6 Immunohistochemistry

All fixations and IHC stains were performed at the same laboratory, which eliminates interlaboratory differences. Potential errors during IHC can be divided into reaction biases (e.g. related to tissue fixation, antigen retrieval, and detection systems) and interpretation biases (e.g. the selection of antibody types and protocols and interpretation of the results) (269). As an example of reaction biases, the antigenicity of FFPE material has been shown to decrease after only 12 months of storage (270). In the same study, vWF was one of the markers that showed decreased staining (breast cancer specimens) (270). Regarding interpretation biases, these are affected by the experience of both the lab personal and the examiner. Inter- and interobserver variability in determining what is regarded as a positive structure is also relevant. Adequate titration of the antibody dilution is necessary to avoid false positive or false negative staining. Factors such as hemorrhages, necrosis, and tissue edges can lead to false positive staining. To account for this in Paper II, we used a glioblastoma with focally present hemorrhages and necroses for optimal antibody titrations of the endothelial markers. Different types of antibodies (polyclonal vs monoclonal) affect the sensitivity and specificity of the staining. Polyclonal antibodies (e.g. GFAP and vWF) react with several epitopes that lead to a higher detection sensitivity, whereas monoclonal antibodies (e.g. IDH1 and CD105) only bind one epitope and are thus more specific

(269). To assure the validity of the findings, all the applied IHC protocols (Table 1, page 39) had external controls that were processed under the same condition as the assessed cases, and all had negative controls where the primary antibodies were omitted. Moreover, the staining procedure for CD105 with overnight incubation with cover glass may dispose to air bubbles and excessive drying, which also could lead to aggregated staining at tissue edges.

9.5.7 Methylation specific PCR

There is currently no consensus regarding the preferred assay to detect the *MGMT* promoter methylation status, and several different techniques are used (93, 95). We used methylation specific PCR (MSP), which is the technique routinely used at the pathology department at St. Olavs Hospital in Trondheim. *MGMT* status determined with MSP has been shown to associate with overall survival in several pivotal clinical studies (10, 11, 95, 96). Our finding of 36% methylated cases corresponds to the 30-60% found in previous studies (10). Unfortunately, intratumoral heterogeneity in *MGMT* status has also been reported (70, 271). Another important technical limitation of the MSP assay, is poor DNA quality that may be caused by bisulfite treatment, tissue fixation, necrosis, and sparse tumor material (10, 94). Some argue that quantitative MSP (real-time PCR) and pyrosequencing are superior to gel-based MSP, as they enable detection of 'intermediate' methylation (94) (i.e. 'weakly methylated' cases) and quantitatively state the degree of methylation as a percentage (93). However, in both assays, the cutoff-value for what is determined as a methylated sample is controversial (93-95). Nevertheless, the primers used in Paper III correspond to an area of the promoter found to best correlate with prognosis and *MGMT* expression in patients with glioblastoma (272, 273). Further technical limitations are discussed in more detail in previous publications (93-95).

9.5.8 Statistics

The statistical analyses in this thesis were explorative, meaning that not all statistical tests were preplanned. This led to a relatively high number of statistical tests, which is especially relevant for Paper I and III. We did not correct for multiple testing despite the increased risk of type I errors (i.e. false positive findings). This was because a correction would lead to decreased power and a higher risk of type II errors (i.e. not detecting associations that are true). To decrease the risk of type I errors, we could have included only features with the most biologically plausible relationships with tumor growth in Paper I. This approach would have been less fit for Paper III, where the knowledge of biological associations with *MGMT* status is more limited. In Paper I, 30

univariable significance tests were performed. Out of these, three (10%) were significant ($p < 0.05$), which suggests that some of the findings are not significant just by chance (i.e. type I error). In Paper III, none of the 29 performed statistical tests were significant. Hence, type II errors were suspected. To calculate the power in Paper III, we assumed a standardized effect size of 0.8, and estimated the power to be >90% for each of the analyses. We realize that a similar approach could have been made to estimate the power in Paper I and II. Altogether, the results must be interpreted with caution and need to be validated.

The grouping of variables causes a loss of information, such as the dichotomization of the growth estimates and the grouping of the two lowest categories of atypia, cellular density, and vascular density (274). The latter could have been avoided by using alternative statistical tests, such as the Kruskal-Wallis analysis. Possible consequences of the dichotomization of the growth data are loss of statistical power, underestimation of the extent of variation, and tumors close to the average (the cut-off) are at risk of being regarded as very different even though they might actually be quite similar (274). We considered other approaches than the dichotomization of the growth data, such as using the magnitude of the residual of the observed volume from the curve (Figure 10, page 27) or compensate for the dependency on tumor volume by using statistical transformation or interaction terms. However, such approaches would have made our data less interpretable.

10 Main conclusions

In this thesis, we have investigated potential relationships between pretreatment biological features and radiological speed of tumor growth or *MGMT* promoter methylation status.

In Paper I and II, only high cellular density and thromboses were significant independent predictors of faster tumor growth. Mitotic count and CD105-MVD were significantly associated with faster growth in univariable analyses of Paper I and II, respectively, but not in the multivariable analyses. Accordingly, these results suggest:

- High cellular density might better reflect a high proliferative activity than quantifications of mitotic count and Ki-67/MIB-1 PI
- Our findings are in line with hypotheses describing thrombosis as an important inductor of hypoxia, which triggers more aggressive tumor biology
- Thrombosis could potentially be used as a histopathological feature of glioblastoma. Hence, it could be considered to be implemented in tumor grading
- Thrombus formation might be a potential target of therapy
- Immunohistochemical quantification of the degree of angiogenesis (i.e. MVD measurement) is inadequate as markers of faster tumor growth
- Tumor growth is not necessarily angiogenesis-dependent (i.e. not in accordance with the Folkman hypothesis)
- It is possible that hypoxia-induced, angiogenesis-independent mechanisms contribute to faster glioblastoma growth
- The findings are in line with that anti-angiogenic therapy has not been shown to improve survival in glioblastomas due to the development of hypoxia-induced resistance mechanisms

In Paper III, we found no significant associations between *MGMT* status and pretreatment phenotypical tumor biology. Methylated *MGMT* status was an independent predictor for improved survival when adjusted for several clinical factors. Our findings suggest:

- The survival benefit of *MGMT* methylated glioblastomas is not due to a less aggressive inherent tumor biology. This further suggests methylated *MGMT* status is not in part a prognostic factor by itself, but merely a predictive marker

- The increased response to chemotherapy in *MGMT* methylated glioblastomas is not due to pretreatment differences in phenotypical tumor biology
- *MGMT* status cannot be non-invasively predicted from preoperative MRI scans

The major strengths of the papers are the preoperative growth estimates in a relatively large number of patients from one center with a population-based referral, and that the analyzed tissue material and MRI images were obtained before radiochemotherapy treatment. However, our studies were explorative, and the findings need to be validated in future studies. Before that, we cannot draw any firm conclusions.

11 Future perspectives

Despite the explorative study design that increases the need for validation, the findings of our studies can be used to generate hypotheses for future research. For example, such as the findings in Paper I were the basis for the aim of Paper II. Because the findings in Paper I and II point to hypoxia and thromboses, we are currently conducting a study with the markers HIF-1 α and tissue factor (TF) with the aim to investigate if these factors are associated with tumor growth. HIF-1 α indicates the degree of hypoxia, whereas upregulation of TF is thought to be important for thrombus formation in glioblastomas (212). TF has also been linked to *IDH* wt status and increased tumor aggressiveness (212). Interestingly, TF has been speculated as an attractive therapeutic target in *IDH* wt glioblastomas (214).

The extensive research on the molecular biology of brain tumors is making an increasing impact on the classification of brain tumors. In this regard, methylation profiling has been shown to be a powerful tool (63, 74). However, the use of methylation profiling is today limited by unresolved methodology, regulatory issues, and that it is unavailable to most institutions (71, 275, 276). Recently, an expert consortium of neuropathologists (277) has recommended substantial changes in the next WHO Classification regarding the typing and grading of diffuse astrocytic tumors (276). They recommend that glioblastoma, *IDH* mt should no longer be called “glioblastoma”, but instead “astrocytoma, *IDH* mt, WHO grade IV”, and that lower-grade *IDH* wt diffuse astrocytomas with molecular features as glioblastoma should be diagnosed as “glioblastomas, *IDH* wt” (276). The main purpose of the WHO Classification is to improve the clinical management of patients through precise communication, being a solid basis for research, improve prognostication, and guide treatment and follow-up (2). However, such substantial changes would make previous research based on the former definitions less valid. We also speculate that such substantial changes might cause confusion due to changes in nomenclature and the increased complexity. Thus, we are worried that this in turn could impede the clinical management of patients. Especially in hospitals and countries where the clinicians and pathologists are generalists (and not e.g. specialized neuropathologists), it is probably harder to keep up with such complex updates. Also, the extended need for molecular testing poses a challenge, particularly in less developed countries with less available resources. In sum, it will be very interesting to see if these recommendations will be incorporated, and especially, what the consequences will be for the clinical management of brain tumor patients in different countries.

Advancements in technology introduce exiting new methodologies and possibilities in glioblastoma research. For example, sequencing of circulating tumor DNA (ctDNA) in cerebrospinal fluid (CSF) is a potential future technique to study the glioma genome without the need for surgery (3, 278). With advances in technology, ctDNA could potentially be evaluated from blood plasma as well (3). Moreover, the introduction of advanced imaging techniques enable increased biological information of human glioblastomas *in vivo*, such as magnetic resonance spectroscopy (MRS) (279) and positron emission tomography (PET) (280). Moreover, the development of biomathematical models enable studies of the dynamic tumor biology, which could potentially model the constant evolution and be used to predict responses to therapies (228). Huge attention has recently been dedicated to artificial intelligence (AI). AI has the potential to discover features, patterns and relationships in large, complex datasets without the limitation of human subjectivity causing observer variability. AI has been shown to accurately perform automatic image segmentation of high-grade gliomas (281), and there is a huge potential in digital pathology where AI can potentially be used for automated tissue diagnosis and feature recognition (282, 283). In our ongoing study about HIF-1 α , TF and tumor growth, we plan to use digital pathology, and potentially AI, to quantitate the immunostainings.

We find ourselves in an exciting time in glioblastoma research, and it will be very interesting to see if the extensive research on glioblastoma biology eventually will lead to improved patient outcomes. Hopefully, new technologies along with high-quality research will enable the discovery of effective treatments of this extremely heterogenous and aggressive disease. As said by the oncologist Robert Gatenby when explaining the challenges of treatment development and treatment resistance in cancers (228):

“Instead of whack-a-mole, we need to be playing chess”

12 Errata

- In Paper III, we state that 30 histopathological features were assessed for associations with tumor growth. However, it was 30 statistical tests that were performed, and 27 histopathological features were assessed. This was because microvascular proliferation irrespective of location, one or more of the secondary structures of Scherer, and all three of the structures were also tested for associations.

13 References

1. Ostrom QT, Cioffi G, Gittleman H, et al. CBTRUS Statistical Report: Primary Brain and Other Central Nervous System Tumors Diagnosed in the United States in 2012-2016. *Neuro-oncology*. 2019;21(Suppl 5):v1-v100.
2. Louis DN, Ohgaki H, Wiestler O, et al. WHO Classification of Tumours of the Central Nervous System. Revised 4th ed. 1211 Geneva 27, Switzerland: International Agency for Research on Cancer (IARC); 2016.
3. Wen PY, Weller M, Lee EQ, et al. Glioblastoma in adults: a Society for Neuro-Oncology (SNO) and European Society of Neuro-Oncology (EANO) consensus review on current management and future directions. *Neuro-oncology*. 2020;22(8):1073-113.
4. Lee JH, Lee JE, Kahng JY, et al. Human glioblastoma arises from subventricular zone cells with low-level driver mutations. *Nature*. 2018;560(7717):243-7.
5. Sottoriva A, Spiteri I, Piccirillo SG, et al. Intratumor heterogeneity in human glioblastoma reflects cancer evolutionary dynamics. *Proc Natl Acad Sci U S A*. 2013;110(10):4009-14.
6. Patel AP, Tirosh I, Trombetta JJ, et al. Single-cell RNA-seq highlights intratumoral heterogeneity in primary glioblastoma. *Science*. 2014;344(6190):1396-401.
7. Parsons DW, Jones S, Zhang X, et al. An integrated genomic analysis of human glioblastoma multiforme. *Science*. 2008;321(5897):1807-12.
8. Kloosterhof NK, Bralten LB, Dubbink HJ, et al. Isocitrate dehydrogenase-1 mutations: a fundamentally new understanding of diffuse glioma? *Lancet Oncol*. 2011;12(1):83-91.
9. Ohgaki H, Kleihues P. Genetic pathways to primary and secondary glioblastoma. *Am J Pathol*. 2007;170(5):1445-53.
10. Weller M, Stupp R, Reifenberger G, et al. MGMT promoter methylation in malignant gliomas: ready for personalized medicine? *Nat Rev Neurol*. 2010;6(1):39-51.
11. Hegi ME, Diserens AC, Gorlia T, et al. MGMT gene silencing and benefit from temozolomide in glioblastoma. *N Engl J Med*. 2005;352(10):997-1003.
12. Weller M, Felsberg J, Hartmann C, et al. Molecular predictors of progression-free and overall survival in patients with newly diagnosed glioblastoma: a prospective translational study of the German Glioma Network. *J Clin Oncol*. 2009;27(34):5743-50.
13. Wick W, Platten M, Meisner C, et al. Temozolomide chemotherapy alone versus radiotherapy alone for malignant astrocytoma in the elderly: the NOA-08 randomised, phase 3 trial. *Lancet Oncol*. 2012;13(7):707-15.
14. Malmstrom A, Gronberg BH, Marosi C, et al. Temozolomide versus standard 6-week radiotherapy versus hypofractionated radiotherapy in patients older than 60 years with glioblastoma: the Nordic randomised, phase 3 trial. *Lancet Oncol*. 2012;13(9):916-26.
15. Perry JR, Laperriere N, O'Callaghan CJ, et al. Short-Course Radiation plus Temozolomide in Elderly Patients with Glioblastoma. *N Engl J Med*. 2017;376(11):1027-37.
16. Yan H, Parsons DW, Jin G, et al. IDH1 and IDH2 mutations in gliomas. *N Engl J Med*. 2009;360(8):765-73.
17. Storstein A, Helseth E, Børge Johannesen T, et al. Høygradige gliomer hos voksne. *Tidsskr Nor Lægeforen*. 2011;131(3):238.
18. Ronning PA, Helseth E, Meling TR, et al. A population-based study on the effect of temozolomide in the treatment of glioblastoma multiforme. *Neuro-oncology*. 2012;14(9):1178-84.
19. Stupp R, Mason WP, van den Bent MJ, et al. Radiotherapy plus concomitant and adjuvant temozolomide for glioblastoma. *N Engl J Med*. 2005;352(10):987-96.
20. Stensjøen AL, Solheim O, Kvistad KA, et al. Growth dynamics of untreated glioblastomas in vivo. *Neuro-oncology*. 2015;17(10):1402-11.
21. Ellingson BM, Nguyen HN, Lai A, et al. Contrast-enhancing tumor growth dynamics of preoperative, treatment-naïve human glioblastoma. *Cancer*. 2016;122(11):1718-27.
22. Omuro A, DeAngelis LM. Glioblastoma and other malignant gliomas: a clinical review. *JAMA*. 2013;310(17):1842-50.
23. Weller M, van den Bent M, Tonn JC, et al. European Association for Neuro-Oncology (EANO) guideline on the diagnosis and treatment of adult astrocytic and oligodendroglial gliomas. *Lancet Oncol*. 2017;18(6):e315-e29.

24. Vogelbaum MA, Jost S, Aghi MK, et al. Application of novel response/progression measures for surgically delivered therapies for gliomas: Response Assessment in Neuro-Oncology (RANO) Working Group. *Neurosurgery*. 2012;70(1):234-43; discussion 43-4.
25. Ellingson BM, Abrey LE, Nelson SJ, et al. Validation of postoperative residual contrast-enhancing tumor volume as an independent prognostic factor for overall survival in newly diagnosed glioblastoma. *Neuro-oncology*. 2018;20(9):1240-50.
26. Lacroix M, Toms SA. Maximum safe resection of glioblastoma multiforme. *J Clin Oncol*. 2014;32(8):727-8.
27. McGirt MJ, Mukherjee D, Chaichana KL, et al. Association of surgically acquired motor and language deficits on overall survival after resection of glioblastoma multiforme. *Neurosurgery*. 2009;65(3):463-9; discussion 9-70.
28. Gulati S, Jakola AS, Nerland US, et al. The risk of getting worse: surgically acquired deficits, perioperative complications, and functional outcomes after primary resection of glioblastoma. *World Neurosurg*. 2011;76(6):572-9.
29. Kelly PJ, Dumas-Duport C, Kispert DB, et al. Imaging-based stereotaxic serial biopsies in untreated intracranial glial neoplasms. *J Neurosurg*. 1987;66(6):865-74.
30. Yamahara T, Numa Y, Oishi T, et al. Morphological and flow cytometric analysis of cell infiltration in glioblastoma: a comparison of autopsy brain and neuroimaging. *Brain Tumor Pathol*. 2010;27(2):81-7.
31. Sahm F, Capper D, Jeibmann A, et al. Addressing diffuse glioma as a systemic brain disease with single-cell analysis. *Arch Neurol*. 2012;69(4):523-6.
32. Hegi ME, Stupp R. Withholding temozolomide in glioblastoma patients with unmethylated MGMT promoter--still a dilemma? *Neuro-oncology*. 2015;17(11):1425-7.
33. Friedman HS, Prados MD, Wen PY, et al. Bevacizumab alone and in combination with irinotecan in recurrent glioblastoma. *J Clin Oncol*. 2009;27(28):4733-40.
34. Kreisl TN, Kim L, Moore K, et al. Phase II trial of single-agent bevacizumab followed by bevacizumab plus irinotecan at tumor progression in recurrent glioblastoma. *J Clin Oncol*. 2009;27(5):740-5.
35. Gilbert MR, Dignam JJ, Armstrong TS, et al. A randomized trial of bevacizumab for newly diagnosed glioblastoma. *N Engl J Med*. 2014;370(8):699-708.
36. Chinot OL, Wick W, Mason W, et al. Bevacizumab plus radiotherapy-temozolomide for newly diagnosed glioblastoma. *N Engl J Med*. 2014;370(8):709-22.
37. Wick W, Gorlia T, Bendszus M, et al. Lomustine and Bevacizumab in Progressive Glioblastoma. *N Engl J Med*. 2017;377(20):1954-63.
38. Ellingson BM, Wen PY, Cloughesy TF. Evidence and context of use for contrast enhancement as a surrogate of disease burden and treatment response in malignant glioma. *Neuro-oncology*. 2018;20(4):457-71.
39. Ellingson BM, Bendszus M, Boxerman J, et al. Consensus recommendations for a standardized Brain Tumor Imaging Protocol in clinical trials. *Neuro-oncology*. 2015;17(9):1188-98.
40. Quant EC, Wen PY. Response assessment in neuro-oncology. *Curr Oncol Rep*. 2011;13(1):50-6.
41. Wen PY, Macdonald DR, Reardon DA, et al. Updated response assessment criteria for high-grade gliomas: response assessment in neuro-oncology working group. *J Clin Oncol*. 2010;28(11):1963-72.
42. Rees JH, Smirniotopoulos JG, Jones RV, et al. Glioblastoma multiforme: radiologic-pathologic correlation. *Radiographics*. 1996;16(6):1413-38; quiz 62-3.
43. Gill BJ, Pisapia DJ, Malone HR, et al. MRI-localized biopsies reveal subtype-specific differences in molecular and cellular composition at the margins of glioblastoma. *Proc Natl Acad Sci U S A*. 2014;111(34):12550-5.
44. Ellingson BM. Radiogenomics and imaging phenotypes in glioblastoma: novel observations and correlation with molecular characteristics. *Curr Neurol Neurosci Rep*. 2015;15(1):506.
45. Kalpathy-Cramer J, Gerstner ER, Emblem KE, et al. Advanced magnetic resonance imaging of the physical processes in human glioblastoma. *Cancer research*. 2014;74(17):4622-37.
46. Suh CH, Kim HS, Jung SC, et al. MRI as a diagnostic biomarker for differentiating primary central nervous system lymphoma from glioblastoma: A systematic review and meta-analysis. *J Magn Reson Imaging*. 2019;50(2):560-72.
47. Law M, Yang S, Babb JS, et al. Comparison of cerebral blood volume and vascular permeability from dynamic susceptibility contrast-enhanced perfusion MR imaging with glioma grade. *AJNR Am J Neuroradiol*. 2004;25(5):746-55.

48. Kickingereder P, Bonekamp D, Nowosielski M, et al. Radiogenomics of Glioblastoma: Machine Learning-based Classification of Molecular Characteristics by Using Multiparametric and Multiregional MR Imaging Features. *Radiology*. 2016;281(3):907-18.
49. Drabycz S, Roldan G, de Robles P, et al. An analysis of image texture, tumor location, and MGMT promoter methylation in glioblastoma using magnetic resonance imaging. *Neuroimage*. 2010;49(2):1398-405.
50. Eoli M, Menghi F, Bruzzone MG, et al. Methylation of O6-methylguanine DNA methyltransferase and loss of heterozygosity on 19q and/or 17p are overlapping features of secondary glioblastomas with prolonged survival. *Clin Cancer Res*. 2007;13(9):2606-13.
51. Ryoo I, Choi SH, Kim JH, et al. Cerebral blood volume calculated by dynamic susceptibility contrast-enhanced perfusion MR imaging: preliminary correlation study with glioblastoma genetic profiles. *PLoS One*. 2013;8(8):e71704.
52. Ellingson BM, Cloughesy TF, Pope WB, et al. Anatomic localization of O6-methylguanine DNA methyltransferase (MGMT) promoter methylated and unmethylated tumors: a radiographic study in 358 de novo human glioblastomas. *Neuroimage*. 2012;59(2):908-16.
53. Han Y, Yan LF, Wang XB, et al. Structural and advanced imaging in predicting MGMT promoter methylation of primary glioblastoma: a region of interest based analysis. *BMC Cancer*. 2018;18(1):215.
54. Romano A, Calabria LF, Tavanti F, et al. Apparent diffusion coefficient obtained by magnetic resonance imaging as a prognostic marker in glioblastomas: correlation with MGMT promoter methylation status. *Eur Radiol*. 2013;23(2):513-20.
55. Pope WB, Lai A, Mehta R, et al. Apparent diffusion coefficient histogram analysis stratifies progression-free survival in newly diagnosed bevacizumab-treated glioblastoma. *AJNR Am J Neuroradiol*. 2011;32(5):882-9.
56. Hempel JM, Schittenhelm J, Klose U, et al. In Vivo Molecular Profiling of Human Glioma : Cross-Sectional Observational Study Using Dynamic Susceptibility Contrast Magnetic Resonance Perfusion Imaging. *Clin Neuroradiol*. 2019;29(3):479-91.
57. Ahn SS, Shin NY, Chang JH, et al. Prediction of methylguanine methyltransferase promoter methylation in glioblastoma using dynamic contrast-enhanced magnetic resonance and diffusion tensor imaging. *J Neurosurg*. 2014;121(2):367-73.
58. Gupta A, Omuro AM, Shah AD, et al. Continuing the search for MR imaging biomarkers for MGMT promoter methylation status: conventional and perfusion MRI revisited. *Neuroradiology*. 2012;54(6):641-3.
59. Korfiatis P, Kline TL, Coufalova L, et al. MRI texture features as biomarkers to predict MGMT methylation status in glioblastomas. *Med Phys*. 2016;43(6):2835-44.
60. Brennan CW, Verhaak RG, McKenna A, et al. The somatic genomic landscape of glioblastoma. *Cell*. 2013;155(2):462-77.
61. Comprehensive genomic characterization defines human glioblastoma genes and core pathways. *Nature*. 2008;455(7216):1061-8.
62. Eckel-Passow JE, Lachance DH, Molinaro AM, et al. Glioma Groups Based on 1p/19q, IDH, and TERT Promoter Mutations in Tumors. *N Engl J Med*. 2015;372(26):2499-508.
63. Capper D, Jones DTW, Sill M, et al. DNA methylation-based classification of central nervous system tumours. *Nature*. 2018;555(7697):469-74.
64. Ceccarelli M, Barthel FP, Malta TM, et al. Molecular Profiling Reveals Biologically Discrete Subsets and Pathways of Progression in Diffuse Glioma. *Cell*. 2016;164(3):550-63.
65. Ohgaki H, Dessen P, Jourde B, et al. Genetic pathways to glioblastoma: a population-based study. *Cancer research*. 2004;64(19):6892-9.
66. Killela PJ, Pirozzi CJ, Healy P, et al. Mutations in IDH1, IDH2, and in the TERT promoter define clinically distinct subgroups of adult malignant gliomas. *Oncotarget*. 2014;5(6):1515-25.
67. Phillips HS, Kharbanda S, Chen R, et al. Molecular subclasses of high-grade glioma predict prognosis, delineate a pattern of disease progression, and resemble stages in neurogenesis. *Cancer Cell*. 2006;9(3):157-73.
68. Verhaak RG, Hoadley KA, Purdom E, et al. Integrated genomic analysis identifies clinically relevant subtypes of glioblastoma characterized by abnormalities in PDGFRA, IDH1, EGFR, and NF1. *Cancer Cell*. 2010;17(1):98-110.
69. Reifenberger G, Wirsching HG, Knobbe-Thomsen CB, et al. Advances in the molecular genetics of gliomas - implications for classification and therapy. *Nat Rev Clin Oncol*. 2017;14(7):434-52.

70. Wenger A, Ferreyra Vega S, Kling T, et al. Intratumor DNA methylation heterogeneity in glioblastoma: implications for DNA methylation-based classification. *Neuro-oncology*. 2019;21(5):616-27.
71. Brat DJ, Aldape K, Colman H, et al. cIMPACT-NOW update 3: recommended diagnostic criteria for "Diffuse astrocytic glioma, IDH-wildtype, with molecular features of glioblastoma, WHO grade IV". *Acta Neuropathol*. 2018;136(5):805-10.
72. van den Bent MJ. Interobserver variation of the histopathological diagnosis in clinical trials on glioma: a clinician's perspective. *Acta Neuropathol*. 2010;120(3):297-304.
73. Coons SW, Johnson PC, Scheithauer BW, et al. Improving diagnostic accuracy and interobserver concordance in the classification and grading of primary gliomas. *Cancer*. 1997;79(7):1381-93.
74. Karimi S, Zuccato JA, Mamatjan Y, et al. The central nervous system tumor methylation classifier changes neuro-oncology practice for challenging brain tumor diagnoses and directly impacts patient care. *Clin Epigenetics*. 2019;11(1):185.
75. Sanai N, Berger MS. Glioma extent of resection and its impact on patient outcome. *Neurosurgery*. 2008;62(4):753-64; discussion 264-6.
76. Lacroix M, Abi-Said D, Fourney DR, et al. A multivariate analysis of 416 patients with glioblastoma multiforme: prognosis, extent of resection, and survival. *J Neurosurg*. 2001;95(2):190-8.
77. Burger PC, Green SB. Patient age, histologic features, and length of survival in patients with glioblastoma multiforme. *Cancer*. 1987;59(9):1617-25.
78. Barker FG, 2nd, Davis RL, Chang SM, et al. Necrosis as a prognostic factor in glioblastoma multiforme. *Cancer*. 1996;77(6):1161-6.
79. Homma T, Fukushima T, Vaccarella S, et al. Correlation among pathology, genotype, and patient outcomes in glioblastoma. *J Neuropathol Exp Neurol*. 2006;65(9):846-54.
80. Burger PC, Vollmer RT. Histologic factors of prognostic significance in the glioblastoma multiforme. *Cancer*. 1980;46(5):1179-86.
81. Kozak KR, Moody JS. Giant cell glioblastoma: a glioblastoma subtype with distinct epidemiology and superior prognosis. *Neuro-oncology*. 2009;11(6):833-41.
82. Ortega A, Nuno M, Walia S, et al. Treatment and survival of patients harboring histological variants of glioblastoma. *J Clin Neurosci*. 2014;21(10):1709-13.
83. Hammoud MA, Sawaya R, Shi W, et al. Prognostic significance of preoperative MRI scans in glioblastoma multiforme. *J Neurooncol*. 1996;27(1):65-73.
84. Weller M, Pfister SM, Wick W, et al. Molecular neuro-oncology in clinical practice: a new horizon. *Lancet Oncol*. 2013;14(9):e370-9.
85. Wesolowski JR, Rajdev P, Mukherji SK. Temozolomide (Temodar). *AJNR Am J Neuroradiol*. 2010;31(8):1383-4.
86. Scheie D, Kufaiishi HHA, Broholm H, et al. Biomarkers in tumors of the central nervous system - a review. *APMIS : acta pathologica, microbiologica, et immunologica Scandinavica*. 2019;127(5):265-87.
87. Krex D, Klink B, Hartmann C, et al. Long-term survival with glioblastoma multiforme. *Brain*. 2007;130(Pt 10):2596-606.
88. Rivera AL, Pelloski CE, Gilbert MR, et al. MGMT promoter methylation is predictive of response to radiotherapy and prognostic in the absence of adjuvant alkylating chemotherapy for glioblastoma. *Neuro-oncology*. 2010;12(2):116-21.
89. Criniere E, Kaloshi G, Laigle-Donadey F, et al. MGMT prognostic impact on glioblastoma is dependent on therapeutic modalities. *J Neurooncol*. 2007;83(2):173-9.
90. Zhao YH, Wang ZF, Cao CJ, et al. The Clinical Significance of O(6)-Methylguanine-DNA Methyltransferase Promoter Methylation Status in Adult Patients With Glioblastoma: A Meta-analysis. *Front Neurol*. 2018;9:127.
91. Wick W, Weller M, van den Bent M, et al. MGMT testing--the challenges for biomarker-based glioma treatment. *Nat Rev Neurol*. 2014;10(7):372-85.
92. Stupp R, Hegi ME, Mason WP, et al. Effects of radiotherapy with concomitant and adjuvant temozolomide versus radiotherapy alone on survival in glioblastoma in a randomised phase III study: 5-year analysis of the EORTC-NCIC trial. *Lancet Oncol*. 2009;10(5):459-66.
93. Malmstrom A, Lysiak M, Kristensen BW, et al. Do we really know who has an MGMT methylated glioma? Results of an international survey regarding use of MGMT analyses for glioma. *Neuro-oncology practice*. 2020;7(1):68-76.
94. Dullea A, Marignol L. MGMT testing allows for personalised therapy in the temozolomide era. *Tumour Biol*. 2016;37(1):87-96.

95. Mansouri A, Hachem LD, Mansouri S, et al. MGMT promoter methylation status testing to guide therapy for glioblastoma: refining the approach based on emerging evidence and current challenges. *Neuro-oncology*. 2019;21(2):167-78.
96. Esteller M, Garcia-Foncillas J, Andion E, et al. Inactivation of the DNA-repair gene MGMT and the clinical response of gliomas to alkylating agents. *N Engl J Med*. 2000;343(19):1350-4.
97. Romani M, Pistillo MP, Banelli B. Epigenetic Targeting of Glioblastoma. *Front Oncol*. 2018;8:448.
98. Aoki K, Natsume A. Overview of DNA methylation in adult diffuse gliomas. *Brain Tumor Pathol*. 2019;36(2):84-91.
99. Persano L, Pistollato F, Rampazzo E, et al. BMP2 sensitizes glioblastoma stem-like cells to Temozolomide by affecting HIF-1 α stability and MGMT expression. *Cell Death Dis*. 2012;3:e412.
100. Tang JH, Ma ZX, Huang GH, et al. Downregulation of HIF-1 α sensitizes U251 glioma cells to the temozolomide (TMZ) treatment. *Exp Cell Res*. 2016;343(2):148-58.
101. Wang P, Lan C, Xiong S, et al. HIF1 α regulates single differentiated glioma cell dedifferentiation to stem-like cell phenotypes with high tumorigenic potential under hypoxia. *Oncotarget*. 2017;8(17):28074-92.
102. Chahal M, Xu Y, Lesniak D, et al. MGMT modulates glioblastoma angiogenesis and response to the tyrosine kinase inhibitor sunitinib. *Neuro-oncology*. 2010;12(8):822-33.
103. Huszthy PC, Daphu I, Niclou SP, et al. In vivo models of primary brain tumors: pitfalls and perspectives. *Neuro-oncology*. 2012;14(8):979-93.
104. Hanahan D, Weinberg RA. Hallmarks of cancer: the next generation. *Cell*. 2011;144(5):646-74.
105. Laird AK. Dynamics of tumor growth. *Br J Cancer*. 1964;13:490-502.
106. Baker GJ, Yadav VN, Motsch S, et al. Mechanisms of glioma formation: iterative perivascular glioma growth and invasion leads to tumor progression, VEGF-independent vascularization, and resistance to antiangiogenic therapy. *Neoplasia (New York, NY)*. 2014;16(7):543-61.
107. Robertson FL, Marqués-Torrejón MA, Morrison GM, et al. Experimental models and tools to tackle glioblastoma. *Dis Model Mech*. 2019;12(9).
108. Gordillo N, Montseny E, Sobrevilla P. State of the art survey on MRI brain tumor segmentation. *Magn Reson Imaging*. 2013;31(8):1426-38.
109. Tubiana M. Tumor cell proliferation kinetics and tumor growth rate. *Acta Oncol*. 1989;28(1):113-21.
110. Retsky MW, Swartzendruber DE, Wardwell RH, et al. Is Gompertzian or exponential kinetics a valid description of individual human cancer growth? *Med Hypotheses*. 1990;33(2):95-106.
111. Bru A, Albertos S, Luis Subiza J, et al. The universal dynamics of tumor growth. *Biophys J*. 2003;85(5):2948-61.
112. Harpold HL, Alvord EC, Jr., Swanson KR. The evolution of mathematical modeling of glioma proliferation and invasion. *J Neuropathol Exp Neurol*. 2007;66(1):1-9.
113. Wang CH, Rockhill JK, Mrugala M, et al. Prognostic significance of growth kinetics in newly diagnosed glioblastomas revealed by combining serial imaging with a novel biomathematical model. *Cancer research*. 2009;69(23):9133-40.
114. Fan Z, Liu Y, Li S, et al. Association of tumor growth rates with molecular biomarker status: a longitudinal study of high-grade glioma. *Aging (Albany NY)*. 2020;12(9):7908-26.
115. Yamashita T, Kuwabara T. Estimation of rate of growth of malignant brain tumors by computed tomography scanning. *Surg Neurol*. 1983;20(6):464-70.
116. Tsuboi K, Yoshii Y, Nakagawa K, et al. Regrowth patterns of supratentorial gliomas: estimation from computed tomographic scans. *Neurosurgery*. 1986;19(6):946-51.
117. Blankenberg FG, Teplitz RL, Ellis W, et al. The influence of volumetric tumor doubling time, DNA ploidy, and histologic grade on the survival of patients with intracranial astrocytomas. *AJNR Am J Neuroradiol*. 1995;16(5):1001-12.
118. Haney SM, Thompson PM, Cloughesy TF, et al. Tracking tumor growth rates in patients with malignant gliomas: a test of two algorithms. *AJNR Am J Neuroradiol*. 2001;22(1):73-82.
119. Pennington C, Kilbride L, Grant R, et al. A pilot study of brain tumour growth between radiotherapy planning and delivery. *Clin Oncol (R Coll Radiol)*. 2006;18(2):104-8.
120. James B, Gillard J, Antoun N, et al. Glioblastoma doubling time and cellular proliferation markers. *Clin Oncol*. 2007;19(3):S33.
121. Lun M, Lok E, Gautam S, et al. The natural history of extracranial metastasis from glioblastoma multiforme. *J Neurooncol*. 2011;105(2):261-73.

122. Silbergeld DL, Rostomily RC, Alvord EC, Jr. The cause of death in patients with glioblastoma is multifactorial: clinical factors and autopsy findings in 117 cases of supratentorial glioblastoma in adults. *J Neurooncol.* 1991;10(2):179-85.
123. Giangaspero F, Burger PC. Correlations between cytologic composition and biologic behavior in the glioblastoma multiforme. A postmortem study of 50 cases. *Cancer.* 1983;52(12):2320-33.
124. Badve C, Sloan AE. Modeling the growth dynamics of glioblastoma using magnetic resonance imaging. *Neuro-oncology.* 2015;17(10):1307-8.
125. Burger PC, Kleihues P. Cytologic composition of the untreated glioblastoma with implications for evaluation of needle biopsies. *Cancer.* 1989;63(10):2014-23.
126. Habberstad AH, Lind-Landstöm T, Torp SH. The Histopathological Spectrum of Primary Human Glioblastomas with Relations to Tumour Biology. *Journal of Clinical & Experimental Pathology.* 2012;2(3).
127. Eder K, Kalman B. Molecular heterogeneity of glioblastoma and its clinical relevance. *Pathol Oncol Res.* 2014;20(4):777-87.
128. Torp SH, Granli US. Proliferative activity in human glioblastomas assessed by various techniques. *APMIS : acta pathologica, microbiologica, et immunologica Scandinavica.* 2001;109(12):865-9.
129. Brem S, Cotran R, Folkman J. Tumor angiogenesis: a quantitative method for histologic grading. *J Natl Cancer Inst.* 1972;48(2):347-56.
130. Lamszus K, Ulbricht U, Matschke J, et al. Levels of soluble vascular endothelial growth factor (VEGF) receptor 1 in astrocytic tumors and its relation to malignancy, vascularity, and VEGF-A. *Clin Cancer Res.* 2003;9(4):1399-405.
131. Zagzag D, Zhong H, Scalzitti JM, et al. Expression of hypoxia-inducible factor 1alpha in brain tumors: association with angiogenesis, invasion, and progression. *Cancer.* 2000;88(11):2606-18.
132. Kaur B, Khwaja FW, Severson EA, et al. Hypoxia and the hypoxia-inducible-factor pathway in glioma growth and angiogenesis. *Neuro-oncology.* 2005;7(2):134-53.
133. Guan M, Jin J, Su B, et al. Tissue factor expression and angiogenesis in human glioma. *Clin Biochem.* 2002;35(4):321-5.
134. Perry JR. Thromboembolic disease in patients with high-grade glioma. *Neuro-oncology.* 2012;14 Suppl 4:iv73-80.
135. Tehrani M, Friedman TM, Olson JJ, et al. Intravascular thrombosis in central nervous system malignancies: a potential role in astrocytoma progression to glioblastoma. *Brain Pathol.* 2008;18(2):164-71.
136. Jackson PR, Juliano J, Hawkins-Daarud A, et al. Patient-specific mathematical neuro-oncology: using a simple proliferation and invasion tumor model to inform clinical practice. *Bull Math Biol.* 2015;77(5):846-56.
137. Shen Y, Grisdale CJ, Islam SA, et al. Comprehensive genomic profiling of glioblastoma tumors, BTICs, and xenografts reveals stability and adaptation to growth environments. *Proc Natl Acad Sci U S A.* 2019;116(38):19098-108.
138. Chignola R, Foroni RI. Estimating the growth kinetics of experimental tumors from as few as two determinations of tumor size: implications for clinical oncology. *IEEE Trans Biomed Eng.* 2005;52(5):808-15.
139. Love S, Budka H, Ironside JW, et al. *Greenfield's Neuropathology.* Ninth Edition ed: Taylor & Francis; 2015.
140. Louis DN. Molecular pathology of malignant gliomas. *Annual review of pathology.* 2006;1:97-117.
141. Louis DN, Ohgaki H, Wiestler O, et al. *WHO Classification of Tumours of the Central Nervous System.* 4th ed. CH-1211 Geneva 27, Switzerland: International Agency for Research on Cancer (IARC); 2007.
142. Hardee ME, Zagzag D. Mechanisms of glioma-associated neovascularization. *Am J Pathol.* 2012;181(4):1126-41.
143. Folkman J. Tumor angiogenesis: therapeutic implications. *N Engl J Med.* 1971;285(21):1182-6.
144. Folkman J. What is the evidence that tumors are angiogenesis dependent? *J Natl Cancer Inst.* 1990;82(1):4-6.
145. Scribner E, Saut O, Province P, et al. Effects of anti-angiogenesis on glioblastoma growth and migration: model to clinical predictions. *PLoS One.* 2014;9(12):e115018.
146. Holash J, Maisonpierre PC, Compton D, et al. Vessel cooption, regression, and growth in tumors mediated by angiopoietins and VEGF. *Science.* 1999;284(5422):1994-8.
147. Lyden D, Hattori K, Dias S, et al. Impaired recruitment of bone-marrow-derived endothelial and hematopoietic precursor cells blocks tumor angiogenesis and growth. *Nat Med.* 2001;7(11):1194-201.

148. Pepper MS. Transforming growth factor-beta: vasculogenesis, angiogenesis, and vessel wall integrity. *Cytokine Growth Factor Rev.* 1997;8(1):21-43.
149. Sun B, Zhang D, Zhang S, et al. Hypoxia influences vasculogenic mimicry channel formation and tumor invasion-related protein expression in melanoma. *Cancer Lett.* 2007;249(2):188-97.
150. Liu XM, Zhang QP, Mu YG, et al. Clinical significance of vasculogenic mimicry in human gliomas. *J Neurooncol.* 2011;105(2):173-9.
151. Wang R, Chadalavada K, Wilshire J, et al. Glioblastoma stem-like cells give rise to tumour endothelium. *Nature.* 2010;468(7325):829-33.
152. Soda Y, Marumoto T, Friedmann-Morvinski D, et al. Transdifferentiation of glioblastoma cells into vascular endothelial cells. *Proc Natl Acad Sci U S A.* 2011;108(11):4274-80.
153. Mahase S, Rattenni RN, Wesseling P, et al. Hypoxia-Mediated Mechanisms Associated with Antiangiogenic Treatment Resistance in Glioblastomas. *Am J Pathol.* 2017;187(5):940-53.
154. Kaur B, Tan C, Brat DJ, et al. Genetic and hypoxic regulation of angiogenesis in gliomas. *J Neurooncol.* 2004;70(2):229-43.
155. Brat DJ, Van Meir EG. Vaso-occlusive and prothrombotic mechanisms associated with tumor hypoxia, necrosis, and accelerated growth in glioblastoma. *Lab Invest.* 2004;84(4):397-405.
156. Leon SP, Folkner RD, Black PM. Microvessel density is a prognostic indicator for patients with astroglial brain tumors. *Cancer.* 1996;77(2):362-72.
157. Fischer I, Gagner JP, Law M, et al. Angiogenesis in gliomas: biology and molecular pathophysiology. *Brain Pathol.* 2005;15(4):297-310.
158. Wolburg H, Noell S, Fallier-Becker P, et al. The disturbed blood-brain barrier in human glioblastoma. *Mol Aspects Med.* 2012;33(5-6):579-89.
159. Pope WB, Sayre J, Perlina A, et al. MR imaging correlates of survival in patients with high-grade gliomas. *AJNR Am J Neuroradiol.* 2005;26(10):2466-74.
160. Cheng SY, Nagane M, Huang HS, et al. Intracerebral tumor-associated hemorrhage caused by overexpression of the vascular endothelial growth factor isoforms VEGF121 and VEGF165 but not VEGF189. *Proc Natl Acad Sci U S A.* 1997;94(22):12081-7.
161. Kim KJ, Li B, Winer J, et al. Inhibition of vascular endothelial growth factor-induced angiogenesis suppresses tumour growth in vivo. *Nature.* 1993;362(6423):841-4.
162. Cheng SY, Huang HJ, Nagane M, et al. Suppression of glioblastoma angiogenicity and tumorigenicity by inhibition of endogenous expression of vascular endothelial growth factor. *Proc Natl Acad Sci U S A.* 1996;93(16):8502-7.
163. Saleh M, Stacker SA, Wilks AF. Inhibition of growth of C6 glioma cells in vivo by expression of antisense vascular endothelial growth factor sequence. *Cancer research.* 1996;56(2):393-401.
164. Plate KH, Breier G, Weich HA, et al. Vascular endothelial growth factor is a potential tumour angiogenesis factor in human gliomas in vivo. *Nature.* 1992;359(6398):845-8.
165. Shweiki D, Itin A, Soffer D, et al. Vascular endothelial growth factor induced by hypoxia may mediate hypoxia-initiated angiogenesis. *Nature.* 1992;359(6398):843-5.
166. Semenza GL, Jiang BH, Leung SW, et al. Hypoxia response elements in the aldolase A, enolase 1, and lactate dehydrogenase A gene promoters contain essential binding sites for hypoxia-inducible factor 1. *J Biol Chem.* 1996;271(51):32529-37.
167. Jiang BH, Agani F, Passaniti A, et al. V-SRC induces expression of hypoxia-inducible factor 1 (HIF-1) and transcription of genes encoding vascular endothelial growth factor and enolase 1: involvement of HIF-1 in tumor progression. *Cancer research.* 1997;57(23):5328-35.
168. Maxwell PH, Dachs GU, Gleadle JM, et al. Hypoxia-inducible factor-1 modulates gene expression in solid tumors and influences both angiogenesis and tumor growth. *Proc Natl Acad Sci U S A.* 1997;94(15):8104-9.
169. Ravi R, Mookerjee B, Bhujwalla ZM, et al. Regulation of tumor angiogenesis by p53-induced degradation of hypoxia-inducible factor 1alpha. *Genes Dev.* 2000;14(1):34-44.
170. Li L, Lin X, Staver M, et al. Evaluating hypoxia-inducible factor-1alpha as a cancer therapeutic target via inducible RNA interference in vivo. *Cancer research.* 2005;65(16):7249-58.
171. Brat DJ, Castellano-Sanchez AA, Hunter SB, et al. Pseudopalisades in glioblastoma are hypoxic, express extracellular matrix proteases, and are formed by an actively migrating cell population. *Cancer research.* 2004;64(3):920-7.
172. Ramos-Vara JA, Miller MA. When tissue antigens and antibodies get along: revisiting the technical aspects of immunohistochemistry--the red, brown, and blue technique. *Vet Pathol.* 2014;51(1):42-87.

173. Leong TY, Leong AS. How does antigen retrieval work? *Adv Anat Pathol*. 2007;14(2):129-31.
174. Rutka JT, Murakami M, Dirks PB, et al. Role of glial filaments in cells and tumors of glial origin: a review. *J Neurosurg*. 1997;87(3):420-30.
175. Deck JH, Eng LF, Bigbee J, et al. The role of glial fibrillary acidic protein in the diagnosis of central nervous system tumors. *Acta Neuropathol*. 1978;42(3):183-90.
176. Eng LF, Rubinstein LJ. Contribution of immunohistochemistry to diagnostic problems of human cerebral tumors. *The journal of histochemistry and cytochemistry : official journal of the Histochemistry Society*. 1978;26(7):513-22.
177. Brat DJ, Prayson RA, Ryken TC, et al. Diagnosis of malignant glioma: role of neuropathology. *J Neurooncol*. 2008;89(3):287-311.
178. Eng LF, Ghirnikar RS, Lee YL. Glial fibrillary acidic protein: GFAP-thirty-one years (1969-2000). *Neurochem Res*. 2000;25(9-10):1439-51.
179. Duffy PE, Huang YY, Rapport MM, et al. Glial fibrillary acidic protein in giant cell tumors of brain and other gliomas. A possible relationship to malignancy, differentiation, and pleomorphism of glia. *Acta Neuropathol*. 1980;52(1):51-7.
180. Peraud A, Mondal S, Hawkins C, et al. Expression of fascin, an actin-bundling protein, in astrocytomas of varying grades. *Brain Tumor Pathol*. 2003;20(2):53-8.
181. Bolduc JM, Dyer DH, Scott WG, et al. Mutagenesis and Laue structures of enzyme intermediates: isocitrate dehydrogenase. *Science*. 1995;268(5215):1312-8.
182. Liu A, Hou C, Chen H, et al. Genetics and Epigenetics of Glioblastoma: Applications and Overall Incidence of IDH1 Mutation. *Front Oncol*. 2016;6:16.
183. Chen L, Voronovich Z, Clark K, et al. Predicting the likelihood of an isocitrate dehydrogenase 1 or 2 mutation in diagnoses of infiltrative glioma. *Neuro-oncology*. 2014;16(11):1478-83.
184. Louis DN, Perry A, Reifenberger G, et al. The 2016 World Health Organization Classification of Tumors of the Central Nervous System: a summary. *Acta Neuropathol*. 2016;131(6):803-20.
185. McComb RD, Jones TR, Pizzo SV, et al. Immunohistochemical detection of factor VIII/von Willebrand factor in hyperplastic endothelial cells in glioblastoma multiforme and mixed glioma-sarcoma. *J Neuropathol Exp Neurol*. 1982;41(5):479-89.
186. Denis CV. Molecular and cellular biology of von Willebrand factor. *Int J Hematol*. 2002;75(1):3-8.
187. McComb RD, Jones TR, Pizzo SV, et al. Specificity and sensitivity of immunohistochemical detection of factor VIII/von Willebrand factor antigen in formalin-fixed paraffin-embedded tissue. *The journal of histochemistry and cytochemistry : official journal of the Histochemistry Society*. 1982;30(4):371-7.
188. Sehested M, Hou-Jensen K. Factor VII related antigen as an endothelial cell marker in benign and malignant diseases. *Virchows Arch A Pathol Anat Histol*. 1981;391(2):217-25.
189. Burrows FJ, Derbyshire EJ, Tazzari PL, et al. Up-regulation of endoglin on vascular endothelial cells in human solid tumors: implications for diagnosis and therapy. *Clin Cancer Res*. 1995;1(12):1623-34.
190. Seon BK, Matsuno F, Haruta Y, et al. Long-lasting complete inhibition of human solid tumors in SCID mice by targeting endothelial cells of tumor vasculature with antihuman endoglin immunotoxin. *Clin Cancer Res*. 1997;3(7):1031-44.
191. Miller DW, Graulich W, Karges B, et al. Elevated expression of endoglin, a component of the TGF-beta-receptor complex, correlates with proliferation of tumor endothelial cells. *Int J Cancer*. 1999;81(4):568-72.
192. Dallas NA, Samuel S, Xia L, et al. Endoglin (CD105): a marker of tumor vasculature and potential target for therapy. *Clin Cancer Res*. 2008;14(7):1931-7.
193. Krupinski J, Kaluza J, Kumar P, et al. Role of angiogenesis in patients with cerebral ischemic stroke. *Stroke*. 1994;25(9):1794-8.
194. Minhaj R, Mori D, Yamasaki F, et al. Organ-specific endoglin (CD105) expression in the angiogenesis of human cancers. *Pathol Int*. 2006;56(12):717-23.
195. Birner P, Piribauer M, Fischer I, et al. Vascular patterns in glioblastoma influence clinical outcome and associate with variable expression of angiogenic proteins: evidence for distinct angiogenic subtypes. *Brain Pathol*. 2003;13(2):133-43.
196. Yao Y, Kubota T, Takeuchi H, et al. Prognostic significance of microvessel density determined by an anti-CD105/endoglin monoclonal antibody in astrocytic tumors: comparison with an anti-CD31 monoclonal antibody. *Neuropathology*. 2005;25(3):201-6.
197. Wang JM, Kumar S, Pye D, et al. Breast carcinoma: comparative study of tumor vasculature using two endothelial cell markers. *J Natl Cancer Inst*. 1994;86(5):386-8.

198. Gerdes J, Li L, Schlueter C, et al. Immunobiochemical and molecular biologic characterization of the cell proliferation-associated nuclear antigen that is defined by monoclonal antibody Ki-67. *Am J Pathol.* 1991;138(4):867-73.
199. Sobecki M, Mrouj K, Colinge J, et al. Cell-Cycle Regulation Accounts for Variability in Ki-67 Expression Levels. *Cancer research.* 2017;77(10):2722-34.
200. Sun X, Kaufman PD. Ki-67: more than a proliferation marker. *Chromosoma.* 2018;127(2):175-86.
201. Key G, Becker MH, Baron B, et al. New Ki-67-equivalent murine monoclonal antibodies (MIB 1-3) generated against bacterially expressed parts of the Ki-67 cDNA containing three 62 base pair repetitive elements encoding for the Ki-67 epitope. *Lab Invest.* 1993;68(6):629-36.
202. Mehrara E, Forssell-Aronsson E, Ahlman H, et al. Specific growth rate versus doubling time for quantitative characterization of tumor growth rate. *Cancer research.* 2007;67(8):3970-5.
203. Osborn AG. Astrocytomas. In: Renlund AR, editor. *Osborn's Brain: Imaging, Pathology and Anatomy.* First ed. Altona, Manitoba, Canada: Amirsys Publishing, Inc.; 2013. p. 484-90.
204. Brat DJ, Aldape K, Colman H, et al. cIMPACT-NOW update 5: recommended grading criteria and terminologies for IDH-mutant astrocytomas. *Acta Neuropathol.* 2020;139(3):603-8.
205. Stensjøen AL, Berntsen EM, Mikkelsen VE, et al. Does Pretreatment Tumor Growth Hold Prognostic Information for Patients with Glioblastoma? *World Neurosurg.* 2017;101:686-94.e4.
206. Kleihues P, Burger P, Aldape K, et al. Glioblastoma. In: Louis DN, Ohgaki H, Wiestler O, Cavenee WK, editors. *WHO Classification of Tumours of the Central Nervous System.* 4th Edition ed. Lyon: International Agency of Research on Cancer (IARC); 2007. p. 33-49.
207. Weidner N, Semple JP, Welch WR, et al. Tumor angiogenesis and metastasis--correlation in invasive breast carcinoma. *N Engl J Med.* 1991;324(1):1-8.
208. Kraby MR, Kruger K, Opdahl S, et al. Microvascular proliferation in luminal A and basal-like breast cancer subtypes. *J Clin Pathol.* 2015;68(11):891-7.
209. Stummer W, Reulen HJ, Meinel T, et al. Extent of resection and survival in glioblastoma multiforme: identification of and adjustment for bias. *Neurosurgery.* 2008;62(3):564-76; discussion -76.
210. Nakajima M, Nakasu S, Morikawa S, et al. Estimation of volume doubling time and cell loss in an experimental rat glioma model in vivo. *Acta neurochirurgica.* 1998;140(6):607-12; discussion 12-3.
211. Rong Y, Durden DL, Van Meir EG, et al. 'Pseudopalisading' necrosis in glioblastoma: a familial morphologic feature that links vascular pathology, hypoxia, and angiogenesis. *J Neuropathol Exp Neurol.* 2006;65(6):529-39.
212. Unruh D, Schwarze SR, Khoury L, et al. Mutant IDH1 and thrombosis in gliomas. *Acta Neuropathol.* 2016;132(6):917-30.
213. Prayson NF, Koch P, Angelov L, et al. Microscopic thrombi in anaplastic astrocytoma predict worse survival? *Ann Diagn Pathol.* 2011;15(6):389-93.
214. Unruh D, Mirkov S, Wray B, et al. Methylation-dependent Tissue Factor Suppression Contributes to the Reduced Malignancy of IDH1-mutant Gliomas. *Clin Cancer Res.* 2019;25(2):747-59.
215. Song Y, Zheng S, Wang J, et al. Hypoxia-induced PLOD2 promotes proliferation, migration and invasion via PI3K/Akt signaling in glioma. *Oncotarget.* 2017;8(26):41947-62.
216. DeLay M, Jahangiri A, Carbonell WS, et al. Microarray analysis verifies two distinct phenotypes of glioblastomas resistant to antiangiogenic therapy. *Clin Cancer Res.* 2012;18(10):2930-42.
217. Keunen O, Johansson M, Oudin A, et al. Anti-VEGF treatment reduces blood supply and increases tumor cell invasion in glioblastoma. *Proc Natl Acad Sci U S A.* 2011;108(9):3749-54.
218. de Groot JF, Fuller G, Kumar AJ, et al. Tumor invasion after treatment of glioblastoma with bevacizumab: radiographic and pathologic correlation in humans and mice. *Neuro-oncology.* 2010;12(3):233-42.
219. Li ZC, Bai H, Sun Q, et al. Multiregional radiomics features from multiparametric MRI for prediction of MGMT methylation status in glioblastoma multiforme: A multicentre study. *Eur Radiol.* 2018;28(9):3640-50.
220. Xi YB, Guo F, Xu ZL, et al. Radiomics signature: A potential biomarker for the prediction of MGMT promoter methylation in glioblastoma. *J Magn Reson Imaging.* 2018;47(5):1380-7.
221. Hajianfar G, Shiri I, Maleki H, et al. Noninvasive O6 Methylguanine-DNA Methyltransferase Status Prediction in Glioblastoma Multiforme Cancer Using Magnetic Resonance Imaging Radiomics Features: Univariate and Multivariate Radiogenomics Analysis. *World Neurosurg.* 2019;132:e140-e61.
222. Wick W, Meisner C, Hentschel B, et al. Prognostic or predictive value of MGMT promoter methylation in gliomas depends on IDH1 mutation. *Neurology.* 2013;81(17):1515-22.

223. Marchevsky AM, Wick MR. Evidence-based pathology: systematic literature reviews as the basis for guidelines and best practices. *Archives of pathology & laboratory medicine*. 2015;139(3):394-9.
224. McShane LM, Altman DG, Sauerbrei W, et al. REporting recommendations for tumour MARKer prognostic studies (REMARK). *Br J Cancer*. 2005;93(4):387-91.
225. Ginsburg GS, Willard HF. Genomic and personalized medicine: foundations and applications. *Transl Res*. 2009;154(6):277-87.
226. Sakariassen PO, Prestegarden L, Wang J, et al. Angiogenesis-independent tumor growth mediated by stem-like cancer cells. *Proc Natl Acad Sci U S A*. 2006;103(44):16466-71.
227. Reardon DA, Galanis E, DeGroot JF, et al. Clinical trial end points for high-grade glioma: the evolving landscape. *Neuro-oncology*. 2011;13(3):353-61.
228. Gammon K. Mathematical modelling: Forecasting cancer. *Nature*. 2012;491(7425):S66-7.
229. Prados MD, Byron SA, Tran NL, et al. Toward precision medicine in glioblastoma: the promise and the challenges. *Neuro-oncology*. 2015;17(8):1051-63.
230. Roth P, Mason WP, Richardson PG, et al. Proteasome inhibition for the treatment of glioblastoma. Expert opinion on investigational drugs. 2020:1-9.
231. Binabaj MM, Bahrami A, ShahidSales S, et al. The prognostic value of MGMT promoter methylation in glioblastoma: A meta-analysis of clinical trials. *J Cell Physiol*. 2018;233(1):378-86.
232. Clark GM. Prognostic factors versus predictive factors: Examples from a clinical trial of erlotinib. *Mol Oncol*. 2008;1(4):406-12.
233. Hegi ME, Liu L, Herman JG, et al. Correlation of O6-methylguanine methyltransferase (MGMT) promoter methylation with clinical outcomes in glioblastoma and clinical strategies to modulate MGMT activity. *J Clin Oncol*. 2008;26(25):4189-99.
234. Brandes AA, Franceschi E, Ermani M, et al. Pattern of care and effectiveness of treatment for glioblastoma patients in the real world: Results from a prospective population-based registry. Could survival differ in a high-volume center? *Neuro-oncology practice*. 2014;1(4):166-71.
235. Yang P, Wang Y, Peng X, et al. Management and survival rates in patients with glioma in China (2004-2010): a retrospective study from a single-institution. *J Neurooncol*. 2013;113(2):259-66.
236. Hegi ME, Janzer RC, Lambiv WL, et al. Presence of an oligodendroglioma-like component in newly diagnosed glioblastoma identifies a pathogenetically heterogeneous subgroup and lacks prognostic value: central pathology review of the EORTC_26981/NCIC_CE.3 trial. *Acta Neuropathol*. 2012;123(6):841-52.
237. Hawkins C, Ellison DW, Sturm D. Diffuse midline glioma, H3 K27M-mutant. In: Louis DN, Ohgaki H, Wiestler OT, Cavenee WK, editors. *WHO Classification of Tumours of the Central Nervous System*. Revised 4th Edition ed. Lyon: International Agency for Research on Cancer (IARC); 2016. p. 57-9.
238. Louis DN, Suva ML, Burger P, et al. Glioblastoma, IDH-wildtype. In: Louis DN, Ohgaki H, Wiestler OT, Cavenee WK, editors. *WHO Classification of Tumours of the Central Nervous System*. Revised 4th Edition ed. Lyon: International Agency for Research on Cancer (IARC); 2016. p. 28-51.
239. Fyllingen EH, Stensj en AL, Berntsen EM, et al. Glioblastoma Segmentation: Comparison of Three Different Software Packages. *PLoS One*. 2016;11(10):e0164891.
240. Jackson RJ, Fuller GN, Abi-Said D, et al. Limitations of stereotactic biopsy in the initial management of gliomas. *Neuro-oncology*. 2001;3(3):193-200.
241. Vaquero J, Martinez R, Manrique M. Stereotactic biopsy for brain tumors: is it always necessary? *Surg Neurol*. 2000;53(5):432-7; discussion 7-8.
242. Muller MB, Schmidt MC, Schmidt O, et al. Molecular genetic analysis as a tool for evaluating stereotactic biopsies of glioma specimens. *J Neuropathol Exp Neurol*. 1999;58(1):40-5.
243. Glantz MJ, Burger PC, Herndon JE, 2nd, et al. Influence of the type of surgery on the histologic diagnosis in patients with anaplastic gliomas. *Neurology*. 1991;41(11):1741-4.
244. Chandrasoma PT, Smith MM, Apuzzo ML. Stereotactic biopsy in the diagnosis of brain masses: comparison of results of biopsy and resected surgical specimen. *Neurosurgery*. 1989;24(2):160-5.
245. Reithmeier T, Lopez WO, Doostkam S, et al. Intraindividual comparison of histopathological diagnosis obtained by stereotactic serial biopsy to open surgical resection specimen in patients with intracranial tumours. *Clin Neurol Neurosurg*. 2013;115(10):1955-60.
246. Bruner JM, Inouye L, Fuller GN, et al. Diagnostic discrepancies and their clinical impact in a neuropathology referral practice. *Cancer*. 1997;79(4):796-803.
247. McCullough BJ, Ader V, Aguedan B, et al. Preoperative relative cerebral blood volume analysis in gliomas predicts survival and mitigates risk of biopsy sampling error. *J Neurooncol*. 2018;136(1):181-8.

248. Kim BYS, Jiang W, Beiko J, et al. Diagnostic discrepancies in malignant astrocytoma due to limited small pathological tumor sample can be overcome by IDH1 testing. *J Neurooncol.* 2014;118(2):405-12.
249. Prayson RA. Cell proliferation and tumors of the central nervous system. Part 1: Evaluation of mitotic activity. *J Neuropathol Exp Neurol.* 2002;61(6):501-9.
250. Preusser M, Heinzl H, Gelpi E, et al. Histopathologic assessment of hot-spot microvessel density and vascular patterns in glioblastoma: Poor observer agreement limits clinical utility as prognostic factors: a translational research project of the European Organization for Research and Treatment of Cancer Brain Tumor Group. *Cancer.* 2006;107(1):162-70.
251. Kumar S, Ghellal A, Li C, et al. Breast carcinoma: vascular density determined using CD105 antibody correlates with tumor prognosis. *Cancer research.* 1999;59(4):856-61.
252. Sica G, Lama G, Anile C, et al. Assessment of angiogenesis by CD105 and nestin expression in peritumor tissue of glioblastoma. *Int J Oncol.* 2011;38(1):41-9.
253. Afshar Moghaddam N, Mahsuni P, Taheri D. Evaluation of Endoglin as an Angiogenesis Marker in Glioblastoma. *Iranian journal of pathology.* 2015;10(2):89-96.
254. Flynn JR, Wang L, Gillespie DL, et al. Hypoxia-regulated protein expression, patient characteristics, and preoperative imaging as predictors of survival in adults with glioblastoma multiforme. *Cancer.* 2008;113(5):1032-42.
255. Behrem S, Zarkovic K, Eskinja N, et al. Endoglin is a better marker than CD31 in evaluation of angiogenesis in glioblastoma. *Croat Med J.* 2005;46(3):417-22.
256. Eberhard A, Kahlert S, Goede V, et al. Heterogeneity of angiogenesis and blood vessel maturation in human tumors: implications for antiangiogenic tumor therapies. *Cancer research.* 2000;60(5):1388-93.
257. Kraby MR, Opdahl S, Russnes HG, et al. Microvessel density in breast cancer: the impact of field area on prognostic informativeness. *J Clin Pathol.* 2019;72(4):304-10.
258. Vermeulen PB, Gasparini G, Fox SB, et al. Second international consensus on the methodology and criteria of evaluation of angiogenesis quantification in solid human tumours. *Eur J Cancer.* 2002;38(12):1564-79.
259. Offersen BV, Borre M, Overgaard J. Quantification of angiogenesis as a prognostic marker in human carcinomas: a critical evaluation of histopathological methods for estimation of vascular density. *Eur J Cancer.* 2003;39(7):881-90.
260. Rakocevic J, Orlic D, Mitrovic-Ajtic O, et al. Endothelial cell markers from clinician's perspective. *Exp Mol Pathol.* 2017;102(2):303-13.
261. Balza E, Castellani P, Zijlstra A, et al. Lack of specificity of endoglin expression for tumor blood vessels. *Int J Cancer.* 2001;94(4):579-85.
262. Matsubara S, Bourdeau A, terBrugge KG, et al. Analysis of endoglin expression in normal brain tissue and in cerebral arteriovenous malformations. *Stroke.* 2000;31(11):2653-60.
263. Hlatky L, Hahnfeldt P, Folkman J. Clinical application of antiangiogenic therapy: microvessel density, what it does and doesn't tell us. *J Natl Cancer Inst.* 2002;94(12):883-93.
264. Prayson RA. Cell proliferation and tumors of the central nervous system, part II: radiolabeling, cytometric, and immunohistochemical techniques. *J Neuropathol Exp Neurol.* 2002;61(8):663-72.
265. Moskowitz SI, Jin T, Prayson RA. Role of MIB1 in predicting survival in patients with glioblastomas. *J Neurooncol.* 2006;76(2):193-200.
266. Grzybicki DM, Liu Y, Moore SA, et al. Interobserver variability associated with the MIB-1 labeling index: high levels suggest limited prognostic usefulness for patients with primary brain tumors. *Cancer.* 2001;92(10):2720-6.
267. McKeever PE, Ross DA, Strawderman MS, et al. A comparison of the predictive power for survival in gliomas provided by MIB-1, bromodeoxyuridine and proliferating cell nuclear antigen with histopathologic and clinical parameters. *J Neuropathol Exp Neurol.* 1997;56(7):798-805.
268. Wakimoto H, Aoyagi M, Nakayama T, et al. Prognostic significance of Ki-67 labeling indices obtained using MIB-1 monoclonal antibody in patients with supratentorial astrocytomas. *Cancer.* 1996;77(2):373-80.
269. Matos LL, Trufelli DC, de Matos MG, et al. Immunohistochemistry as an important tool in biomarkers detection and clinical practice. *Biomarker insights.* 2010;5:9-20.
270. Jacobs TW, Prioleau JE, Stillman IE, et al. Loss of tumor marker-immunostaining intensity on stored paraffin slides of breast cancer. *J Natl Cancer Inst.* 1996;88(15):1054-9.
271. Parker NR, Hudson AL, Khong P, et al. Intratumoral heterogeneity identified at the epigenetic, genetic and transcriptional level in glioblastoma. *Sci Rep.* 2016;6:22477.

272. Bady P, Sciuscio D, Diserens AC, et al. MGMT methylation analysis of glioblastoma on the Infinium methylation BeadChip identifies two distinct CpG regions associated with gene silencing and outcome, yielding a prediction model for comparisons across datasets, tumor grades, and CIMP-status. *Acta Neuropathol.* 2012;124(4):547-60.
273. Malley DS, Hamoudi RA, Kociałkowski S, et al. A distinct region of the MGMT CpG island critical for transcriptional regulation is preferentially methylated in glioblastoma cells and xenografts. *Acta Neuropathol.* 2011;121(5):651-61.
274. Altman DG, Royston P. The cost of dichotomising continuous variables. *BMJ.* 2006;332(7549):1080.
275. Reuss DE, Kratz A, Sahm F, et al. Adult IDH wild type astrocytomas biologically and clinically resolve into other tumor entities. *Acta Neuropathol.* 2015;130(3):407-17.
276. Louis DN, Wesseling P, Aldape K, et al. cIMPACT-NOW update 6: new entity and diagnostic principle recommendations of the cIMPACT-Utrecht meeting on future CNS tumor classification and grading. *Brain Pathol.* 2020;30(4):844-56.
277. Louis DN, Aldape K, Brat DJ, et al. Announcing cIMPACT-NOW: the Consortium to Inform Molecular and Practical Approaches to CNS Tumor Taxonomy. *Acta Neuropathol.* 2017;133(1):1-3.
278. Miller AM, Shah RH, Pentsova EI, et al. Tracking tumour evolution in glioma through liquid biopsies of cerebrospinal fluid. *Nature.* 2019;565(7741):654-8.
279. Andronesi OC, Rapalino O, Gerstner E, et al. Detection of oncogenic IDH1 mutations using magnetic resonance spectroscopy of 2-hydroxyglutarate. *J Clin Invest.* 2013;123(9):3659-63.
280. Szeto MD, Chakraborty G, Hadley J, et al. Quantitative metrics of net proliferation and invasion link biological aggressiveness assessed by MRI with hypoxia assessed by FMISO-PET in newly diagnosed glioblastomas. *Cancer research.* 2009;69(10):4502-9.
281. Menze BH, Jakab A, Bauer S, et al. The Multimodal Brain Tumor Image Segmentation Benchmark (BRATS). *IEEE Trans Med Imaging.* 2015;34(10):1993-2024.
282. Rathore S, Niazi T, Iftikhar MA, et al. Glioma Grading via Analysis of Digital Pathology Images Using Machine Learning. *Cancers (Basel).* 2020;12(3).
283. Mobadersany P, Yousefi S, Amgad M, et al. Predicting cancer outcomes from histology and genomics using convolutional networks. *Proc Natl Acad Sci U S A.* 2018;115(13):E2970-e9.

14 Publications

Paper I



Histopathologic Features in Relation to Pretreatment Tumor Growth in Patients with Glioblastoma

Vilde Elisabeth Mikkelsen¹, Anne Line Stensjøen^{2,3}, Erik Magnus Berntsen^{2,3}, Ivar Skjåk Nordrum^{1,7}, Øyvind Salvesen¹, Ole Solheim^{4,6}, Sverre Helge Torp^{1,7}

■ BACKGROUND: Rapid growth is a well-known property of glioblastoma (GBM); however, growth rates vary among patients. Mechanisms behind such variation have not been widely studied in human patients. We sought to investigate relationships between histopathologic features and tumor growth estimated from pretreatment magnetic resonance imaging scans.

■ METHODS: In 106 patients with GBM, 2 preoperative T1-weighted magnetic resonance imaging scans obtained at least 14 days apart were segmented to assess tumor growth. A fitted Gompertzian growth curve based on the segmented volumes divided the tumors into 2 groups: faster and slower growth than expected based on the initial tumor volume. Histopathologic features were investigated for associations with these groups, using univariable and multivariable logistic regression analyses.

■ RESULTS: The presence of high cellular density and thromboses was significantly associated with radiologic growth in the multivariable analysis ($P = 0.018$ and 0.019 , respectively), with respective odds ratios of 3.0 (95% confidence interval, 1.2–7.4) and 4.3 (95% confidence interval, 1.3–14.5) for faster growing tumors.

■ CONCLUSIONS: Our findings show that high cellular density and thromboses are significant independent predictors of faster growth in human GBM. This finding underlines the importance of hypercellularity as a criterion

in glioma grading. Furthermore, our findings are concordant with hypotheses suggesting hypoxia triggered by thromboses to be relevant for growth of GBM.

INTRODUCTION

Human glioblastomas (GBMs) are known for their rapid growth,^{1,2} short overall survival,³ lack of effective therapies,⁴ and vast intertumoral and intratumoral heterogeneity both genetically and histologically.⁵

Because GBMs are highly aggressive, patients with GBM are often operated on rapidly after being detected with computed tomography or magnetic resonance imaging (MRI). This factor makes it difficult to obtain pretreatment growth data necessary for studying unaffected growth mechanisms of human GBM. We have recently examined the pretreatment growth dynamics of 106 patients with GBM based on volume segmentation acquired from preoperative MRI scans.¹ The results showed a median daily volumetric growth of 1.4% and an equivalent volume doubling time of 49.6 days. However, there was considerable variation in growth rates across the patients examined. Large tumors grew significantly slower than their smaller counterparts, and our findings supported the assumption that GBMs follow a Gompertzian growth pattern (Figure 1).¹ This growth pattern is characterized by a progressive decrease in speed of growth because of lack of nutrients as the tumor volume increases, leading to a final plateau phase.⁶

Key words

- Glioblastoma
- Histopathology
- Magnetic resonance imaging
- Tumor biology
- Tumor growth
- Tumor hypoxia

Abbreviations and Acronyms

- GBM:** Glioblastoma
- HIF-1 α :** Hypoxia inducible factor 1 α
- IDH:** Isocitrate dehydrogenase
- MRI:** Magnetic resonance imaging
- PI:** Proliferative index

From the Departments of ¹Clinical and Molecular Medicine and ²Circulation and Medical Imaging, Faculty of Medicine and Health Sciences, NTNU—Norwegian University of Science and Technology, Trondheim; Departments of ³Radiology and Nuclear Medicine, ⁴Neurosurgery, and ⁵National Advisory Unit for Ultrasound and Image-Guided Therapy, St. Olavs University Hospital, Trondheim, Norway; ⁶Department of Neuromedicine and Movement Science, Faculty of Medicine and Health Sciences, NTNU—Norwegian University of Science and Technology, Trondheim; ⁷Department of Pathology, St. Olavs University Hospital, Trondheim, Norway

To whom correspondence should be addressed: Vilde Elisabeth Mikkelsen [E-mail: vildeem@stud.ntnu.no]

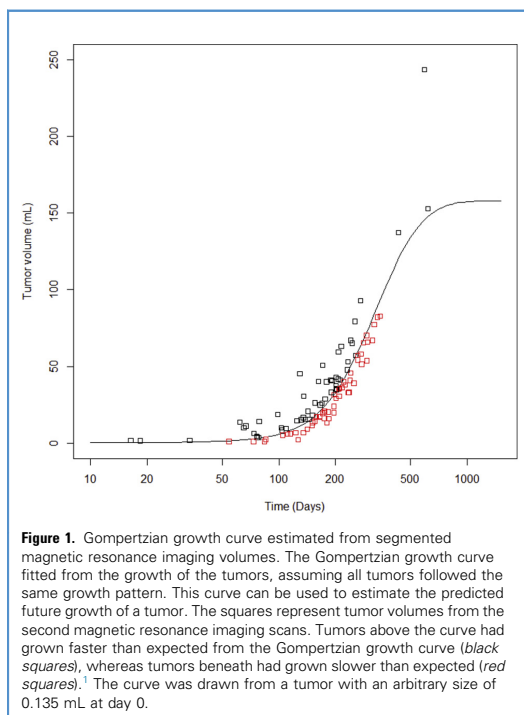
Citation: World Neurosurg. (2018) 109:e50–e58.

<https://doi.org/10.1016/j.wneu.2017.09.102>

Journal homepage: www.WORLDNEUROSURGERY.org

Available online: www.sciencedirect.com

1878-8750/\$ - see front matter © 2017 Elsevier Inc. All rights reserved.



Few studies have explored the growth dynamics of human GBM,^{1,2,7-13} and even fewer have examined the biological processes behind growth rate variability.^{9,13} We aimed to investigate possible associations between histopathologic features and pre-operative tumor growth, to clarify whether variations in tumor growth can be explained by such features.

METHODS

Inclusion and Exclusion Criteria

All patients ≥ 18 years old with assumed primary GBMs (without clinical evidence of a previous lower-grade lesion) operated on between January 2004 and May 2014 at St. Olavs Hospital—Trondheim University Hospital, Norway (262 patients) were retrospectively evaluated for inclusion. Here, patients had to have at least 2 preoperative contrast-enhanced T1-weighted MRIs, separated by a minimum gap of 14 days (i.e., initially the diagnostic scan and subsequently the preoperative scan). The median time interval between the 2 MRIs was 23.5 days (range, 14–98 days). Patients with tumors lacking contrast enhancement and/or gliomatosis cerebri according to radiologic criteria¹⁴ were excluded. All cases were microscopically revised for diagnosis by V.E.M. (a medical student) and controlled by S.H.T. (an experienced pathologist), using the 2007 World Health Organization classification system.¹⁵ One case was rediagnosed as an anaplastic astrocytoma grade III and excluded. This action

left a total of 106 patients eligible for further analyses. The study was approved by the regional committee for medical and health research ethics and adhered to the Declaration of Helsinki.

Histopathologic Evaluation

Histologic sections from surgical specimens (89 cases) and biopsies (17 cases) were examined on all available hematoxylin-eosin–stained formalin-fixed paraffin-embedded sections (including formalin-fixed paraffin-embedded frozen sections) for 30 histopathologic features possibly affecting tumor growth (listed in Table 1). The assessment of histopathologic features was performed by V.E.M. and controlled by S.H.T. All cases except 1 had available paraffin sections for the evaluation, and almost all cases (except 9) had additional formalin-fixed paraffin-embedded frozen sections. Moreover, all cases were recorded for histologic presence of central tumor areas (105 cases), infiltration zones (i.e., presence of normal brain tissue intermingled with tumor cells) (78 cases), infiltration zones into gray matter (i.e., presence of neurons) (66 cases), and outer brain surface (45 cases).

Most histopathologic features were registered as either present or absent, and only conspicuous features were recorded to reduce observer variability. Cellular density, atypia, and vascular density were semiquantitatively graded. Mitoses were counted in hotspots from 10 high power fields, preferably in paraffin sections with adequate morphology for identification and counting of mitotic figures. However, 3 cases were counted on formalin-fixed paraffin-embedded frozen sections because of insufficient morphology on the paraffin sections, and 1 case could not be counted because of inadequate morphology on all paraffin and frozen sections. The amount of tumor tissue varied across cases, and 49 contained small amounts of viable tissue material as a result of extensive necrosis or small biopsies. Nonetheless, the amount of material in these cases was still sufficient for evaluation of the histopathologic features.

Immunohistochemical Analyses

All cases underwent standard immunohistochemical analyses carried out on a Dako Autostainer (Dako Denmark AS, Glostrup, Denmark). Visualization of immunoreactivity was performed with the Dako Envision system. Paraffin sections, 4 μ m thick, were incubated with antibodies against glial fibrillary acidic protein (rabbit, polyclonal, dilution 1:2000 for 65 cases and 1:10 000 for the others [Dako Denmark AS]) and isocitrate dehydrogenase 1 mutation (IDH1 R132H, monoclonal, dilution 1:100 [Dianova, Hamburg, Germany]) using standard procedures as described earlier.¹⁶

Tumor Volume Segmentation and Growth Estimates

A.L.S. performed the manual segmentation of tumor volumes using the software BrainVoyager QX (Brain Innovation, Maastricht, The Netherlands), and a neuroradiologist, E.M.B., validated the segmentations. Total tumor volume was defined as the combined volume of contrast-enhancing and central non-contrast-enhancing compartments (i.e., necrosis). In cases with multiple lesions per patient, all were segmented and combined in the total tumor volume. A more elaborate description of the segmentation procedure was reported previously.¹

Table 1. Frequencies of Histopathologic Features and Criteria for Categorization

Histopathologic Features	% (n), n = 106	Comments and Criteria for Categorization
Necroses		
Large	90 (95)	Large areas of infarct-like tumor necrosis
Small	83 (88)	Smaller areas of necrotic tissue, with or without pseudopalisades
Both	73 (77)	
Microvascular proliferation	76 (81)	Two or more layers of cells in the vascular wall
Central	69 (73/105*)	
Peripheral	41 (32/78†)	
Pseudopalisades	70 (74/105*)	Accumulated cells present at the rim of either large or small necrotic areas
Cellular density		Categorization based on a subjective assessment of the mean distances between neoplastic cells for all available viable tumor material, preferably in central tumor areas. See Figure 2A–C , for examples of each of the respective categories
Low	5 (5)	
Intermediate	65 (69)	
High	30 (32)	
Atypia		Subjective assessment of the variability in cellular and nuclear size and shape of all available viable tumor material. See Figure 2E, B, and D for examples of each of the respective categories
Mild	3 (3)	
Moderate	76 (81)	
Severe	21 (22)	
Mitotic count	Median count: 11 Range, 0–65	Number of cases with 0 mitoses: 6 Total number of cases: 105‡ Mitotic figures counted in 10 high power fields with the highest density of mitotic figures (hot spots)
Vascular features		
Thromboses	83 (88)	Vessels either partly or completely occluded with fibrin. See Figure 2D , as an example
Hemorrhage	79 (84)	Extravascular erythrocytes and fibrin, often co-occurring with perivascular neutrophils, damaged vascular walls, or cellular debris. Also, the mere presence of hemosiderin-containing macrophages was sufficient for the categorization
Pseudorosettes	21 (22/103§)	Perivascular tumor cells forming rosettes surrounding smaller vessels with sparse amounts of vascular connective tissue. Distinct eosinophilic area between the vascular wall and the nuclei of the surrounding cells
Vascular density		Subjective assessment of the mean distances between separate blood vessels for all available viable tumor material, preferably in central tumor areas. See Figure 2F, B, and C , for examples of each of the respective categories
Low	6 (6)	
Intermediate	59 (62)	
High	36 (38)	
Secondary structures of Scherer		These phenomena were assessed solely in cases containing infiltration zones into gray matter (n = 66)
Perineuronal satellitosis	50 (33/66)	Neoplastic cells surrounding neurons
Angiocentric structures	41 (27/66)	Neoplastic cells located adjacent to capillaries or smaller vessels
Subpial clustering	27 (12/45)	Densely packed neoplastic cells just below the pial layer of the meninges
One or more feature	67 (45/66)	
All 3 features	12 (8/66)	
Desmoplasia	63 (67)	Areas of distinct fibrovascular tissue with extracellular collagen deposits
Leukocytes		
Macrophages	93 (99)	Cells with distinct and characteristic morphology of microglia/macrophages
Lymphocytic infiltration	64 (68)	Perivascular accumulation or larger infiltrates in viable tumor tissue
Glioblastoma subtypes		

Continues

Table 1. Continued

Histopathologic Features	% (n), n = 106	Comments and Criteria for Categorization
Small cell glioblastoma	15 (16)	Tumor tissue containing >75% small cells with high nucleocytoplasmic ratio and round, oval, or angular shapes
Giant cell glioblastoma	1 (1)	Tumor tissue dominated by giant cells (see definition below)
Gliosarcoma	1 (1)	Biphasic pattern of sarcomatous and classic glioblastoma morphology. Sarcomatous component clearly demarcated and negatively stained for glial fibrillary acidic protein
Cell types		
Gemistocytes	22 (23)	Tumor cells with large eosinophilic cytoplasm and eccentric nuclei
Small cell component	20 (21)	Focal areas with small cells (see above)
Sarcomatous cells	18 (19)	Elongated spindle cells, often in bundles
Myxomatoid component	13 (14)	Loosely woven tissue of elongated cells with mucinous extracellular substance
Giant cells	9 (10)	Abnormally large and bizarre cells with irregular nuclei
Primitive neuronal component	8 (8)	Densely packed small hyperchromatic neuroblast-like cells with high nucleocytoplasmic ratio
Oligodendroglial component	7 (7)	Smaller, monotonous hyperchromatic cells with perinuclear haloes, chicken wire vasculature, and/or microcalcifications
<p>*Assessed only in tumors with central tumor morphology (n = 105).</p> <p>†Assessed only in cases with present infiltration zones into either gray or white matter (n = 78).</p> <p>‡Assessed only in cases with adequate morphology for counting of mitoses (n = 105).</p> <p>§Assessed only in cases with paraffin sections with viable central tumor areas (n = 103).</p> <p> Assessed only in cases containing outer brain surface (i.e., cases containing leptomeninges or, alternatively, cases containing ≥2 of the following features: molecular cortical layer, corpora amylacea, or glia limitans (n = 45)).</p>		

Because growth rates were correlated with tumor volume for these 106 patients,¹ a point estimate of growth is likely a poor representation of tumor biology. In our previous study,¹ we concluded that the growth of untreated GBMs was best described by a Gompertzian growth curve, as shown in Figure 1. In the current study, the Gompertzian growth curve, with growth parameters estimated as described previously,¹ was used to separate the patients into 2 groups: patients with tumors growing faster than expected from their initial volume (volumes above the curve) and patients with tumors growing slower than expected (volumes beneath the curve) (Figure 1). These growth groups have previously been shown to be associated with patient survival.¹⁷ In the current study, these groups formed the basis for the investigation of relations to histopathologic features.

Statistical Analyses

Statistical analyses regarding growth estimates and fitted growth patterns were computed using R version 2.13.1 (R Foundation for Statistical Computing, Vienna, Austria), whereas analyses investigating relations between histopathology and speed of growth were conducted using SPSS Statistics version 21 (IBM Corp., Armonk, New Jersey, USA). The significance level was set to $P < 0.05$. Before the logistic regression analyses were conducted, the 3 ordinal variables (cellular density, atypia, and vascular density) were dichotomized by merging the 2 lower categories; few cases were assigned to the lowest of these. Possible associations between the group of faster growing tumors and the histopathologic features were examined using univariable and multivariable

binary logistic regression analyses. The multivariable analysis with the highest number of significant independent predictors was selected.

RESULTS

Patient Characteristics

The age and sex distributions of the 106 patients included, with 72 men (68%) and a mean age of 63 years (range, 26–83 years), were not significantly different from the excluded patients.¹ Eighty-six patients (81%) received corticosteroids before surgery, and the median tumor volume was 17.7 mL (range, 0.05–146.5 mL) in the first MRI scans and 27.5 mL (range, 0.98–243.5 mL) in the second MRI scans.

Immunohistochemical Analyses

All cases were immunoreactive for glial fibrillary acidic protein and 2 for IDH1 R132H.

Histopathology

Frequencies of the recorded histopathologic features are listed in Table 1. Necroses were present in all cases, and perinecrotic pseudopalisades were observed in relation to both large and small necroses. Microvascular proliferation was frequently encountered, most commonly in central tumor areas. The secondary structures of Scherer were possible to assess in most of the cases, and 1 or more of these phenomena appeared frequently (most commonly, perineuronal satellitosis).

Table 2. Proportions of Histologic Features in the Two Groups of Growth with *P* Values from Univariable Binary Logistic Regression Analyses

Histopathologic Features	Tumors Growing Slower Than Expected (n = 53), n (%)	Tumors Growing Faster Than Expected (n = 53), n (%)	<i>P</i> Values*
Necroses			
Large	87 (46)	93 (49)	0.345
Small	83 (44)	83 (44)	1.000
Microvascular proliferation	79 (42)	74 (39)	0.493
Central (n = 105†)	69 (36/52)	70 (37)	0.948
Peripheral (n = 78§)	50 (20/40)	32 (12/38)	0.101
Pseudopalisade (n = 105‡)	71 (37/52)	70 (37)	0.880
High cellular density	19 (10)	42 (22)	0.013†
Severe atypia	21 (11)	21 (11)	1.000
Mitotic count (n = 105)	Median count: 7 Range, 0–64	Median count: 15 Range, 0–65	0.026†
Vascular features			
Thromboses	74 (39)	93 (49)	0.015†
Hemorrhage	81 (43)	77 (41)	0.632
Pseudorosettes (n=103¶)	18 (9/51)	25 (13/52)	0.365
High vascular density	36 (19)	36 (19)	1.000
Secondary structures of Scherer			
One or more feature (n=66#)	65 (22/34)	69 (22/32)	0.728
Perineuronal satellitosis (n=66#)	44 (15/34)	56 (18/32)	0.326
Angiocentric structures (n=66#)	35 (12/34)	47 (15/32)	0.340
Subpial clustering (n=45**)	25 (6/24)	29 (6/21)	0.787
Desmoplasia	72 (38)	55 (29)	0.072
Leukocytes			
Macrophages	93 (49)	94 (50)	0.697
Lymphocytes	68 (36)	60 (32)	0.419
Glioblastoma subtypes			
Small cell glioblastoma	9 (5)	21 (11)	0.111
Giant cell glioblastoma	2 (1)	0 (0)	1.000
Gliosarcoma	2 (1)	0 (0)	1.000
Continues			

Table 2. Continued

Histopathologic Features	Tumors Growing Slower Than Expected (n = 53), n (%)	Tumors Growing Faster Than Expected (n = 53), n (%)	<i>P</i> Values*
Cell types			
Gemistocytes	23 (12)	21 (11)	0.814
Small cells	26 (14)	13 (7)	0.093
Sarcomatous cells	23 (12)	13 (7)	0.210
Myxomatoid areas	17 (9)	9 (5)	0.257
Giant cells	8 (4)	11 (6)	0.509
Primitive neuronal-like cells	4 (2)	11 (6)	0.161
Oligodendroglial areas	9 (5)	4 (2)	0.256

**P* values obtained from univariable binary logistic regression analyses.

†Statistically significant features, *P* < 0.05.

‡Assessed only in tumors with central tumor morphology (n = 105).

§Assessed only in cases with present infiltration zones into either gray or white matter (n = 78).

||Assessed only in cases with adequate morphology for counting of mitoses (n = 105).

¶Assessed only in cases with paraffin sections with viable central tumor areas (n = 103).

#Assessed only in cases containing infiltration zones into gray matter (n = 66).

**Assessed only in cases containing outer brain surface (i.e., cases containing leptomeninges or, alternatively, cases containing ≥2 of the following features: molecular cortical layer, corpora amylacea, or glia limitans [n = 45]).

Associations Between Histopathology and Growth Groups

Of all histopathologic features listed in **Table 1**, only mitotic count, high cellular density, and thromboses were significantly associated with tumor growth in the univariable analyses (**Tables 2** and **3**). In the multivariable analysis with the highest number of significant independent predictors, only high cellular density and thromboses remained significant, and were positively associated with faster growing tumors (**Table 3**).

Associations Between Histopathologic Features

To investigate why mitotic count did not reach statistical significance in the multivariable models, we examined associations between the 3 significant features in the univariable analyses. Thromboses and high cellular density were not significantly associated (χ^2 test, *P* = 0.419). Increasing mitotic counts were significantly associated both with high cellular density (Mann-Whitney *U* test, *P* < 0.001) and with the presence of thromboses (Mann-Whitney *U* test, *P* = 0.006).

DISCUSSION

In the present study, we found that high cellular density and thromboses were histopathologic features significantly associated with faster radiologic growth of human GBM in a multivariable analysis.

This relatively large set of pretreatment growth data from patients with GBM enables us to study virtually unaffected growth

Table 3. Univariable and Multivariable Odds Ratios from Binary Logistic Regression Analyses

Histopathologic Feature	Univariable Odds Ratio (95% Confidence Interval)	Multivariable Odds Ratio (95% Confidence Interval)	P Values from Multivariable Analysis
High cellular density	3.05 (1.27–7.35)	2.98 (1.21–7.39)	0.018*
Thromboses	4.40 (1.34–14.43)	4.28 (1.27–14.47)	0.019*
Mitotic count (n = 105)	1.03 (1.00–1.06)		

*Significant features, $P < 0.05$. Features with odds ratio >1 were positively associated with faster tumor growth.

mechanisms in human GBMs. Growth mechanisms of GBM have been studied extensively in both in vitro and in vivo animal studies, but such models can never fully mimic the unique intratumoral genetic and phenotypic heterogeneity of human GBM, because of microenvironmental dissimilarities.¹⁸ Although preoperative corticosteroids (received by 81% of the patients in our study) could affect the microenvironment, it did not affect radiologic speed of growth.¹ Moreover, because it is unethical to withhold symptomatic corticosteroid treatment, the biology of these tumors is as unaffected as can be ethically justified. To better assess the impact of steroids, we performed the same statistical analyses as previously described for this steroid-treated subgroup. Here, we found the same results as for all patients (data not shown).

Although speed of growth is not a hard clinical end point such as overall survival, we believe it might better capture the biology of the disease because of the numerous factors affecting survival. Such factors are age and tumor size at diagnosis, tumor location, extent of surgical resection, adjuvant therapy, neurologic deficits, and comorbidity, which all might introduce bias in search of markers associated with GBM biology. Such potential interfering parameters could explain why many molecular biomarkers have failed to be associated with survival of grade IV gliomas in numerous large studies.^{19–21} By assessing relations between histopathologic features and pretreatment growth, we could investigate tumor biology without significant interference of these clinical factors.

High Cellular Density Is a Significant Independent Predictor of Faster Growth

High cellular density was significantly associated with faster growing tumors in the multivariable analysis. The cellularity of tumors is believed to increase along with higher proliferation rates, and these 2 features were significantly associated in our study. However, mitotic count was not a significantly independent predictor of tumor growth. Studies investigating the prognostic value of Ki-67 proliferative index (PI) have shown diverging results, and the importance of proliferation assessments in GBM is not clarified.^{22–26} In addition, the method of evaluating Ki-67 PI has been shown to have a large interobserver variability.²⁷ In a recently published study of the same patients, we found Ki-67 PI to be significantly associated neither with faster growth nor with prognosis,¹⁷ which further substantiates a possible inadequacy of histopathologic evaluation of proliferative activity in GBM. Mitotic activity is known to be highly heterogeneously distributed, both between and within different GBMs.²⁸ This factor presents challenges in selecting and counting hot spots representative of the true proliferative value of

the tumor. We therefore speculate that high cellular density may be more representative of the true proliferation rate of the tumor than is histopathologically evaluated proliferative activity. In any case, these findings support hypercellularity as an important criterion in glioma grading.²⁸

Intravascular Thrombosis Is a Significant Independent Predictor of Faster Growth

Intravascular thrombosis is a frequent and well-known macroscopic and microscopic feature of GBM.^{29,30} In the current study, thromboses were associated independently with faster growing tumors. Thromboses are observed more frequently in GBMs than in lower-grade astrocytomas, and it has been hypothesized that thromboses trigger more aggressive tumor behavior.²⁹ It has been proposed that thromboses initiate tumor hypoxia,^{31,32} which leads to upregulation of the transcription factor HIF-1 α (hypoxia inducible factor 1 α), stimulating invasion and angiogenesis.^{33,34} It is plausible that increased angiogenesis promotes a more aggressive tumor phenotype and tumor expansion.^{31,32} However, antiangiogenic treatment with the vascular endothelial growth factor antagonist bevacizumab has not been shown to increase survival in phase 3 clinical trials,³⁵ with the possible exception of the proneural subtype.³⁶ In animal models, bevacizumab treatment reduces tumor blood supply and increases hypoxia (induction of HIF-1 α) and glycolysis (through activation of the phosphatidylinositol 3-kinase/Akt pathway), leading to increased tumor invasion.³⁷ Thus, the increase of hypoxia after bevacizumab treatment might explain the lack of therapeutic benefit, and it has been speculated that adding drugs targeting HIF-1 α and phosphatidylinositol 3-kinase/Akt pathways could circumvent this issue.³⁷

Hypoxia quantitated from positron emission tomography scans has been found to correlate with a radiologic index of aggressiveness in human GBMs.³⁸ This index is computed from a biomathematical model based on preoperative MRI scans, which estimates net proliferation and dispersal rates of glioma cells.³⁹ Szeto et al.³⁸ argue that high proliferation rates might cause the observed hypoxia. However, reverse causation may also be possible, (i.e., hypoxia could cause higher proliferation by acquisition of a more aggressive phenotype). Both causal chains may contribute to the aggressive biology of the highly heterogeneous GBM.

The pathogenesis underlying the formation of intravascular thromboses in GBM is not fully comprehended.²⁸ Tissue factor is expressed in higher levels in GBMs than in lower-grade

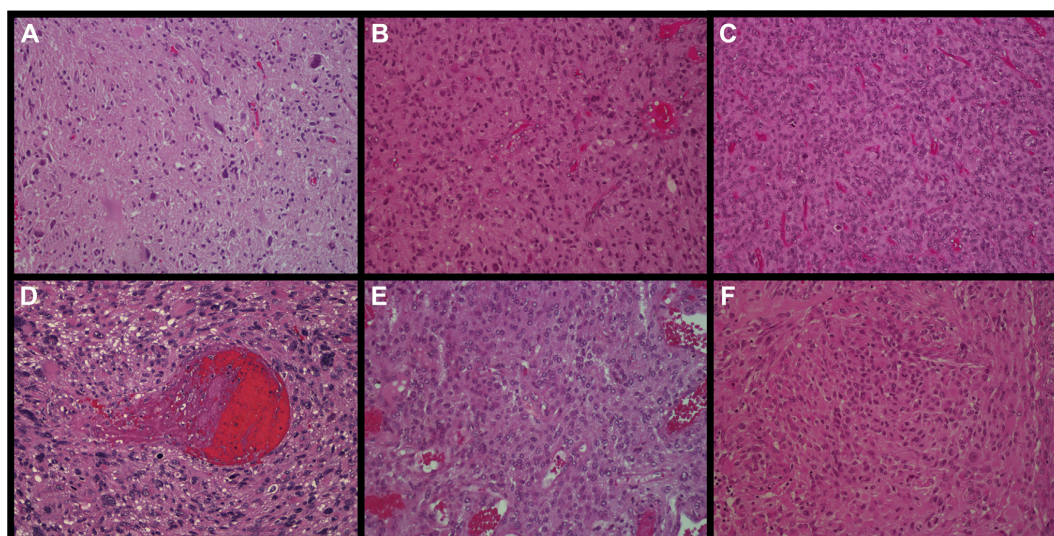


Figure 2. Histopathologic features. Hematoxylin-eosin stains from glioblastoma tissue on 200× magnification. (A–C) Low, moderate, and high cellular density, respectively. (B, C) Moderate and high vascular density, respectively. In addition, (B) shows moderate atypia, whereas (C)

shows an area with small cell morphology. (D) A partly thrombosed vessel surrounded by severely atypical neoplastic cells. (E, F) Mild atypia and low vascular density, respectively.

gliomas,^{40,41} and upregulation of tissue factor has been suggested to be important for thrombus formation in GBM. Another possible explanation is that the co-option of native vasculature by tumor cells leads to destabilization of the vessels and thereby promotes vaso-occlusion.⁴² A third possible mechanism is that a breached blood-brain barrier leads to activation of the coagulation cascade and thereby formation of thromboses.³¹ Although several mechanisms for increased coagulability have been proposed, it is unclear why some tumors are more procoagulant than others.

Histopathologic Features Linked to Slower Growth

The presence of desmoplasia and small cell compartments showed increased proportions in slower growing tumors, with near-significant *P* values in the univariable analyses (Table 2). However, their role remains unclear, because there is a lack of studies covering how they could impede the growth of GBM.

Other Relevant Histopathologic Features

Other relevant histopathologic features did not achieve statistical significance in the univariable analyses. As previously described, thrombosis has been postulated as an initiator of hypoxia, which in turn leads to increased neovascular stimuli, facilitating outward tumor expansion. Still, neither vascular features nor necroses showed any significant associations with tumor growth in this study. With regard to vascularization, it is difficult to fully recognize all vessels in routine sections of GBM tissue.⁴³ Therefore, immunohistochemical analyses with endothelial markers can aid in developing more

definite documentation on this issue. Regarding necroses, random tissue samples of GBMs may not be representative of the necrotic part. It might thus be better to quantify the degree of necrosis on MRI scans to study its role in GBM growth. Radiologic necrosis in histopathologic grade III tumors harbors the same prognosis as GBMs.⁴⁴ To better understand the roles of neovascularization and necroses in human GBM growth, future studies are required.

Strengths and Limitations

The main strength of the study is the repeated preoperative MRI assessments in a relatively large number of patients, all treated at 1 neurosurgical center with a population-based referral. Distributions of both age and gender were nonsignificantly different from the excluded patients, and the distribution of age was similar to all patients with GBM in Norway.¹ The exclusion of patients with serial images separated by less than 14 days can be a source of selection biases. Although 81% of the patients received symptomatic corticosteroid treatment before surgery, the steroid intervention did not show a significant impact on tumor growth when adjusted for diagnostic tumor volume.¹

Errors in obtaining reliable growth estimates may have occurred because of the variability of MRI scanners performing the diagnostic scans (performed in 15 different radiology clinics), the timing of administration of the contrast agent, and other factors that could have altered the contrast enhancement (such as infarctions).⁴⁵ To minimize such errors, the segmentations were controlled by a neuroradiologist (E.B.M.), and the reproducibility of the MRI segmentations assessed using

measures suggested by Bland and Altman.⁴⁶ The reproducibility assessment showed good reliability of the volume estimates.¹

GBMs show a pronounced infiltrative growth, and tumor cells are present far outside the contrast-enhancing rim.^{47,48} Nevertheless, bulk tumor volume as seen on contrast-enhanced T1-weighted MRI scans is used for evaluation of resection grades and treatment responses.^{49,50}

Regarding the histopathologic examination, all cases had adequate material for evaluating histologic features, although 49 had sparse amounts of viable tumor material. Variation in the amount of tissue pertaining to each case and the vast intratumor and intertumor heterogeneity of GBM histopathology^{5,30} could decrease the representability, especially in cases with sparse tissue amount. Nevertheless, representability probably increases because of the large number of cases reviewed. Despite stringent criteria for recognizing histopathologic features, all recognition was carried out subjectively and thus with varying degrees of intra-observer variability. In this regard, we found thromboses to be fairly conspicuous on routine hematoxylin-eosin slides (Figure 2D), plausibly minimizing the intraobserver variability for this particular feature. Regarding the mitotic count, the assessment has many potential sources of errors.⁵¹ Moreover, the second observer (S.H.T.) was not completely blinded because he was more experienced and therefore controlled the first observer's (V.E.M.) histopathologic findings. However, we were well aware of this issue and strived to maximize blinding when possible.

In our data set, only 2% (2/106) were immunopositive for IDH1, which is concordant with the 5% observed in de novo occurring

GBMs in a literature review.⁵² According to the 2016 World Health Organization classification, IDH1 R132H-negative patients younger than 55 years should be sequenced in addition for adequate determination of IDH status.²⁸ However, additional gene sequencing was unavailable for the 22 patients (21%) negative for IDH1 R132H and younger than 55 years in our study.

Multiple significance tests were performed because of the exploratory design of our study, thus increasing the chance of false findings. Also, the novel approach has made it impossible to calculate statistical power upfront. Our findings should therefore be validated in future studies. However, we believe this study can form a basis for future studies on growth mechanisms in patients with GBM.

CONCLUSIONS

In this explorative study, we found that high cellular density and thromboses were significant independent predictors of faster tumor growth in a multivariable analysis. Furthermore, our results are in accordance with hypotheses describing thrombosis as a main initiator of hypoxia, which triggers more aggressive tumor biology.

ACKNOWLEDGMENTS

We would like to thank the staff at the Cellular and Molecular Imaging Core Facility (CMIC) for excellent laboratory work, and Iris Alexandra Kummen for exquisite language editing.

REFERENCES

- Stensjoen AL, Solheim O, Kvistad KA, Haberg AK, Salvesen O, Berntsen EM. Growth dynamics of untreated glioblastomas in vivo. *Neuro Oncol*. 2015;17:1402-1411.
- Ellingson BM, Nguyen HN, Lai A, Nechifor RE, Zaw O, Pope WB, et al. Contrast-enhancing tumor growth dynamics of preoperative, treatment-naïve human glioblastoma. *Cancer*. 2016;122:1718-1727.
- Helseth R, Helseth E, Johannessen TB, Langberg CW, Lote K, Ronning P, et al. Overall survival, prognostic factors, and repeated surgery in a consecutive series of 516 patients with glioblastoma multiforme. *Acta Neurol Scand*. 2010;122:159-167.
- Stupp R, Mason WP, van den Bent MJ, Weller M, Fisher B, Taphoorn MJ, et al. Radiotherapy plus concomitant and adjuvant temozolomide for glioblastoma. *N Engl J Med*. 2005;352:987-996.
- Eder K, Kalman B. Molecular heterogeneity of glioblastoma and its clinical relevance. *Pathol Oncol Res*. 2014;20:777-787.
- Laird AK. Dynamics of tumor growth. *Br J Cancer*. 1964;13:490-502.
- Yamashita T, Kuwabara T. Estimation of rate of growth of malignant brain tumors by computed tomography scanning. *Surg Neurol*. 1983;20:464-470.
- Tsuboi K, Yoshii Y, Nakagawa K, Maki Y. Regrowth patterns of supratentorial gliomas: estimation from computed tomographic scans. *Neurosurgery*. 1986;19:946-951.
- Blankenberg FG, Teplitz RL, Ellis W, Salamat MS, Min BH, Hall L, et al. The influence of volumetric tumor doubling time, DNA ploidy, and histologic grade on the survival of patients with intracranial astrocytomas. *AJNR Am J Neuroradiol*. 1995;16:1001-1012.
- Haney SM, Thompson PM, Cloughesy TF, Alger JR, Toga AW. Tracking tumor growth rates in patients with malignant gliomas: a test of two algorithms. *AJNR Am J Neuroradiol*. 2001;22:73-82.
- Pennington C, Kilbride L, Grant R, Wardlaw JM. A pilot study of brain tumour growth between radiotherapy planning and delivery. *Clin Oncol (R Coll Radiol)*. 2006;18:104-108.
- James B, Gillard J, Antoun N, Scott I, Coleman N, Pinto E, et al. Glioblastoma doubling time and cellular proliferation markers. *Clin Oncol*. 2007;19:533.
- Wang CH, Rockhill JK, Mrugala M, Peacock DL, Lai A, Jusenius K, et al. Prognostic significance of growth kinetics in newly diagnosed glioblastomas revealed by combining serial imaging with a novel biomathematical model. *Cancer Res*. 2009;69:9133-9140.
- Osborn AG. Astrocytomas. In: Renlund AR, ed. *Osborn's Brain: Imaging, Pathology and Anatomy*. Altona, Manitoba, Canada: Amirsys Publishing; 2013:484-490.
- Louis DN, Ohgaki H, Wiestler O, Cavenee WK. *WHO Classification of Tumours of the Central Nervous System*. 4th ed. Geneva, Switzerland: International Agency for Research on Cancer (IARC); 2007.
- Vettkattil R, Gulati M, Sjobakk TE, Jakola AS, Kvernmo NA, Torp SH, et al. Differentiating diffuse World Health Organization grade II and IV astrocytomas with ex vivo magnetic resonance spectroscopy. *Neurosurgery*. 2013;72:186-195 [discussion: 195].
- Stensjoen AL, Berntsen EM, Mikkelsen VE, Torp SH, Jakola AS, Salvesen O, et al. Does pre-treatment tumor growth hold prognostic information for patients with glioblastoma? *World Neurosurg*. 2017;101:686-694.e684.
- Huszthy PC, Daphu I, Niclou SP, Stieber D, Nigro JM, Sakariassen PO, et al. In vivo models of primary brain tumors: pitfalls and perspectives. *Neuro Oncol*. 2012;14:979-993.
- Weller M, Pfister SM, Wick W, Hegi ME, Reifenberger G, Stupp R. Molecular neuro-oncology in clinical practice: a new horizon. *Lancet Oncol*. 2013;14:e370-e379.
- Weller M, Felsberg J, Hartmann C, Berger H, Steinbach JP, Schramm J, et al. Molecular predictors of progression-free and overall survival in patients with newly diagnosed glioblastoma: a

- prospective translational study of the German Glioma Network. *J Clin Oncol*. 2009;27:5743-5750.
21. Eckel-Passow JE, Lachance DH, Molinaro AM, Walsh KM, Decker PA, Sciotte H, et al. Glioma groups based on 1p/19q, IDH, and TERT promoter mutations in tumors. *N Engl J Med*. 2015;372:2499-2508.
 22. Brat DJ, Prayson RA, Ryken TC, Olson JJ. Diagnosis of malignant glioma: role of neuropathology. *J Neurooncol*. 2008;89:287-311.
 23. Giannini C, Scheithauer BW, Burger PC, Christensen MR, Wollan PC, Sebo TJ, et al. Cellular proliferation in pilocytic and diffuse astrocytomas. *J Neuropathol Exp Neurol*. 1999;58:46-53.
 24. McKeever PE, Ross DA, Strawderman MS, Brunberg JA, Greenberg HS, Junck L. A comparison of the predictive power for survival in gliomas provided by MIB-1, bromodeoxyuridine and proliferating cell nuclear antigen with histopathologic and clinical parameters. *J Neuropathol Exp Neurol*. 1997;56:798-805.
 25. Wakimoto H, Aoyagi M, Nakayama T, Nagashima G, Yamamoto S, Tamaki M, et al. Prognostic significance of Ki-67 labeling indices obtained using MIB-1 monoclonal antibody in patients with supratentorial astrocytomas. *Cancer*. 1996;77:373-380.
 26. Moskowitz SI, Jin T, Prayson RA. Role of MIB-1 in predicting survival in patients with glioblastomas. *J Neurooncol*. 2006;76:193-200.
 27. Grzybicki DM, Liu Y, Moore SA, Brown HG, Silverman JF, D'Amico F, et al. Interobserver variability associated with the MIB-1 labeling index: high levels suggest limited prognostic usefulness for patients with primary brain tumors. *Cancer*. 2001;92:2720-2726.
 28. Louis DN, Ohgaki H, Wiestler O, Cavenee WK, Ellison DW, Figarella-Branger D, et al. WHO Classification of Tumours of the Central Nervous System. 4th ed. Geneva, Switzerland: International Agency for Research on Cancer (IARC); 2016.
 29. Tehrani M, Friedman TM, Olson JJ, Brat DJ. Intravascular thrombosis in central nervous system malignancies: a potential role in astrocytoma progression to glioblastoma. *Brain Pathol*. 2008;18:164-171.
 30. Habberstad AH, Lind-Landstöm T, Torp SH. The histopathological spectrum of primary human glioblastomas with relations to tumour biology. *J Clin Exp Pathol*. 2012;2:110.
 31. Brat DJ, Van Meir EG. Vaso-occlusive and prothrombotic mechanisms associated with tumor hypoxia, necrosis, and accelerated growth in glioblastoma. *Lab Invest*. 2004;84:397-405.
 32. Rong Y, Durden DL, Van Meir EG, Brat DJ. "Pseudopalisading" necrosis in glioblastoma: a familiar morphologic feature that links vascular pathology, hypoxia, and angiogenesis. *J Neuropathol Exp Neurol*. 2006;65:529-539.
 33. Zagzag D, Zhong H, Scalzitti JM, Laughner E, Simons JW, Semenza GL. Expression of hypoxia-inducible factor 1alpha in brain tumors: association with angiogenesis, invasion, and progression. *Cancer*. 2000;88:2606-2618.
 34. Mendez O, Zavadil J, Esencay M, Lukyanov Y, Santovasi D, Wang SC, et al. Knock down of HIF-1alpha in glioma cells reduces migration in vitro and invasion in vivo and impairs their ability to form tumor spheres. *Mol Cancer*. 2010;9:133.
 35. Gilbert MR, Dignam JJ, Armstrong TS, Wefel JS, Blumenthal DT, Vogelbaum MA, et al. A randomized trial of bevacizumab for newly diagnosed glioblastoma. *N Engl J Med*. 2014;370:699-708.
 36. Sandmann T, Bourgon R, Garcia J, Li C, Cloughesy T, Chinot OL, et al. Patients with proneural glioblastoma may derive overall survival benefit from the addition of bevacizumab to first-line radiotherapy and temozolomide: retrospective analysis of the AVAglio trial. *J Clin Oncol*. 2015;33:2735-2744.
 37. Keunen O, Johansson M, Oudin A, Sanzey M, Rahim SA, Fack F, et al. Anti-VEGF treatment reduces blood supply and increases tumor cell invasion in glioblastoma. *Proc Natl Acad Sci U S A*. 2011;108:3749-3754.
 38. Szeto MD, Chakraborty G, Hadley J, Rockne R, Muzi M, Alvord EC Jr, et al. Quantitative metrics of net proliferation and invasion link biological aggressiveness assessed by MRI with hypoxia assessed by FMISO-PET in newly diagnosed glioblastomas. *Cancer Res*. 2009;69:4502-4509.
 39. Swanson KR, Bridge C, Murray JD, Alvord EC Jr. Virtual and real brain tumors: using mathematical modeling to quantify glioma growth and invasion. *J Neurol Sci*. 2003;216:1-10.
 40. Guan M, Jin J, Su B, Liu WW, Lu Y. Tissue factor expression and angiogenesis in human glioma. *Clin Biochem*. 2002;35:321-325.
 41. Hamada K, Kuratsu J, Saitoh Y, Takeshima H, Nishi T, Ushio Y. Expression of tissue factor correlates with grade of malignancy in human glioma. *Cancer*. 1996;77:1877-1883.
 42. Fischer I, Gagner JP, Law M, Newcomb EW, Zagzag D. Angiogenesis in gliomas: biology and molecular pathophysiology. *Brain Pathol*. 2005;15:297-310.
 43. Louis DN. Molecular pathology of malignant gliomas. *Annu Rev Pathol*. 2006;1:97-117.
 44. Lasocki A, Tsui A, Tacey MA, Drummond KJ, Field KM, Gaillard F. MRI grading versus histology: predicting survival of World Health Organization grade II-IV astrocytomas. *AJNR Am J Neuroradiol*. 2015;36:77-83.
 45. Quant EC, Wen PY. Response assessment in neuro-oncology. *Curr Oncol Rep*. 2011;13:50-56.
 46. Bland JM, Altman DG. Statistical methods for assessing agreement between two methods of clinical measurement. *Lancet*. 1986;1:307-310.
 47. Kelly PJ, Daumas-Duport C, Kispert DB, Kall BA, Scheithauer BW, Illig JJ. Imaging-based stereotaxic serial biopsies in untreated intracranial glial neoplasms. *J Neurosurg*. 1987;66:865-874.
 48. Yamahara T, Numa Y, Oishi T, Kawaguchi T, Seno T, Asai A, et al. Morphological and flow cytometric analysis of cell infiltration in glioblastoma: a comparison of autopsy brain and neuroimaging. *Brain Tumor Pathol*. 2010;27:81-87.
 49. Lacroix M, Abi-Said D, Fournier DR, Gokaslan ZL, Shi W, DeMonte F, et al. A multivariate analysis of 416 patients with glioblastoma multiforme: prognosis, extent of resection, and survival. *J Neurosurg*. 2001;95:190-198.
 50. Wen PY, Macdonald DR, Reardon DA, Cloughesy TF, Sorensen AG, Galanis E, et al. Updated response assessment criteria for high-grade gliomas: response assessment in neuro-oncology working group. *J Clin Oncol*. 2010;28:1963-1972.
 51. Prayson RA. Cell proliferation and tumors of the central nervous system. Part 1: Evaluation of mitotic activity. *J Neuropathol Exp Neurol*. 2002;61:501-509.
 52. Kloosterhof NK, Bralten LB, Dubbink HJ, French PJ, van den Bent MJ. Isocitrate dehydrogenase-1 mutations: a fundamentally new understanding of diffuse glioma? *Lancet Oncol*. 2011;12:83-91.

Conflict of interest statement: O.S. has previously been an unpaid member of a national advisory committee on treatment guidelines for brain tumors. All other authors disclose no potential conflicts of interest.

Received 8 May 2017; accepted 16 September 2017

Citation: *World Neurosurg.* (2018) 109:e50-e58.

<https://doi.org/10.1016/j.wneu.2017.09.102>

Journal homepage: www.WORLDNEUROSURGERY.org

Available online: www.sciencedirect.com

1878-8750/\$ - see front matter © 2017 Elsevier Inc. All rights reserved.

Paper II

RESEARCH ARTICLE

Open Access



Angiogenesis and radiological tumor growth in patients with glioblastoma

Vilde Elisabeth Mikkelsen^{1*}, Anne Line Stensj  en^{2,3}, Unn Sophie Granli^{1,4}, Erik Magnus Berntsen^{2,5}, Øyvind Salvesen⁶, Ole Solheim^{3,7,8} and Sverre Helge Torp^{1,9}

Abstract

Background: The preoperative growth of human glioblastomas (GBMs) has been shown to vary among patients. In animal studies, angiogenesis has been linked to hypoxia and faster growth of GBM, however, its relation to the growth of human GBMs is sparsely studied. We have therefore aimed to look for associations between radiological speed of growth and microvessel density (MVD) counts of the endothelial markers vWF (Factor VIII related antigen) and CD105 (endoglin).

Methods: Preoperative growth was estimated from segmented tumor volumes of two preoperative T1-weighted postcontrast magnetic resonance imaging scans taken ≥ 14 days apart in patients with newly diagnosed GBMs. A Gompertzian growth curve was computed from the volume data and separated the patients into two groups of either faster or slower tumor growth than expected. MVD counts of the immunohistochemical markers von Willebrand factor (vWF) (a pan-endothelial marker) and CD105 (a marker of proliferating endothelial cells) were assessed for associations with fast-growing tumors using Mann-Whitney U tests and a multivariable binary logistic regression analysis.

Results: We found that only CD105-MVD was significantly associated with faster growth in a univariable analysis ($p = 0.049$). However, CD105-MVD was no longer significant when corrected for the presence of thromboses and high cellular density in a multivariable model, where the latter features were significant independent predictors of faster growth with respective odds ratios 4.2 (95% confidence interval, 1.2, 14.3), $p = 0.021$ and 2.6 (95% confidence interval, 1.0, 6.5), $p = 0.048$.

Conclusions: MVDs of neither endothelial marker were independently associated with faster growth, suggesting angiogenesis-independent processes contribute to faster glioblastoma growth.

Keywords: Angiogenesis, Glioblastoma, Histopathology, Magnetic resonance imaging, Microvessel density, Tumor growth, Tumor biology, Tumor hypoxia

Background

Glioblastoma (GBM) is the most common primary malignant brain tumor in adults [1], with a median overall survival of only 10 months in unselected patients [2]. GBMs are characterized by a highly heterogeneous histopathology [3–5], a high secretion of pro-angiogenic factors [6, 7], extensive vascularity [8, 9], and rapid pretreatment growth [10, 11]. The pretreatment growth has been shown to vary considerably among patients [10] and slower growth to be

an independent predictor of long term survival in patients with GBM [12].

It is of major interest to understand biological processes behind the variations in speed of growth observed in human GBMs, which in turn could reveal future targets of therapies hampering growth. We have recently studied relations between histopathological features and radiological speed of pretreatment tumor growth [13]. We found that thromboses and high cellular density were significant independent predictors of faster preoperative tumor growth [13]. These findings are in line with hypotheses suggesting thrombosis as an initiator of hypoxia facilitating outward tumor expansion, plausibly through stimulation of

* Correspondence: vildeem@stud.ntnu.no

¹Department of Clinical and Molecular Medicine, Faculty of Medicine and Health Sciences, NTNU - Norwegian University of Science and Technology, Erling Skjalgssons gate 1, 7030 Trondheim, Norway

Full list of author information is available at the end of the article



  The Author(s). 2018 **Open Access** This article is distributed under the terms of the Creative Commons Attribution 4.0 International License (<http://creativecommons.org/licenses/by/4.0/>), which permits unrestricted use, distribution, and reproduction in any medium, provided you give appropriate credit to the original author(s) and the source, provide a link to the Creative Commons license, and indicate if changes were made. The Creative Commons Public Domain Dedication waiver (<http://creativecommons.org/publicdomain/zero/1.0/>) applies to the data made available in this article, unless otherwise stated.

angiogenesis [9, 14]. Neovascularization is fundamental for the survival and expansion of tumors [15], and angiogenesis has been extensively linked to hypoxia and growth of GBM in animal studies [16–19]. However, in randomized trials, antiangiogenic therapy has not shown any significant survival benefit in GBMs [20, 21]. Still, the degree of angiogenesis has not been assessed for relations with radiological speed of pretreatment growth in human GBMs.

In a cohort of 102 GBMs previously assessed for radiological speed of growth [10], we sought to investigate possible associations between pretreatment speed of tumor growth and the degree of angiogenesis quantified by microvessel density (MVD) measurements. The MVDs were immunohistochemically assessed by means of two endothelial markers: von Willebrand factor (vWF or FVIII related antigen), a pan-endothelial marker [22], which illustrates the metabolic demand of the tumor [23]; and endoglin (CD105), a marker of proliferating endothelial cells [24], which reflects the degree of angiogenesis [23]. In addition, we investigated the correlation between the MVDs and their associations with the histopathological features thromboses, high cellular density, high vascular density, and mitotic count.

Methods

Inclusion and exclusion criteria

As previously described, patients were retrospectively selected from all newly diagnosed GBM patients ≥ 18 years of age operated at St Olavs Hospital – Trondheim University Hospital, Norway between January 2004 and May 2014 (262 patients) [10]. Selection criteria were ≥ 2 pretreatment T₁-weighted postcontrast magnetic resonance imaging (MRI) scans separated by ≥ 14 days and histopathologically verified GBMs according to the 2007 World Health Organization (WHO) Classification [25]. Exclusion criteria were non-contrast-enhancing tumors and gliomatosis cerebri (defined by radiological criteria [26]). In addition, four cases were excluded because of insufficient tissue amount or morphology for the MVD assessments, which left 102 patients eligible for further analyses.

Volume segmentation and growth rates

The segmentation of tumor volumes and establishment of growth rates have previously been described in detail [10]. The volume segmentation was performed by ALS and controlled by EMB (a neuroradiologist) using the software BrainVoyager QX (Brain Innovation, Maastricht, The Netherlands). Both preoperative MRI scans were segmented for total tumor volumes, defined as the combined volume of the non-contrast-enhancing central part (i. e. necrosis) and the contrast-enhancing rim. In addition, the

reproducibility of the tumor volume assessments has been assessed and concluded as satisfactory [10].

The fitness of different growth patterns based on the segmented tumor volumes and the time intervals between the scans, have previously been assessed [10]. The Gompertzian growth pattern (Fig. 1) was concluded as the most biologically reasonable growth pattern [10], and all tumors were assumed to follow this growth pattern. Since growth rates were highly dependent upon tumor volume [10], a point estimate (such as doubling time) would be a wrong representation of tumor growth. To account for this issue, we calculated an expected Gompertzian growth curve based on the volume data from 106 patients [10]. The curve dichotomized the patients into having tumors with a larger or smaller volume increase than expected from the curve (i.e. fast-growing or slow-growing tumors) (Fig. 1) [10]. These two groups have previously been shown to associate with survival of GBM patients [12]. In the current study, these groups were assessed for associations with the MVDs.

Histopathology

All routine hematoxylin-eosin (HE) sections for each case have previously been microscopically assessed by VEM (a medical research student) and controlled by SHT (an experienced neuropathologist) for the presence of 30 different histopathological features, which have previously been described in detail [13]. These features were assessed for associations with the same groups of growth, and thromboses, high cellular density, vascular density, and mitotic count were of interest to this study. Thromboses were defined as vascular structures partly or completely occluded with fibrin. The general cellular and vascular densities of viable tumor areas were subjectively graded as low, moderate, or high. For statistical analyses, the 2 lowest categories were merged, because very few cases were graded as low in both variables. Mitoses were counted in 10 high-power fields (HPFs) in areas of highest mitotic counts (hotspots).

Immunohistochemistry

From each patient, one representative tumor sample from formalin-fixed paraffin-embedded (FFPE) tissue were cut at 4 μ m, dried, deparaffinized, and rehydrated. Of the 102 cases, 11 cases had sections from FFPE frozen tissue. We applied vWF (vWF, 1:2000, polyclonal rabbit, EnV+/HRP, Dako Denmark AS, Glostrup, Denmark) and CD105 (CD105, SN6h, 1:50, monoclonal mouse, LSAB/HRP, Dako Denmark AS, Glostrup, Denmark). Optimum antibody concentrations were determined by titrations. For CD105, antigen retrieval was achieved with proteolytic enzymes, endogenous peroxidase activity was quenched with peroxidase block, and sections were incubated with the primary antibody for

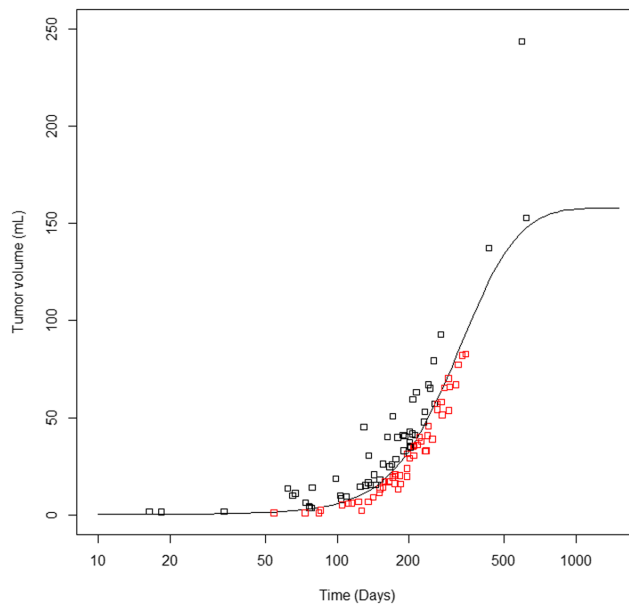


Fig. 1 Gompertzian growth pattern. The expected Gompertzian growth curve computed from segmented tumor volumes of two preoperative MRI scans and the interval between them in 106 patients [10]. Time is presented as a logarithmic scale. The squares represent tumor volumes at the second MRI scans: the black squares are tumor volumes with a larger increase in size than expected from their initial volume (fast-growing tumors), while the red squares are tumors with a smaller volume increase than expected from the curve (slow-growing tumors). For illustration purposes, the curve was drawn from a tumor with an arbitrary size of 0.135 mL at day 0

24 h at 4 °C with cover glass after pretreatment with serumfree proteinblock. Both endothelial markers had negative controls and positive internal controls.

Quantification of microvessel densities

MVDs of vWF and CD105 were assessed by VEM, who was blinded to the growth data. A Nikon Eclipse 80i microscope and a Nikon CFI 10×/22 grid at × 400 magnification (area within the grid equal to 0.059 mm²) were used for the MVD assessments. MVDs were assessed after the methods of Weider et al. [27] with some modifications. MVDs were computed as the mean count of vessels within the grid for three HPFs of highest vascular densities (i. e. hotspots). Hotspots were identified by scanning using × 4 and × 10 objectives on vWF sections; corresponding hotspots were identified on CD105 sections. Only areas with ≥50% of viable central tumor tissue were counted. Tissue edges and areas with excessive hemorrhage and/or desmoplasia were avoided. Any individually stained endothelial cell or vessel within or in contact with the grid were counted. Moreover, because of the heterogeneous morphology of GBM vessels [28], each lumen was counted for long branched vessels and glomeruloid tufts as described by Kraby et al. [29]. In addition, separate units of ≥2 staining endothelial cells

within the same vascular structure were counted as one vascular unit. Altogether, one case was not assessed for vWF-MVD due to high background staining, and another case was not evaluated for CD105-MVD due to non-existent antigenicity.

Statistical analyses

The estimation of growth rates and curves were computed using R version 2.13.1 [10] and analyses involving histopathology and MVDs were performed using IBM SPSS Statistics 24. Statistical significance was defined as $p < 0.05$ without corrections for multiple testing. The correlation between vWF-MVD and CD105-MVD was assessed using the Spearman rank correlation test. Associations between both MVDs and histopathological features were assessed using Mann-Whitney U tests (categorical vs continuous) and Spearman rank correlation tests (continuous vs continuous). vWF-MVD and CD105-MVD were further investigated for associations with fast-growing tumors using Mann-Whitney U tests. Finally, CD105-MVD was included in a multivariable binary logistic regression model with the histopathological features previously found to be significantly associated with faster growth in the same patients (thromboses, high cellular density, and mitotic

count) [13]. Mitotic count was excluded from the model due to significant associations with all other features included [13].

Results

Patient characteristics

Of the 102 included patients, 69% (70 patients) were male. The mean age was 63 years, range 26–83 years old. All cases were immunopositive for glial fibrillary acidic protein (GFAP) and two for isocitrate dehydrogenase mutation (IDH1-R132H) [12]. Eighty-two patients (80%) were preoperatively treated with corticosteroids. The median tumor volume was 17.7 mL (range 0.05–146.45 mL) from the first MRI scans and 27.5 mL (range 0.98–243.52 mL) from the second MRI scans. The median interval between the scans was 22.5 days, range 14–98 days. Overall, 52 patients (51%) had fast-growing tumors, and patient characteristics within the growth groups have previously been reported [12].

Descriptive data

We observed that both markers stained endothelial cells quite specifically. vWF had a strong and granular cytoplasmic staining pattern, whereas CD105 had a more even and occasionally weaker cytoplasmic stain (Fig. 2). Generally, little background staining was observed, except in a few vWF sections. The distributions of both vWF-MVD and CD105-MVD were skewed, and the median vWF-MVD was 15.5 per field (range 0.7–62.0) and the median CD105-MVD was 12.7 (range 0.7–50.0).

Relationships between MVDs of the endothelial markers

vWF-MVDs and CD105-MVDs were significantly correlated ($p < 0.001$, $\rho = 0.92$). A scatterplot showing the relationship is found in Fig. 3. The median CD105-MVD/vWF-MVD ratio was 0.91 with 95% confidence interval (0.87, 0.95).

MVD and histopathology

Of the features previously found to significantly associate with faster growth in univariable analyses (thromboses, high cellular density, and mitotic count) [13], only mitotic count was significantly associated with any MVD in this study (Table 1). However, CD105-MVD tended to be higher in cases with present thromboses or high cellular density despite the non-significant associations. The same tendency was observed for vWF-MVD and thromboses (Table 1). Interestingly, both MVDs were significantly associated with subjectively evaluated high vascular densities on HE sections.

MVD and growth

In this study, only CD105-MVD was significantly associated with faster tumor growth in the univariable analyses (Table 2). However, the ranges of both MVDs were quite wide within both fast and slow-growing tumors (Table 2, Fig. 4). Nevertheless, CD105-MVD was no longer significant in a multivariable model including thromboses and high cellular density, where the two latter features were significant independent predictors of faster growth (Table 3).

Discussion

In this study, CD105-MVD, and not vWF-MVD, was significantly associated with faster growth in the univariable analyses. However, the relation was lost when adjusted for the presence of thromboses and high cellular density in a multivariable model, where these two latter features were significant independent predictors of faster growth. Both MVDs associated significantly with mitotic count, but neither with the presence of thromboses nor high cellular density.

Biological reasons for why some GBMs grow faster than others are sparsely studied in human patients, which is mainly due to difficulties in acquiring in vivo pretreatment growth estimates [10, 11]. In addition, most research on growth processes have been conducted

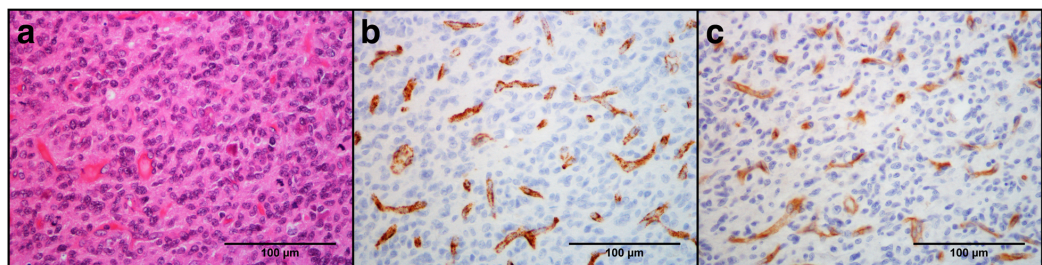


Fig. 2 Vascular structures at HE, vWF, and CD105 stains. Pictures are taken from corresponding HPFs in the same tumor of an area of high vascular density at $\times 400$ magnification. **a** HE stain. Plenty of visible small vascular structures in an area of central tumor with small cell morphology. **b** vWF stain. Granular cytoplasmic staining. **c** CD105 stain. More even cytoplasmic staining

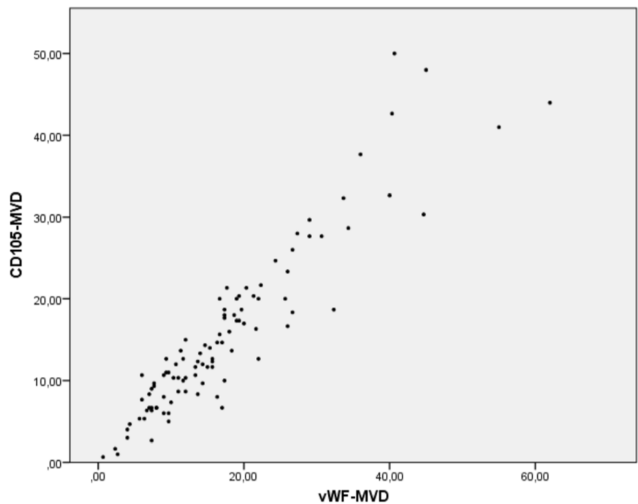


Fig. 3 Scatterplot of vWF-MVD and CD105-MVD. The scatterplot shows the close correlation between the markers, with dots forming a close-to-linear pattern in line with the high correlation coefficient ($p = 0.92$). However, the spread increases for higher MVD counts

on in vitro or animal models which fail to accurately imitate the unique micro-milieu of the human GBM [30]. Moreover, by having preoperative growth as an outcome variable instead of overall survival, we avoid the effects of clinical factors found to be influential on survival, such as age at diagnosis, tumor size at diagnosis, Karnofsky performance status, comorbidity, and effects of treatment. Corticosteroid treatment was the only preoperative treatment received by our patients (82

patients); however, it was not significantly associated with tumor growth when corrected for tumor volume [10], and associations between histopathology and growth were independent of such treatment [13]. Altogether, these aspects of the study made it possible to study the biology of GBM growth as unaffected as clinically justifiable.

Endothelial markers and angiogenesis

The prognostic role of MVD measurements in glioblastomas is unclarified [31–35]. However, a few studies have reported that vWF-MVD and CD105-MVD may predict the malignancy grade and prognosis of gliomas [36, 37]. The finding that only CD105-MVD was significantly associated with growth in the univariable analyses, is in line with other univariable studies which have found more promising results for CD105-MVD than for CD31-MVD (a pan-endothelial marker) as prognostic markers of GBM [33, 34]. These studies speculated the potential prognostic inferiority of pan-endothelial markers (i.e vWF, CD31, CD34) was caused by the additional staining of pre-existing angiogenically inactive vessels [23]. In contrast, many studies have shown that CD105 predominantly stain proliferating endothelial cells [22, 33, 38–46]. However, a few studies have observed CD105-positive vessels in normal [47] and GBM-adjacent brain tissue [48], and the marker needs further validation. Moreover, it has been shown that vWF sometimes fail to stain microvessels in both normal and neoplastic tissue [46].

vWF-MVD and CD105-MVD were highly correlated (Fig. 3), with a higher median and upper range for vWF-MVD. In addition, the high CD105-MVD/vWF-MVD

Table 1 Associations between MVDs and histopathological features

Histopathological features ^a	vWF-MVD (Median, 95% CI, ρ)	CD105-MVD (Median, 95% CI, ρ)
Thromboses	$p = 0.160$	$p = 0.125$
- Not present	12.0 (8.0, 21.8)	9.3 (7.2, 17.2)
- Present	15.7 (15.5, 20.2)	13.3 (13.9, 18.4)
High cellular density	$p = 0.345$	$p = 0.082$
- Not present	14.7 (14.0, 19.3)	12.0 (12.1, 16.8)
- Present	17.3 (14.6, 23.2)	16.3 (13.9, 21.9)
Mitotic count ^b	$p = 0.004^*$	$p = 0.001^*$
	$\rho = 0.29$	$\rho = 0.33$
High vascular density	$p = 0.016^*$	$p = 0.004^*$
- Not present	13.5 (12.9, 18.5)	11.3 (11.3, 15.8)
- Present	17.5 (16.5, 24.0)	16.5 (15.2, 22.9)

vWF-MVD Microvessel density count of von Willebrand factor. CD105-MVD Microvessel density count of CD105. CI Confidence interval. p : p -value. ρ Spearman correlation coefficient. ^a Subjectively assessed on hematoxylin-eosin sections. ^b Counted in hotspots for 10 high-power fields. *Statistically significant associations, $p < 0.05$

Table 2 Univariable analyses of associations between MVDs and tumor growth, Mann-Whitney U tests

	Slow-growing tumors	Fast-growing tumors	<i>p</i> -values
vWF-MVD	Median: 13.7 95% CI (12.9, 18.2) Range: 2.7–44.7 <i>N</i> = 49	Median: 17.3 95% CI (15.5, 22.7) Range: 0.7–62.0 <i>N</i> = 52	<i>p</i> = 0.211
CD105-MVD	Median: 11.7 95% CI (11.0, 16.2) Range: 1.0–42.7 <i>N</i> = 50 ^a	Median: 16.3 95% CI (14.2, 20.5) Range: 0.7–50.0 <i>N</i> = 51 ^a	<i>p</i> = 0.049*

vWF-MVD Microvessel density count of von Willebrand factor. CD105-MVD Microvessel density count of CD105. CI Confidence interval. *N* Number of cases.
* Statistically significant associations, *p* < 0.05. ^a One case was excluded from the vWF-MVD assessment, and another from the CD105-MVD assessment. These two cases were in different growth groups, which caused the change in number of cases for each group

ratio suggests most vasculature of GBM are angiogenically active. Because the markers were counted in corresponding HPFs, a high correlation coefficient was expected. However, some of the differences in the MVDs could be caused by random variations in vascular densities of different sections and the granular staining of vWF (Fig. 2), which sometimes made it more difficult to distinguish separate vascular units than in CD105 sections.

Neovasculature and tumor growth

CD105-MVD was no longer significantly associated with preoperative tumor growth in a multivariable model with thromboses and high cellular density, where both latter features were significant independent predictors of faster growth (Table 3). However, reverse causation may also be possible: faster growth could lead to thromboses and high cellular density. Furthermore, we observed that fast-growing tumors could have quite low CD105-MVD scores and slow-growing tumors quite high (Table 2, Fig. 4), which was in line with the finding that CD105-MVD explained very little of the variance in speed of growth (3%) in the univariable analysis (data not shown). Similar ranges of CD105-MVD were observed within the growth groups when patients with sparse tissue amounts (46 cases) were excluded (Additional file 1), and the weak association was thus unlikely a result of sampling errors.

Altogether, our results suggest that vWF-MVD and CD105-MVD are not predictive of faster GBM growth.

There are several biological mechanisms which could potentially explain the inferiority of CD105-MVD as an independent predictor of tumor growth. One reason could be that tumors can create a surplus of or ineffective vasculature due to excessive angiogenic stimuli [23], potentially leading to an overrepresentation of MVD counts. Excessive angiogenic stimuli may be caused by oncogenic mutations (known as hypoxia-independent angiogenesis [49]). Other explanations could be that other mechanisms of glioma-associated neovascularization account for additionally needed vasculature in fast-growing tumors [49], such as vascular co-option [50], vasculogenesis [51, 52], vascular mimicry (non-endothelial vasculature) [53], and glioblastoma-endothelial cell transdifferentiation [42]. Vascular mimicry is the process most likely to be overlooked by our methodology due to the lack of endothelial cells. In addition, the presence of vascular mimicry has been found to significantly predict higher glioma grades and worse prognosis [53]. However, it is uncertain to which degree and how the different processes of neovascularization interact, and further studies are needed [49].

In our previous study, we speculated that hypoxia initiated by thromboses facilitated growth through an induction of angiogenesis [13]. However, the finding that the presence of thromboses was still a significant independent

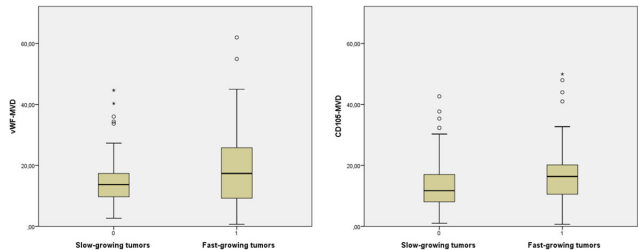


Fig. 4 Boxplots of vWF-MVD and CD105-MVD in slow and fast-growing tumors. Both MVDs show tendencies towards higher counts in fast-growing tumors, however, the spreads are large within both growth groups

Table 3 Multivariable binary logistic regression analysis of morphologic features and faster growth

Morphological features	Multivariable odds ratio (95% CI)	Multivariable <i>p</i> -values
High cellular density ^a	2.55 (1.007, 6.475)	0.048*
Thromboses ^a	4.21 (1.245, 14.253)	0.021*
CD105-MVD	1.03 (0.982, 1.070)	0.255

CI Confidence interval. CD105-MVD Microvessel density count of CD105.
^aSubjectively assessed on hematoxylin-eosin sections. *Statistically significant associations, *p* < 0.05

predictor of faster tumor growth when the degree of angiogenesis was not, suggests angiogenesis-independent mechanisms driven by hypoxia contribute to faster GBM growth. Such hypoxia induced mechanisms may act through other mechanisms of glioma-associated vascularization [49], augmentation of proliferation [54, 55], and initiation of invasiveness [19, 55]. Increased invasiveness is one of the proposed mechanisms of resistance to anti-VEGF (bevacizumab) treatment [55–59], and thus the lack of survival benefit in randomized trials [20, 21]. Some studies even suggest GBM growth is possible without an induction of angiogenesis [19, 60]. Such angiogenesis-independent growth may be described by the “go-or-grow” hypothesis, where tumor cells switch between two mutually exclusive phenotypes of either proliferative or invasive characteristics [61, 62]. Hypoxia has been proposed to induce the switch to the invasive phenotype [62]. In this way, hypoxic tumor cells migrate away from hypoxic areas and switch back to a proliferative phenotype when nutrients are adequate without an induction of angiogenesis [60]. In addition, Sakariassen et al. [19], discovered that xenotransplanted GBMs in nude rats could present as fatal diseases without signs of angiogenesis. Nevertheless, invading cells are unlikely to be captured as contrast enhancement without an induction of angiogenesis [19, 59, 63], and are therefore unlikely to have been measured in our study. Additionally, the non-significant multivariable association for CD105-MVD could perhaps be caused by the nearly significant associations between CD105-MVD and thromboses and high cellularity (Table 1). Collectively, our findings support that angiogenesis-independent mechanisms driven by hypoxia contribute to faster GBM growth, which might explain the lack of survival benefit of anti-VEGF treatment.

As thromboses, high cellular density maintained its role as a significant independent predictor of faster growth in our study (Table 3). This finding substantiates our previous speculation that it is a better marker of high proliferation rates than high mitotic counts, because mitotic count has many potential sources of errors [64], and higher counts were significantly associated with the

presence of thromboses [13] and increasing CD105-MVD counts (Table 1).

Microvessel methodology

So far, there is no standard method for quantification of MVD, however, initiatives on international standardizations have been made [65]. Like in our study, most studies are based on the methods described by Weidner et al. [27] with modifications: they count single positive cells and avoid areas of sclerosis, necrosis, and non-neoplastic tissue. However, few have specified their handling of glomeruloid tufts and longer vessels. We believe as Leon et al. [36], that counting a glomeruloid tuft as one vascular unit might underestimate the angiogenic stimuli of the tumor. Furthermore, the subjective assessment of hotspots and interpretation of positive immunostaining give rise to problematic inter-observer variability, which has been reported as quite high for MVD assessments in GBMs [66].

Even though we found significant associations with both MVDs and subjectively assessed high vascular densities on HE slides, the spreads of the MVDs were wide within and overlapping between the categories of vascular density (Table 1). These findings were in line with the fact that capillaries is known to be inconspicuous on HE slides [28].

Strengths and limitations

Limitations of the assessments of tumor volumes on MRI scans, growth rates, and histopathological features have previously been described in detail [10, 13]. The main strengths are the relatively large number of patients with a population based referral and the reproducibility assessment of tumor volumes [10]. Potential biases are selection biases, preoperative steroid treatment, differences in diagnostic MRI scanners, different timing and administration of the contrast agent, tumor cells existing beyond the contrast enhancing rim [67, 68], and sampling errors and inter-observer variability of the histopathological assessments. Additionally, our analyses were exploratory and should be validated in future studies.

Conclusions

Our results showed that MVD assessments of vWF and CD105 were not independent predictors of radiological speed of growth, although CD105-MVD was significantly associated with faster growth in the univariable analysis. In contrast, thromboses and high cellular density were significant independent predictors of faster growth. In summary, our findings suggest angiogenesis-independent mechanisms contribute to faster GBM growth.

Additional files

Additional file 1: Univariable analysis of associations between CD105-MVD and tumor growth when cases with sparse tissue amount are excluded (46 cases). Mann-Whitney U tests. CD105-MVD: Microvessel density count of CD105. CI: Confidence interval. N: Number of cases. (DOCX 12 kb)

Additional file 2: Dataset supporting conclusions. The minimal dataset necessary to replicate the findings reported in the article. Microvessel densities (MVDs) of both markers are presented as mean counts for 3 high-power fields (HPFs). Regarding the categorical histopathological features (thromboses, high cellular density, and high vascular density), "1" indicates that features are present, while "0" indicates that they are not. Mitotic counts are counted in 10 HPFs. Tumors growing faster than expected are indicated by "1", whereas slow-growing tumors are indicated by "0". Patients preoperatively treated with corticosteroids or having sparse amount of tissue available for the histopathological evaluation are indicated by "1" in the respective variables. (XLSX 15 kb)

Abbreviations

CD: Clusters of differentiation; FFPE: Formalin-fixed paraffin-embedded; GBM: Glioblastoma; GFAP: Glial fibrillary acidic protein; HE: Hematoxylin-eosin; HPF: High-power field; HRP: Horseradish peroxidase; IDH1: Isocitrate dehydrogenase 1; LSAB: Labeled streptavidin-biotin; MRI: Magnetic resonance imaging; MVD: Microvessel density; OR: Odds ratio; VEGF: Vascular endothelial growth factor; vWF: von Willebrand factor; WHO: World Health Organization

Acknowledgements

We thank the staff at the Cellular and Molecular Imaging Core Facility (CMIC) for excellent laboratory work.

Funding

VEM and ALS received research scholarship from the Norwegian University of Science and Technology (NTNU). OS received research salaries from the National Competence Centre for Ultrasound and Image Guided Therapy. EMB received research funding from the Norwegian National Advisory Unit on Functional MRI Methods and the Central Norwegian Brain Tumor Registry. The funding sources had no role in the design of the study, and collection, analysis, and interpretation of the data, or writing of the manuscript.

Availability of data and materials

The dataset supporting the conclusions of this article are included in its additional files (see Additional file 2).

Authors' contributions

VEM and SHT conceived and designed the study. VEM and SHT confirmed the histopathological diagnoses and performed the assessment of histopathological features. VEM did the microvessel density assessments. USG performed the immunohistochemical staining of vWF and CD105. ALS and EMB performed the segmentations of tumor volumes on MRI scans. ALS and ØS computed the growth data. VEM, ALS, ØS, OS, and SHT were involved in the analysis and interpretation of data. VEM wrote the manuscript, and all authors have critically revised the manuscript. The study was supervised by OS and SHT. All authors read and approved the final manuscript.

Ethics approval and consent to participate

The study was approved by the Regional Ethics Committee (Central) as part of a larger project (references 2011/974 and 2013/1348) and adhered with the Declaration of Helsinki. Most patients had provided written informed consent to be included in a related glioma outcome study (reference 2011/974). The regional ethics committee waived informed consent for retrospective evaluation of patient data for the remaining patients, and did not require obtained written informed consent from a relative/guardian.

Consent for publication

Not applicable.

Competing interests

OS has previously been an unpaid member of a national advisory committee on treatment guidelines for brain tumors. All other authors disclose no potential conflicts of interest.

Publisher's Note

Springer Nature remains neutral with regard to jurisdictional claims in published maps and institutional affiliations.

Author details

¹Department of Clinical and Molecular Medicine, Faculty of Medicine and Health Sciences, NTNU - Norwegian University of Science and Technology, Erling Skjalgssons gate 1, 7030 Trondheim, Norway. ²Department of Circulation and Medical Imaging, Faculty of Medicine and Health Sciences, NTNU - Norwegian University of Science and Technology, Trondheim, Norway. ³Department of Neurosurgery, St. Olavs University Hospital, Trondheim, Norway. ⁴Cellular and Molecular Imaging Core Facility (CMIC), Faculty of Medicine and Health Sciences, Norwegian University of Science and Technology (NTNU), Trondheim, Norway. ⁵Department of Radiology and Nuclear Medicine, St. Olavs University Hospital, Trondheim, Norway. ⁶Department of Public Health and Nursing, Faculty of Medicine and Health Sciences, NTNU - Norwegian University of Science and Technology, Trondheim, Norway. ⁷National Advisory Unit for Ultrasound and Image Guided Therapy, St. Olavs University Hospital, Trondheim, Norway. ⁸Department of Neuromedicine and Movement Science, Faculty of Medicine and Health Sciences, NTNU - Norwegian University of Science and Technology, Trondheim, Norway. ⁹Department of Pathology, St. Olavs University Hospital, Trondheim, Norway.

Received: 19 December 2017 Accepted: 22 August 2018

Published online: 03 September 2018

References

- Ostrom QT, Gittleman H, Xu J, Kromer C, Wolinsky Y, Kruchko C, et al. CBTRUS statistical report: primary brain and other central nervous system tumors diagnosed in the United States in 2009-2013. *Neuro-Oncology*. 2016; 18:v1–v75. <https://doi.org/10.1093/neuonc/nov207>.
- Ronning PA, Helseth E, Meling TR, Johannessen TB. A population-based study on the effect of temozolomide in the treatment of glioblastoma multiforme. *Neuro-Oncology*. 2012;14:1178–84. <https://doi.org/10.1093/neuonc/nos153>.
- Burger PC, Kleihues P. Cytologic composition of the untreated glioblastoma with implications for evaluation of needle biopsies. *Cancer*. 1989;63:2014–23.
- Eder K, Kalman B. Molecular heterogeneity of glioblastoma and its clinical relevance. *Pathol Oncol Res*. 2014;20:777–87. <https://doi.org/10.1007/s12253-014-9833-3>.
- Miller CR, Perry A. Glioblastoma. *Arch Pathol Lab Med*. 2007;131:397–406. [https://doi.org/10.1043/1543-2165\(2007\)131\[397:gj2.0.co;2](https://doi.org/10.1043/1543-2165(2007)131[397:gj2.0.co;2).
- Kaur B, Khwaja FW, Severson EA, Matheny SL, Brat DJ, Van Meir EG. Hypoxia and the hypoxia-inducible-factor pathway in glioma growth and angiogenesis. *Neuro-Oncology*. 2005;7:134–53. <https://doi.org/10.1215/s152851704001115>.
- Fischer I, Gagner JP, Law M, Newcomb EW, Zagzag D. Angiogenesis in gliomas: biology and molecular pathophysiology. *Brain Pathol*. 2005;15:297–310.
- Onishi M, Kurozumi K, Ichikawa T, Date I. Mechanisms of tumor development and anti-angiogenic therapy in glioblastoma multiforme. *Neurol Med Chir (Tokyo)*. 2013;53:755–63.
- Brat DJ, Van Meir EG. Vaso-occlusive and prothrombotic mechanisms associated with tumor hypoxia, necrosis, and accelerated growth in glioblastoma. *Lab Invest*. 2004;84:397–405. <https://doi.org/10.1038/labinvest.3700070>.
- Stensjoen AL, Solheim O, Kvistad KA, Haberg AK, Salvesen O, Berntsen EM. Growth dynamics of untreated glioblastomas in vivo. *Neuro-Oncology*. 2015;17:1402–11. <https://doi.org/10.1093/neuonc/nov029>.
- Ellingson BM, Nguyen HN, Lai A, Nechifor RE, Zaw O, Pope WB, et al. Contrast-enhancing tumor growth dynamics of preoperative, treatment-naïve human glioblastoma. *Cancer*. 2016;122:1718–27. <https://doi.org/10.1002/cncr.29957>.
- Stensjoen AL, Berntsen EM, Mikkelsen VE, Torp SH, Jakola AS, Salvesen O, et al. Does Pretreatment Tumor Growth Hold Prognostic Information for

- Patients with Glioblastoma? *World Neurosurg.* 2017;101:686–94.e4. <https://doi.org/10.1016/j.wneu.2017.03.012>.
13. Mikkelsen VE, Stensjoen AL, Berntsen EM, Nordrum IS, Salvesen O, Solheim O, et al. Histopathologic features in relation to pretreatment tumor growth in patients with glioblastoma. *World Neurosurg.* 2018;109:e50–e8. <https://doi.org/10.1016/j.wneu.2017.09.102>.
 14. Rong Y, Durden DL, Van Meir EG, Brat DJ. 'Pseudopalisading' necrosis in glioblastoma: a familiar morphologic feature that links vascular pathology, hypoxia, and angiogenesis. *J Neuropathol Exp Neurol.* 2006;65:529–39.
 15. Hanahan D, Weinberg RA. Hallmarks of cancer: the next generation. *Cell.* 2011;144:646–74. <https://doi.org/10.1016/j.cell.2011.02.013>.
 16. Maxwell PH, Dachs GU, Gleadle JM, Nicholls LG, Harris AL, Stratford IJ, et al. Hypoxia-inducible factor-1 modulates gene expression in solid tumors and influences both angiogenesis and tumor growth. *Proc Natl Acad Sci U S A.* 1997;94:8104–9.
 17. Blouw B, Song H, Tihan T, Bosze J, Ferrara N, Gerber HP, et al. The hypoxic response of tumors is dependent on their microenvironment. *Cancer Cell.* 2003;4:133–46.
 18. Gillespie DL, Whang K, Ragel BT, Flynn JR, Kelly DA, Jensen RL. Silencing of hypoxia inducible factor-1alpha by RNA interference attenuates human glioma cell growth in vivo. *Clin Cancer Res.* 2007;13:2441–8. <https://doi.org/10.1158/1078-0432.ccr-06-2692>.
 19. Sakariassen PO, Prestegarden L, Wang J, Skafnesmo KO, Mahesparan R, Molthoff C, et al. Angiogenesis-independent tumor growth mediated by stem-like cancer cells. *Proc Natl Acad Sci U S A.* 2006;103:16466–71. <https://doi.org/10.1073/pnas.0607668103>.
 20. Chinot OL, Wick W, Mason W, Henriksson R, Saran F, Nishikawa R, et al. Bevacizumab plus radiotherapy-temozolomide for newly diagnosed glioblastoma. *N Engl J Med.* 2014;370:709–22. <https://doi.org/10.1056/NEJMoa1308345>.
 21. Gilbert MR, Dignam JJ, Armstrong TS, Wefel JS, Blumenthal DT, Vogelbaum MA, et al. A randomized trial of bevacizumab for newly diagnosed glioblastoma. *N Engl J Med.* 2014;370:699–708. <https://doi.org/10.1056/NEJMoa1308573>.
 22. Rakocevic J, Orlie D, Mitrovic-Ajtic O, Tomasevic M, Dobric M, Zlati N, et al. Endothelial cell markers from clinician's perspective. *Exp Mol Pathol.* 2017;102:303–13. <https://doi.org/10.1016/j.jexmp.2017.02.005>.
 23. Hlatky L, Hahnfeldt P, Folkman J. Clinical application of antiangiogenic therapy: microvessel density, what it does and doesn't tell us. *J Natl Cancer Inst.* 2002;94:883–93.
 24. Nassiri F, Cusimano MD, Scheithauer BW, Rotondo F, Fazio A, Yousef GM, et al. Endoglin (CD105): a review of its role in angiogenesis and tumor diagnosis, progression and therapy. *Anticancer Res.* 2011;31:2283–90.
 25. Louis DN, Ohgaki H, Wiestler O, Cavenee WK. WHO Classification of Tumours of the Central Nervous System. 4th ed. CH-1211 Geneva 27, Switzerland: International Agency for Research on Cancer (IARC); 2007.
 26. Osborn AG. Astrocytomas. In: Renlund AR, editor. Osborn's brain: imaging, pathology and anatomy. First ed. Altona, Manitoba, Canada: Amirsys Publishing, Inc.; 2013. p. 484–90.
 27. Weidner N, Semple JP, Welch WR, Folkman J. Tumor angiogenesis and metastasis—correlation in invasive breast carcinoma. *N Engl J Med.* 1991;324:1–8. <https://doi.org/10.1056/nejm19910103324101>.
 28. Louis DN. Molecular pathology of malignant gliomas. *Annu Rev Pathol.* 2006;1:97–117. <https://doi.org/10.1146/annurev.pathol.1.110304.100043>.
 29. Kraby MR, Kruger K, Opdahl S, Vatten LJ, Akslen LA, Bofin AM. Microvascular proliferation in luminal a and basal-like breast cancer subtypes. *J Clin Pathol.* 2015;68:891–7. <https://doi.org/10.1136/clinpath-2015-203037>.
 30. Huszthy PC, Daphu I, Nicolou SP, Stieber D, Nigro JM, Sakariassen PO, et al. In vivo models of primary brain tumors: pitfalls and perspectives. *Neuro-Oncology.* 2012;14:979–93. <https://doi.org/10.1093/neuonc/nos135>.
 31. Tastekin E, Caloglu VY, Puyan FO, Tokuc B, Caloglu M, Yalta TD, et al. Prognostic value of angiogenesis and Survivin expression in patients with glioblastoma. *Turk Neurosurg.* 2016;26:484–90. <https://doi.org/10.5137/1019-5149.jtn.16552-15.1>.
 32. Flynn JR, Wang L, Gillespie DL, Stoddard GJ, Reid JK, Owens J, et al. Hypoxia-regulated protein expression, patient characteristics, and preoperative imaging as predictors of survival in adults with glioblastoma multiforme. *Cancer.* 2008;113:1032–42. <https://doi.org/10.1002/cncr.23678>.
 33. Yao Y, Kubota T, Takeuchi H, Sato K. Prognostic significance of microvessel density determined by an anti-CD105/endoglin monoclonal antibody in astrocytic tumors: comparison with an anti-CD31 monoclonal antibody. *Neuropathology.* 2005;25:201–6.
 34. Behrem S, Zarkovic K, Eskinja N, Jonjic N. Endoglin is a better marker than CD31 in evaluation of angiogenesis in glioblastoma. *Croat Med J.* 2005;46:417–22.
 35. Sica G, Lama G, Anile C, Geloso MC, La Torre G, De Bonis P, et al. Assessment of angiogenesis by CD105 and nestin expression in peritumor tissue of glioblastoma. *Int J Oncol.* 2011;38:41–9.
 36. Leon SP, Folkherth RD, Black PM. Microvessel density is a prognostic indicator for patients with astroglial brain tumors. *Cancer.* 1996;77:362–72. [https://doi.org/10.1002/\(sici\)1097-0142\(19960115\)77:2<362::aid-cncr20>3.0.co;2-z](https://doi.org/10.1002/(sici)1097-0142(19960115)77:2<362::aid-cncr20>3.0.co;2-z).
 37. Kong X, Wang Y, Liu S, Xing B, Yang Y, Li Y, et al. CD105 over-expression is associated with higher WHO grades for gliomas. *Mol Neurobiol.* 2016; <https://doi.org/10.1007/s12035-015-9677-1>.
 38. Burrows FJ, Derbyshire EJ, Tazzari PL, Amlot P, Gazdar AF, King SW, et al. Up-regulation of endoglin on vascular endothelial cells in human solid tumors: implications for diagnosis and therapy. *Clin Cancer Res.* 1995;1:1623–34.
 39. Seon BK, Matsuno F, Haruta Y, Kondo M, Barcos M. Long-lasting complete inhibition of human solid tumors in SCID mice by targeting endothelial cells of tumor vasculature with antihuman endoglin immunotoxin. *Clin Cancer Res.* 1997;3:1031–44.
 40. Miller DW, Graulich W, Karges B, Stahl S, Ernst M, Ramaswamy A, et al. Elevated expression of endoglin, a component of the TGF-beta-receptor complex, correlates with proliferation of tumor endothelial cells. *Int J Cancer.* 1999;81:568–72.
 41. Dallas NA, Samuel S, Xia L, Fan F, Gray MJ, Lim SJ, et al. Endoglin (CD105): a marker of tumor vasculature and potential target for therapy. *Clin Cancer Res.* 2008;14:1931–7. <https://doi.org/10.1158/1078-0432.ccr-07-4478>.
 42. Wang R, Chadalavada K, Wilshire J, Kowalik U, Hovinga KE, Geber A, et al. Glioblastoma stem-like cells give rise to tumour endothelium. *Nature.* 2010;468:829–33. <https://doi.org/10.1038/nature09624>.
 43. Krupinski J, Kaluza J, Kumar P, Kumar S, Wang JM. Role of angiogenesis in patients with cerebral ischemic stroke. *Stroke.* 1994;25:1794–8.
 44. Minhajit R, Mori D, Yamasaki F, Sugita Y, Satoh T, Tokunaga O. Organ-specific endoglin (CD105) expression in the angiogenesis of human cancers. *Pathol Int.* 2006;56:717–23. <https://doi.org/10.1111/j.1440-1827.2006.02037.x>.
 45. Birner P, Piribauer M, Fischer I, Gatterbauer B, Marosi C, Ambros PF, et al. Vascular patterns in glioblastoma influence clinical outcome and associate with variable expression of angiogenic proteins: evidence for distinct angiogenic subtypes. *Brain Pathol.* 2003;13:133–43.
 46. Wang JM, Kumar S, Pye D, Haboubi N, al-Nakib L. Breast carcinoma: comparative study of tumor vasculature using two endothelial cell markers. *J Natl Cancer Inst.* 1994;86:386–8.
 47. Matsubara S, Bourdeau A, terBrugge KG, Wallace C, Letarte M. Analysis of endoglin expression in normal brain tissue and in cerebral arteriovenous malformations. *Stroke.* 2000;31:2653–60.
 48. Balza E, Castellani P, Zijlstra A, Neri D, Zardi L, Siri A. Lack of specificity of endoglin expression for tumor blood vessels. *Int J Cancer.* 2001;94:579–85.
 49. Hardee ME, Zagzag D. Mechanisms of glioma-associated neovascularization. *Am J Pathol.* 2012;181:1126–41. <https://doi.org/10.1016/j.ajpath.2012.06.030>.
 50. Holash J, Maisonpierre PC, Compton D, Boland P, Alexander CR, Zagzag D, et al. Vessel cooption, regression, and growth in tumors mediated by angiopoietins and VEGF. *Science.* 1999;284:1994–8.
 51. Lyden D, Hattori K, Dias S, Costa C, Baikie P, Butros L, et al. Impaired recruitment of bone-marrow-derived endothelial and hematopoietic precursor cells blocks tumor angiogenesis and growth. *Nat Med.* 2001;7:1194–201. <https://doi.org/10.1038/nm1101-1194>.
 52. Pepper MS. Transforming growth factor-beta: vasculogenesis, angiogenesis, and vessel wall integrity. *Cytokine Growth Factor Rev.* 1997;8:21–43.
 53. Liu XM, Zhang QP, Mu YG, Zhang XH, Sai K, Pang JC, et al. Clinical significance of vasculogenic mimicry in human gliomas. *J Neuro-Oncol.* 2011;105:173–9. <https://doi.org/10.1007/s11060-011-0578-5>.
 54. Song Y, Zheng S, Wang J, Long H, Fang L, Wang G, et al. Hypoxia-induced PLOD2 promotes proliferation, migration and invasion via PI3K/Akt signaling in glioma. *Oncotarget.* 2017;8:41947–62. <https://doi.org/10.18632/oncotarget.16710>.
 55. Xu H, Rahimpour S, Nesvick CL, Zhang X, Ma J, Zhang M, et al. Activation of hypoxia signaling induces phenotypic transformation of glioma cells: implications for bevacizumab antiangiogenic therapy. *Oncotarget.* 2015;6:11882–93. <https://doi.org/10.18632/oncotarget.3592>.
 56. de Groot JF, Fuller G, Kumar AJ, Piao Y, Eterovic K, Ji Y, et al. Tumor invasion after treatment of glioblastoma with bevacizumab: radiographic and

- pathologic correlation in humans and mice. *Neuro-Oncology*. 2010;12:233–42. <https://doi.org/10.1093/neuonc/nop027>.
57. Nowosielski M, Ellingson BM, Chinot OL, Garcia J, Revil C, Radbruch A, et al. Radiologic progression of glioblastoma under therapy - an exploratory analysis of AVAglio. *Neuro-Oncology*. 2017; <https://doi.org/10.1093/neuonc/nox162>.
 58. Obad N, Espedal H, Jirik R, Sakariassen PO, Brekke Rygh C, Lund-Johansen M, et al. Lack of functional normalisation of tumour vessels following anti-angiogenic therapy in glioblastoma. *J Cereb Blood Flow Metab*. 2017; 271678x17714656. <https://doi.org/10.1177/0271678x17714656>.
 59. Keunen O, Johansson M, Oudin A, Sanzey M, Rahim SA, Fack F, et al. Anti-VEGF treatment reduces blood supply and increases tumor cell invasion in glioblastoma. *Proc Natl Acad Sci U S A*. 2011;108:3749–54. <https://doi.org/10.1073/pnas.1014480108>.
 60. Scribner E, Saut O, Province P, Bag A, Colin T, Fathallah-Shaykh HM. Effects of anti-angiogenesis on glioblastoma growth and migration: model to clinical predictions. *PLoS One*. 2014;9:e115018. <https://doi.org/10.1371/journal.pone.0115018>.
 61. Giese A, Loo MA, Tran N, Haskett D, Coons SW, Berens ME. Dichotomy of astrocytoma migration and proliferation. *Int J Cancer*. 1996;67:275–82. [https://doi.org/10.1002/\(sici\)1097-0215\(199607\)767:2<275::aid-ijc20>3.0.co;2-9](https://doi.org/10.1002/(sici)1097-0215(199607)767:2<275::aid-ijc20>3.0.co;2-9).
 62. Hatzikiro H, Basanta D, Simon M, Schaller K, Deutsch A. 'Go or grow': the key to the emergence of invasion in tumour progression? *Math Med Biol*. 2012;29:49–65. <https://doi.org/10.1093/imammb/dq011>.
 63. Onishi M, Ichikawa T, Kurozumi K, Date I. Angiogenesis and invasion in glioma. *Brain Tumor Pathol*. 2011;28:13–24. <https://doi.org/10.1007/s10014-010-0007-z>.
 64. Prayson RA. Cell proliferation and tumors of the central nervous system. Part 1: evaluation of mitotic activity. *J Neuropathol Exp Neurol*. 2002;61:501–9.
 65. Vermeulen PB, Gasparini G, Fox SB, Colpaert C, Marson LP, Gion M, et al. Second international consensus on the methodology and criteria of evaluation of angiogenesis quantification in solid human tumours. *Eur J Cancer*. 2002;38:1564–79.
 66. Preusser M, Heinzl H, Gelpi E, Schonegger K, Haberler C, Birner P, et al. Histopathologic assessment of hot-spot microvessel density and vascular patterns in glioblastoma: poor observer agreement limits clinical utility as prognostic factors: a translational research project of the European Organization for Research and Treatment of Cancer brain tumor group. *Cancer*. 2006;107:162–70. <https://doi.org/10.1002/cncr.21973>.
 67. Kelly PJ, Daumas-Duport C, Kispert DB, Kall BA, Scheithauer BW, Illig JJ. Imaging-based stereotaxic serial biopsies in untreated intracranial glial neoplasms. *J Neurosurg*. 1987;66:865–74. <https://doi.org/10.3171/jns.1987.66.6.0865>.
 68. Yamahara T, Numa Y, Oishi T, Kawaguchi T, Seno T, Asai A, et al. Morphological and flow cytometric analysis of cell infiltration in glioblastoma: a comparison of autopsy brain and neuroimaging. *Brain Tumor Pathol*. 2010;27:81–7. <https://doi.org/10.1007/s10014-010-0275-7>.

Ready to submit your research? Choose BMC and benefit from:

- fast, convenient online submission
- thorough peer review by experienced researchers in your field
- rapid publication on acceptance
- support for research data, including large and complex data types
- gold Open Access which fosters wider collaboration and increased citations
- maximum visibility for your research: over 100M website views per year

At BMC, research is always in progress.





Learn more biomedcentral.com/submissions



Paper III

ORIGINAL ARTICLE

MGMT Promoter Methylation Status Is Not Related to Histological or Radiological Features in IDH Wild-type Glioblastomas

Vilde Elisabeth Mikkelsen , MD, Hong Yan Dai, PhD, Anne Line Stensjøen, MD, PhD, Erik Magnus Berntsen , MD, PhD, Øyvind Salvesen, PhD, Ole Solheim , MD, PhD, and Sverre Helge Torp , MD, PhD

Abstract

O⁶-methylguanine DNA methyltransferase (*MGMT*) promoter methylation is an important favorable predictive marker in patients with glioblastoma (GBM). We hypothesized that *MGMT* status could be a surrogate marker of pretreatment tumor biology observed as histopathological and radiological features. Apart from some radiological studies aiming to noninvasively predict the *MGMT* status, few studies have investigated relationships between *MGMT* status and phenotypical tumor biology. We have therefore aimed to investigate such relationships in 85 isocitrate dehydrogenase (*IDH*) wild-type GBMs. *MGMT* status was determined by methylation-specific PCR and was assessed for associations with 22 histopathological features, immunohistochemical proliferative index and microvessel density measurements, conventional magnetic resonance imaging characteristics, preoperative speed of tumor growth, and overall sur-

vival. None of the investigated histological or radiological features were significantly associated with *MGMT* status. Methylated *MGMT* status was a significant independent predictor of improved overall survival. In conclusion, our results suggest that *MGMT* status is not related to the pretreatment phenotypical biology in *IDH* wild-type GBMs. Furthermore, our findings suggest the survival benefit of *MGMT* methylated GBMs is not due to an inherently less aggressive tumor biology, and that conventional magnetic resonance imaging features cannot be used to noninvasively predict the *MGMT* status.

Key Words: Angiogenesis, Glioblastoma, Histopathology, Magnetic resonance imaging, *MGMT* promoter methylation, Tumor growth.

INTRODUCTION

Glioblastomas (GBMs) are the most common of the primary malignant brain tumors in adults (1). The overall survival is only 14–16 months despite standard treatment of surgical resection and adjuvant concomitant radiation and chemotherapy (temozolomide) (2, 3). GBMs are biologically highly complex and aggressive tumors, illustrated by their rapid growth (4) and heterogeneous histological and molecular pathology (5–7).

O⁶-methylguanine DNA methyltransferase (*MGMT*) promoter methylation is an important predictive biomarker of improved response to temozolomide in GBMs (8, 9). *MGMT* is a DNA-repair enzyme that removes alkylated guanine residues on DNA, and hence counteracts the effect of alkylating agents, such as temozolomide (10). Methylation of the *MGMT* promoter leads to inactivation of the enzyme, which is believed to cause the predictive effect (10). However, it is not yet established whether it is purely a predictive marker or in part prognostic by itself, as previous studies have shown conflicting results regarding its prognostic value among patients who did not receive chemotherapy (8, 11–15). As *MGMT* promoter methylation status guides treatment decisions regarding chemotherapy (9), several radiological studies have sought to

From the Department of Clinical and Molecular Medicine, Faculty of Medicine and Health Sciences, NTNU—Norwegian University of Science and Technology (VEM, SHT); Department of Pathology, St Olav's University Hospital (HYD, SHT); Department of Circulation and Medical Imaging, Faculty of Medicine and Health Sciences, NTNU—Norwegian University of Science and Technology (ALS, EMB); Department of Radiology and Nuclear Medicine, St. Olav's University Hospital (EMB); Department of Public Health and Nursing (OS); Department of Neuromedicine and Movement Science (OS), Faculty of Medicine and Health Sciences, NTNU—Norwegian University of Science and Technology; and Department of Neurosurgery, St. Olav's University Hospital (OS), Trondheim, Norway.

Send correspondence to: Vilde Elisabeth Mikkelsen, MD, Department of Clinical and Molecular Medicine, Faculty of Medicine and Health Sciences, NTNU—Norwegian University of Science and Technology, 7491 Trondheim, Norway; E-mail: vilde.e.mikkelsen@ntnu.no

V.E.M. and A.L.S. have received research scholarships from NTNU—Norwegian University of Science and Technology. O.S. has received research salaries from the National Competence Centre for Ultrasound and Image Guided Therapy, and E.M.B. has received research funding from the Central Norwegian Brain Tumor Registry. The funding sources had no role in the design of the study, writing of the manuscript, or collection, analysis, and interpretation of data.

O.S. is a previous unpaid member of a National Advisory Committee on Treatment Guidelines for Brain Tumors. All other authors have no dual-ity or conflicts of interest to declare.

noninvasively predict the methylation status. However, results from these studies have also been conflicting (16).

We hypothesized that *MGMT* promoter methylation status could be a surrogate marker of pretreatment phenotypical tumor biology assessed by histopathology and magnetic resonance imaging (MRI) in GBMs. Apart from some radiological studies, few studies have investigated such relationships. By exploring these potential relationships using tissue material and MRI scans collected before treatment, we aimed to discover if there are differences in the inherent aggressiveness between *MGMT* methylated and unmethylated patients (i.e. a prognostic value). Moreover, such potential biological differences may also partially explain the different responses to chemotherapy. Our study could also further elucidate whether *MGMT* status can be predicted from preoperative MRI scans. In a cohort of treatment-naïve, isocitrate dehydrogenase (*IDH*) wild-type (wt) GBMs previously assessed for preoperative growth characteristics (4), we have therefore aimed to investigate whether *MGMT* status was associated with histological and radiological features.

MATERIALS AND METHODS

Patients and Samples

The selection of patients was based on the previous work by Stensjøen et al in which the preoperative growth dynamics of GBMs were investigated (4). Patients were retrospectively selected from all patients >18 years operated for newly diagnosed GBMs at St. Olav's University Hospital, Trondheim, Norway between January 2004 and May 2014 (n = 262) (4). Patients with 2 preoperative contrast-enhancing T1-weighted (T1wGd) MRI scans taken 14 days apart were eligible, and patients without contrast enhancement and/or gliomatosis cerebri were excluded (4). All cases were microscopically revised and *IDH* mutation status assessed according to the 2016 World Health Organization (WHO) Classification of Tumors of the Central Nervous System (17). *IDH* mutation status was first assessed using immunohistochemistry (18), and all immune-negative patients <55 years (18 patients) were additionally sequenced using Sanger sequencing according to previously described methods (using the BigDye Terminator v3.1 cycle sequencing kit and the 3130 genetic analyzer from Applied Biosystems, Foster City, CA) (19). Three patients were *IDH* mutated and were therefore excluded from the study. In 5 patients, *IDH2* could not be sequenced; however, these were all *IDH1* wt on sequencing. Due to the very low frequency of *IDH2* mutations in newly diagnosed GBMs (20, 21), these were categorized as *IDH* wt and included in the study. The collection of clinical data regarding survival, treatment, sex, age at diagnosis, and Karnofsky performance status have previously been accounted for (18). Furthermore, of the 106 patients (4) analyzed for *MGMT* promoter methylation status, 18 were excluded (17%) due to inconclusive results. Hence, 85 patients were included in the current study.

DNA Extraction and *MGMT* Methylation-Specific PCR

For DNA isolation, an area of central tumor morphology (visually 100% tumor cells) was marked on hematoxylin and eosin (H&E) slides from formalin-fixed paraffin-embedded (FFPE) tissue blocks for each patient. Necrotic areas were avoided. Due to a lack of tumor material, 4 cases had a tumor cell content of 40%–70% in the marked areas. The marked areas were manually dissected, and tumor DNA then extracted using the QIAamp DNA FFPE Tissue Kit (Qiagen, Hilden, Germany). QIAcube (Qiagen) was used for automated spin column process of DNA purification following the manufacturer's instructions.

Methylation-specific PCR (MSP) was performed following bisulfite treatment of the isolated DNA using the EpiTect Fast Bisulfite Conversion kit (Qiagen). According to the method by Esteller et al (22), PCR amplification was performed using specific primers covering methylation of the *MGMT* promoter and exon 1 region. Methylated and unmethylated PCR products were detected with 4% agarose gel. An *MGMT* methylation-positive and a negative tissue control were applied during the whole process. The investigator who analyzed and interpreted the MSP data was blinded to other data.

Histopathology and Immunohistochemistry

All available H&E-stained FFPE sections from each case were assessed for the presence of 22 histopathological features. Definitions of each feature can be found in our previous publication (23). Most features were defined as either present or absent, while cellular density and atypia were semiquantitatively graded. Mitoses were counted in 10 high-power fields in hotspots. In 32 cases (38%), the amount of tissue on H&E slides has previously been subjectively categorized as sparse (23). This semiquantitative categorization was based on the collective area of viable (i.e. nonnecrotic) tumor tissue on all available H&E slides from each patient. Sparse tissue amount was often due to the patient being biopsied or having extensive necrosis in the resected material (23).

The immunohistochemical examinations of IDH1 R132H (monoclonal, IDH1 R132H/H09, 1:100, Dianova, Hamburg, Germany) (18), Ki-67/MIB-1 (monoclonal, Ki-67/MIB-1, 1:800 or 1:50, Dako, Glostrup, Denmark) (18), and CD105/endothelin (monoclonal, CD105/endothelin/SN6h, 1:50, Dako) (24) have previously been done and described in detail. The proliferative index (PI) of Ki-67/MIB-1 was quantified as described in our previous publication (18). The degree of angiogenesis has previously been quantified using microvessel density measurements of endoglin/CD105 (24). In short, the microvessel density was computed as the mean count of the number of vascular structures within a grid for 3 high-power fields in hotspots at ×400 magnification.

MRI Characteristics and Preoperative Tumor Growth

The MRI segmentations of total tumor volumes, volumes of the contrast enhancing and noncontrast enhancing

compartments, and estimation of speed of tumor growth have previously been accounted for (4, 18). The software Brain-Voyager QX (Brain Innovation, Maastricht, the Netherlands) was used for the volume segmentations (4). The tumor volumes were segmented from 2 preoperative T1wGd MRI scans from each patient (first scan taken at radiological diagnosis and the second preoperative scan for neuronavigation). The MRI characteristics assessed for associations with *MGMT* status were segmented from the second, preoperative scan. Total tumor volume was defined as the combined volume of the contrast enhancing rim and the noncontrast enhancing (necrotic) core. Preoperative speed of growth was estimated from the total tumor volumes at both scans and the interval between them (4, 18). A fitted Gompertzian growth curve from 106 patients was used to dichotomize the patients into having tumors growing faster or slower than expected, as previously described (18).

Statistical Analyses

Statistical analyses were performed using Stata version 16 (StataCorp LLC, College Station, TX). Statistical significance was set at $p \leq 0.05$. Associations between *MGMT* status and categorical variables were analyzed using Chi-square/Fisher’s exact tests, while associations between *MGMT* status and continuous variables were assessed using Mann-Whitney *U* analyses. A Kaplan-Meier plot and the log-rank test were used for the univariable analyses between *MGMT* status and overall survival and a Cox proportional hazard model was used for multivariable survival analyses. The selection of variables in the multivariable model has previously been accounted for (18). All included variables followed the proportional hazard assumption, which was tested using Schoenfeld residuals in Stata.

Ethics

This study was approved by the Regional Ethics Committee (Central) as part of a larger project (reference numbers 2011/974 and 2013/1348) in accordance with the 1964 Helsinki declaration and later amendments. Most of the patients had provided written informed consent to be included (reference 2011/974), and the Regional Ethics Committee waived informed consent for retrospective evaluation of patient data for the remaining patients.

RESULTS

MGMT and Clinical and Radiological Factors

In the 85 included patients, the distributions of age, sex, Karnofsky performance status, Ki-67/MIB-1 PI, and microvessel density of CD105 corresponded to previous reports (18, 24). The relationships between *MGMT* status and clinical and radiological factors are shown in Table 1. *MGMT* status was not significantly associated with any of the clinical factors or MRI volumetrics (Table 1). There was no significant association between *MGMT* status and MRI assessed preoperative speed of growth (Table 1).

MGMT and Histological Features

Distributions of the 22 histopathological features and the immunohistochemical markers (Ki-67/MIB-1 PI and microvessel density of CD105) in the *MGMT* methylated and unmethylated groups are presented in Table 2. There were no significant associations between *MGMT* status and any of the histological features assessed (Table 2). The difference in the presence of microvascular proliferation in the *MGMT* methylated and unmethylated groups was likely confounded by sparse tissue amount. In our previous work, we found that microvascular proliferation was significantly less present in

TABLE 1. *MGMT* and Clinical and Radiological Factors. Distributions of Clinical and Radiological Parameters Within the *MGMT* Methylated and Unmethylated Patient Groups

	Methylated <i>MGMT</i> (n = 31)	Unmethylated <i>MGMT</i> (n = 54)	p Value	Test Performed
Mean age (SD)	65 (10.4)	63 (11.2)	0.230	Two-sample <i>t</i> -test
Male	71%	69%	0.814	Chi-square
Median preoperative total tumor volume (range)	28.8 mL (1.0–243.5)	31.6 mL (1.0–153.0)	0.777	Mann-Whitney <i>U</i>
Median preoperative contrast enhancing volume (range)	16.6 mL (1.0–215.4)	18.3 mL (0.9–63.9)	0.913	Mann-Whitney <i>U</i>
Median preoperative necrotic core volume (range)	9.7 mL (0.0–89.9)	8.1 mL (0.1–106.5)	0.695	Mann-Whitney <i>U</i>
Median preoperative percentage necrosis (range)	27.8% (1.4–78.6)	34.9% (3.5–69.9)	0.204	Mann-Whitney <i>U</i>
Fast-growing tumors ^a	48%	50%	0.886	Chi-square
Median KPS (range)	7.5 (4–10)	8 (5–10)	0.552	Mann-Whitney <i>U</i>
GTR	35%	26%	0.352	Chi-square
Chemotherapy	81%	81%	0.924	Chi-square
Radiotherapy	90%	94%	0.664	Fisher’s exact
Median survival	15.9 months 95% CI (12.5–26.2)	10.2 months 95% CI (8.6–13.7)	0.048*	Log-rank

MGMT, O⁶-methylguanine DNA methyltransferase; SD, standard deviation; KPS, Karnofsky performance status; GTR, gross total resection; CI, confidence interval.
^aSpeed of tumor growth was estimated from segmented tumor volumes from 2 preoperative MRI scans and the interval between them. A fitted Gompertzian growth curve based on the volume data was used to dichotomize the tumors into growing faster or slower than expected from the curve (18).
*Statistically significant, $p \leq 0.05$.

Downloaded from https://academic.oup.com/jnen/article/79/8/855/5674024 by Norges Teknisk-Naturvitenskapelige Universitet user on 08 October 2020

TABLE 2. *MGMT* and Histological Features. Distributions of the Histological Features Within the *MGMT* Methylated and Unmethylated Patient Groups

	Methylated <i>MGMT</i> (n = 31)	Unmethylated <i>MGMT</i> (n = 54)	p Value	Test Performed
Necrosis				
Small	84%	81%	0.781	Chi-square
Large	94%	89%	0.705	Fisher's exact
Palisades ^a	84%	72%	0.206	Chi-square
Microvascular proliferation ^b	100%	90%	0.249	Fisher's exact
High cellular density	42%	33%	0.428	Chi-square
Severe atypia	16%	26%	0.297	Chi-square
Median mitotic count (range)	16.0 (0–43)	11.5 (0–65)	0.109	Mann-Whitney U
Vascular features				
Thrombosis	81%	87%	0.534	Fisher's exact
Hemorrhage	87%	78%	0.290	Chi-square
Pseudorosettes ^c	29%	25%	0.726	Chi-square
Secondary structures of Scherer ^d	70%	71%	0.911	Chi-square
Desmoplasia	65%	67%	0.840	Chi-square
Leukocytes				
Macrophages	97%	91%	0.409	Fisher's exact
Lymphocytic infiltrates	58%	76%	0.085	Chi-square
Small cell glioblastoma	23%	17%	0.502	Chi-square
Cell types				
Gemistocytes	29%	19%	0.263	Chi-square
Small cells	29%	22%	0.483	Chi-square
Sarcomatous cells	13%	20%	0.385	Chi-square
Myxomatoid	6%	17%	0.314	Fisher's exact
Giant cells	6%	11%	0.705	Fisher's exact
Primitive neuronal component	6%	11%	0.705	Fisher's exact
Oligodendroglial cells	10%	6%	0.664	Fisher's exact
Median Ki-67/MIB-1 PI (range)	17.5% (4.3–40.7)	13.2% (1.4–57.3)	0.333	Mann-Whitney U
Median microvessel density count of CD105 ^e (range)	15.2 (4–42.7)	11.8 (0.7–50)	0.216	Mann-Whitney U

MGMT, O⁶-methylguanine DNA methyltransferase; PI, proliferative index.
^aIncludes only tumors with central tumor morphology in the analysis (n = 84) (23).
^bTumors with sparse tissue amount were excluded from the analysis (53 included cases), because sparse tissue amount was likely a confounder of the association between microvascular proliferation and *MGMT* status.
^cIncludes only tumors with paraffin sections with viable central tumor morphology (n = 82) (23).
^dRecorded as present when 1 of the following features were observed: Perineuronal satellitosis, angiocentric structures, or subpial clustering, as previously defined (23). Only recorded in tumors containing infiltration zones into gray matter (n = 55).
^eIncludes only tumors with enough tissue amount or adequate morphology for the microvessel density assessment (n = 82) (24).

cases with sparse tissue amount ($p < 0.001$, Chi-square test, unpublished student thesis). In addition, there was a near-significant trend of more *MGMT* unmethylated cases in cases with sparse tissue material ($p = 0.088$, Chi-square test) in the current study. To avoid this confounding effect, microvascular proliferation was redefined to only include well-sampled cases (Table 2). Microvascular proliferation was significantly associated with methylated *MGMT* status when not corrected for tissue amount ($p = 0.018$, Chi-square test).

MGMT and Survival

The median overall survival was 13.3 months (95% confidence interval [CI] 9.9–15.7). Methylated *MGMT* status was

significantly associated with overall survival both in the univariable analysis (Table 1; Fig. 1) and in the multivariable Cox model (Table 3).

DISCUSSION

MGMT promoter methylation is a pivotal predictive marker in *IDH* wt GBMs. However, we did not find any significant associations between the *MGMT* promoter methylation status and several biological parameters in treatment-naïve patients. These parameters included 22 histopathological features, proliferative activity, degree of angiogenesis, quantitative MRI volumetrics, and preoperative speed of radiological tumor growth. Altogether, these findings suggest

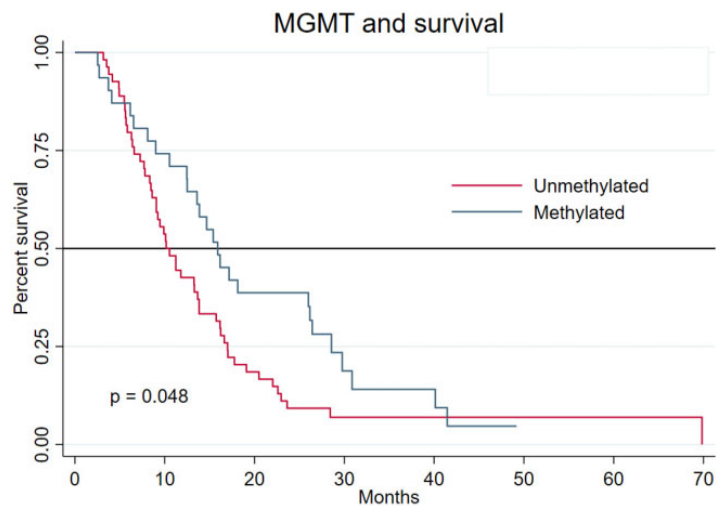


FIGURE 1. Kaplan-Meier plot of overall survival of *MGMT* methylated (blue line) and *MGMT* unmethylated (red line) patients. *MGMT* methylated patients survived significantly longer than unmethylated ($p=0.048$, log-rank test). *MGMT*, *O*⁶-methylguanine DNA methyltransferase.

TABLE 3. Survival Analyses. Univariable and Multivariable Cox Analyses				
	Univariable HR (95% CI)	p Value	Multivariable HR (95% CI)	p Value
Age	1.01 (0.99–1.03)	0.332	1.00 (0.98–1.03)	0.790
KPS	0.68 (0.57–0.82)	<0.001*	0.75 (0.60–0.95)	0.017*
Preoperative tumor volume	1.01 (1.00–1.01)	0.042*	1.00 (0.99–1.01)	0.956
GTR	0.69 (0.42–1.14)	0.150	0.66 (0.37–1.18)	0.162
Chemotherapy	0.17 (0.09–0.32)	<0.001*	0.27 (0.13–0.58)	0.001*
Radiation	0.05 (0.02–0.14)	<0.001*	0.12 (0.04–0.38)	<0.001*
Methylated <i>MGMT</i> status	0.62 (0.39–1.00)	0.051	0.60 (0.37–0.97)	0.038*

HR, hazard ratio; CI, confidence interval; KPS, Karnofsky performance status; GTR, gross total resection; *MGMT*, *O*⁶-methylguanine DNA methyltransferase.
*Statistically significant, $p \leq 0.05$.

that *MGMT* status is not a surrogate marker of the pretreatment phenotypical biology of *IDH* wt GBMs.

Tumor biology has been extensively studied using experimental models; however, these models will never fully mimic the unique micro-environment of human GBMs (25). In this study, tissue samples were obtained from the first surgical intervention and only preoperative MRI scans were assessed. Hence, the assessed biological features were unaffected by radiochemotherapy. Nevertheless, 82% ($n=70$) were preoperatively treated with corticosteroids, and there was a nonsignificant trend ($p=0.144$) of more corticosteroid use in *MGMT* methylated tumors (data not shown). Therefore, we cannot entirely exclude corticosteroid use as a confounding factor. In summary, our study enabled us to study links between the phenotypical biology and *MGMT* status occurring during the natural history of human *IDH* wt GBMs.

MGMT and Histology

We could not find any significant associations between *MGMT* status and the histopathological features or immunohistochemically assessed degree of proliferation and angiogenesis (Table 2). Few previous studies have investigated relationships between *MGMT* status and histological features. However, Hegi et al investigated such relationships by looking at 13 morphological features in newly diagnosed GBM patients (26). Yet, they only found a significant association between methylated *MGMT* status and higher Ki-67/MIB-1 PI. However, this association is limited by various aspects of the assessments of Ki-67/MIB-1 PI (23, 27, 28). Pistollato et al found a higher *MGMT* expression (corresponding to unmethylated tumors) in the hypoxic, inner core of GBMs (29). They also found that cells derived from these areas were more resistant to temozolomide, which was further related to the higher *MGMT* expression (29). In our previous studies, we found that

thromboses independently predicted faster tumor growth, which indicated that hypoxia drives faster tumor growth (23, 24). Because our previous publications included *IDH* mutant tumors and that thromboses have been found to associate with *IDH1* wt status (30), we reanalyzed the data from our previous publications while including only *IDH* wt GBMs. The reanalysis showed similar results, suggesting that thromboses promote aggressiveness also among *IDH* wt GBMs. Interestingly, neither thromboses nor faster preoperative growth were associated with *MGMT* status in the current study (Tables 1 and 2).

Previous experimental studies have also linked *MGMT* expression to increased hypoxia (31–33) and decreased angiogenesis (34) in GBM cell lines. However, these results are conflicting, as hypoxia is known to be an important inductor of angiogenesis (35). Furthermore, a recent comprehensive genomic study showed considerable differences in mRNA expression profiles and DNA methylation profiles between GBM patient material and the in vitro and in vivo models derived from it (36). These findings illustrate challenges in extrapolating findings from experimental models on *MGMT* methylation status and expression. Altogether, the inconsistent results from previous pathological and experimental studies are in line with our findings, which suggest *MGMT* methylation status is not linked to pretreatment histology in GBMs.

***MGMT* and MRI**

We found no significant associations between *MGMT* status and total tumor volumes, contrast enhancing volumes, necrotic volumes, the percentage of necrosis, or preoperative speed of growth (Table 1). As mentioned, previous radiological studies have aimed to noninvasively predict *MGMT* status using conventional and advanced MRI characteristics. However, results have been conflicting and derived no expert consensus (16). Still, most studies have found significant associations between unmethylated *MGMT* status and MRI parameters indicating increased aggressiveness, such as more necrosis (37) and higher vascularity. Higher vascularity was in these studies measured as (i) ring enhancement (37, 38), (ii) higher normalized relative cerebral blood volume (39), (iii) higher relative cerebral blood flow (16), (iv) more edema (40), and (v) lower apparent diffusion coefficient (also indicating increased cellularity) (16, 41). On the contrary, others have found methylated *MGMT* status to significantly associate with necrosis (16), lower apparent diffusion coefficient (42), and higher relative cerebral blood volume (43). In line with our study, others found no significant associations between *MGMT* status and conventional MRI features (44–47). Nevertheless, machine learning approaches might be a way to advance and have thus far shown both promising (47–50) and negative results (45). In summary, our results along with the previous conflicting studies indicate that *MGMT* status cannot yet be noninvasively predicted from MRI scans.

***MGMT* and Survival**

MGMT promoter methylation was an independent predictor for improved survival when adjusted for several clinical factors in the multivariable analyses (Table 3). However, this

does not necessarily mean that methylated *MGMT* status is an independent prognostic factor, as *MGMT* status may have affected the temozolomide use in the studied patients. As defined by Clark, a prognostic factor is “associated with clinical outcome in the absence of therapy or with the application of a standard therapy that patients are likely to receive” (51). Hence, it is a feature of the natural history of the disease. A predictive factor is “associated with response or lack of response to a particular therapy” (51). Ideally, predictive factors should be studied in randomized controlled trials (RCTs), isolating the effect of the potential biomarker related to treatment. Prognostic factors are better studied in cohort studies where treatment is not dependent on the studied biomarker. In our study, most patients received chemotherapy regardless of the *MGMT* status (Table 1). However, among elderly GBM patients, the Stupp protocol is more seldom given and patients with *MGMT* methylated tumors may be selected for chemotherapy alone (12). Second-line chemotherapy is also more likely to be given to patients with *MGMT* methylated lesions. Thus, since *MGMT* status is to some extent used for treatment decisions, the seemingly independent effect of *MGMT* status on survival in the multivariable analyses may be colored by the use of *MGMT* status for treatment selection.

Our finding that *MGMT* status was not related to pretreatment phenotypical tumor biology indicates that methylated *MGMT* status is not associated with an intrinsically less aggressive tumor biology. This further suggests methylated *MGMT* status is not a prognostic factor by itself but merely a predictive marker. As mentioned, previous studies have shown conflicting results regarding the prognostic value of *MGMT* status among patients who were not treated with chemotherapy. Three RCTs on elderly patients (11–13) and a retrospective cohort from the preStupp area (14) did not find a significant difference in overall survival according to *MGMT* status in the radiotherapy-only treated group. Conversely, the EORTC-NCIC RCT on younger patients (8, 52) and a retrospective study by Rivera et al (15) found a prognostic value of *MGMT* status within the same patient group. However, second-line therapy with temozolomide was given to a higher percentage of the radiotherapy-only patients in the EORTC-NCIC trial (~60%) than in the 3 other RCTs (~30% in all) (11–13). Furthermore, in the EORTC-NCIC trial, they argue that the survival benefit is probably due to an effect of second-line chemotherapy, as the progression-free survival was short and the overall survival relatively long in the *MGMT* methylated cases in the radiotherapy-only group (8, 52). Moreover, Rivera et al found that methylated *MGMT* status also predicted an increased response to radiotherapy (15). They further speculated whether methylated *MGMT* status could represent a surrogate marker of improved treatment response in general or of undiscovered processes causing an inherently less aggressive tumor biology (15). However, our study suggests the latter speculation is not the case in *IDH* wt GBMs. Moreover, our results also indicate that the increased response to chemotherapy in *MGMT* methylated GBMs is not due to pretreatment differences in phenotypical tumor biology. Altogether, our findings along with previous studies indicate the increased survival of *MGMT* promoter methylated patients is due to an

increased response to therapy, and not due to an intrinsically less aggressive tumor biology.

Methodological Aspects

To date there is no consensus regarding the best assay for detecting the *MGMT* methylation status (53, 54). We used MSP, which has been related to survival in several pivotal clinical studies (8, 10, 22, 53). The finding of 36% *MGMT* methylated cases corresponds to the 30%–60% in previous studies (10). Interestingly, there was a near-significant trend of more *MGMT* unmethylated tumors when tumor material was sparse ($p = 0.088$). This association is perhaps due to the assay's propensity toward more false negatives when the amount of isolated DNA is low. Intratumoral heterogeneity in *MGMT* status has also been reported (55, 56), which may contribute to a higher risk of false negative results in cases with sparse tissue. Further technical limitations of the MSP assay have been elaborated elsewhere (10, 54, 57). Still, the primers used in this study correspond to an area of the promoter found to best correlate with survival and *MGMT* expression in patients with GBM (58, 59).

Limitations regarding the collection of clinical data, the histopathological and immunohistochemical assessments, the segmentation of tumor volumes and different tumor compartments, and the estimation of growth rates have previously been described in detail (4, 18, 23, 24). The relatively large population of treatment-naïve patients with a population-based referral and the preoperative MRI assessments are the main strengths of the study. Important limitations are potential selection biases, preoperative corticosteroid treatment, sampling errors and interobserver variability of the histological assessments, and the explorative nature of the statistical analyses. We chose not to correct for multiple statistical testing despite the increased risk of false positive findings. Interestingly, based on the set p value of ≤ 0.05 , one would expect at least one false positive finding of the 29 performed statistical tests between *MGMT* status and biological features. Hence, the fact that none of these tests were significant further supports our conclusion that *MGMT* status is not related to pretreatment phenotypical tumor biology. Assuming a standardized effect size of 0.8, the power was estimated to be ~90% for each analysis between *MGMT* status and the biological features. The results should be validated in future studies.

Conclusion

In conclusion, we did not find any significant associations between *MGMT* promoter methylation status and histological or MRI features in treatment-naïve *IDH* wt GBM patients. These findings suggest *MGMT* status is not related to the pretreatment phenotypical biology in *IDH* wt GBMs, which indicate that the increased survival of *MGMT* methylated patients is not due to an inherently less aggressive tumor biology. Also, our findings suggest that preoperative conventional MRI characteristics cannot be used for noninvasive prediction of the *MGMT* status.

ACKNOWLEDGMENTS

We would like to thank Mona Jonsson, Tore Skaldebø, Tone Furre, Ingeborg Engesvold, and Torild Gladø for the excellent laboratory work with the methylation-specific PCR analyses of the *MGMT* promoter methylation status at the Department of Pathology, St. Olav's University Hospital. We would also like to thank the staff at the Cellular and Molecular Imaging Core Facility (CMIC), NTNU-Norwegian University of Science and Technology for outstanding laboratory work with the histological and immunohistochemical analyses. Open Access funding provided by NTNU-Norwegian University of Science and Technology.

REFERENCES

- Ostrom QT, Gittleman H, Truitt G, et al. CBTRUS statistical report: Primary brain and other central nervous system tumors diagnosed in the United States in 2011–2015. *Neuro-Oncology* 2018;20:iv1–iv86
- Ronning PA, Helseth E, Meling TR, et al. A population-based study on the effect of temozolomide in the treatment of glioblastoma multiforme. *Neuro-Oncology* 2012;14:1178–84
- Stupp R, Mason WP, van den Bent MJ, et al. Radiotherapy plus concomitant and adjuvant temozolomide for glioblastoma. *N Engl J Med* 2005;352:987–96
- Stensj en AL, Solheim O, Kvistad KA, et al. Growth dynamics of untreated glioblastomas in vivo. *Neuro Oncol* 2015;17:1402–11
- Burger PC, Kleihues P. Cytologic composition of the untreated glioblastoma with implications for evaluation of needle biopsies. *Cancer* 1989;63:2014–23
- Habberstad AH, Lind-Landst m T, Torp SH. The histopathological spectrum of primary human glioblastomas with relations to tumour biology. *J Clin Exp Pathol* 2012;2:110
- Sottoriva A, Spiteri I, Piccirillo SG, et al. Intratumor heterogeneity in human glioblastoma reflects cancer evolutionary dynamics. *Proc Natl Acad Sci USA* 2013;110:4009–14
- Hegi ME, Diserens AC, Gorlia T, et al. *MGMT* gene silencing and benefit from temozolomide in glioblastoma. *N Engl J Med* 2005;352:997–1003
- Weller M, van den Bent M, Tonn JC, et al. European Association for Neuro-Oncology (EANO) guideline on the diagnosis and treatment of adult astrocytic and oligodendroglial gliomas. *Lancet Oncol* 2017;18:e315–e29
- Weller M, Stupp R, Reifenberger G, et al. *MGMT* promoter methylation in malignant gliomas: Ready for personalized medicine? *Nat Rev Neurol* 2010;6:39–51
- Wick W, Platten M, Meisner C, et al. Temozolomide chemotherapy alone versus radiotherapy alone for malignant astrocytoma in the elderly: The NOA-08 randomised, phase 3 trial. *Lancet Oncol* 2012;13:707–15
- Malmstr m A, Gronberg BH, Marosi C, et al. Temozolomide versus standard 6-week radiotherapy versus hypofractionated radiotherapy in patients older than 60 years with glioblastoma: The Nordic randomised, phase 3 trial. *Lancet Oncol* 2012;13:916–26
- Perry JR, Laperriere N, O'Callaghan CJ, et al. Short-course radiation plus temozolomide in elderly patients with glioblastoma. *N Engl J Med* 2017;376:1027–37
- Criniere E, Kaloshi G, Laigle-Donadey F, et al. *MGMT* prognostic impact on glioblastoma is dependent on therapeutic modalities. *J Neurooncol* 2007;83:173–9
- Rivera AL, Pelloski CE, Gilbert MR, et al. *MGMT* promoter methylation is predictive of response to radiotherapy and prognostic in the absence of adjuvant alkylating chemotherapy for glioblastoma. *Neuro-Oncology* 2010;12:116–21
- Han Y, Yan LF, Wang XB, et al. Structural and advanced imaging in predicting *MGMT* promoter methylation of primary glioblastoma: A region of interest based analysis. *BMC Cancer* 2018;18:215
- Louis DN, Ohgaki H, Wiestler O, et al. WHO Classification of Tumours of the Central Nervous System. Revised 4th ed. 1211 Geneva 27, Switzerland: International Agency for Research on Cancer (IARC) 2016

18. Stensj  en AL, Berntsen EM, Mikkelsen VE, et al. Does pretreatment tumor growth hold prognostic information for patients with glioblastoma? *World Neurosurg* 2017;101:686–94.e4
19. Jakola AS, Skjulsvik AJ, Myrnes KS, et al. Surgical resection versus watchful waiting in low-grade gliomas. *Ann Oncol* 2017;28:1942–8
20. Brennan CW, Verhaak RG, McKenna A, et al. The somatic genomic landscape of glioblastoma. *Cell* 2013;155:462–77
21. Kloosterhof NK, Bralten LB, Dubbink HJ, et al. Isocitrate dehydrogenase-1 mutations: A fundamentally new understanding of diffuse glioma? *Lancet Oncol* 2011;12:83–91
22. Esteller M, Garcia-Foncillas J, Andion E, et al. Inactivation of the DNA-repair gene MGMT and the clinical response of gliomas to alkylating agents. *N Engl J Med* 2000;343:1350–4
23. Mikkelsen VE, Stensj  en AL, Berntsen EM, et al. Histopathologic features in relation to pretreatment tumor growth in patients with glioblastoma. *World Neurosurg* 2018;109:e50–e8
24. Mikkelsen VE, Stensj  en AL, Granli US, et al. Angiogenesis and radiological tumor growth in patients with glioblastoma. *BMC Cancer* 2018;18:862
25. Huszthy PC, Daphu I, Niclou SP, et al. In vivo models of primary brain tumors: Pitfalls and perspectives. *Neuro-Oncology* 2012;14:979–93
26. Hegi ME, Janzer RC, Lambiv WL, et al. Presence of an oligodendroglioma-like component in newly diagnosed glioblastoma identifies a pathogenetically heterogeneous subgroup and lacks prognostic value: Central pathology review of the EORTC_26981/NCIC_CE.3 trial. *Acta Neuropathol* 2012;123:841–52
27. Prayson RA. Cell proliferation and tumors of the central nervous system, part II: Radiolabeling, cytometric, and immunohistochemical techniques. *J Neuropathol Exp Neurol* 2002;61:663–72
28. Skjulsvik AJ, Mork JN, Torp MO, et al. Ki-67/MIB-1 immunostaining in a cohort of human gliomas. *Int J Clin Exp Pathol* 2014;7:8905–10
29. Pistollato F, Abbadi S, Rampazzo E, et al. Intratumoral hypoxic gradient drives stem cells distribution and MGMT expression in glioblastoma. *Stem Cells* 2010;28:851–62
30. Unruh D, Schwarze SR, Khoury L, et al. Mutant IDH1 and thrombosis in gliomas. *Acta Neuropathol* 2016;132:917–30
31. Persano L, Pistollato F, Rampazzo E, et al. BMP2 sensitizes glioblastoma stem-like cells to Temozolomide by affecting HIF-1alpha stability and MGMT expression. *Cell Death Dis* 2012;3:e412
32. Tang JH, Ma ZX, Huang GH, et al. Downregulation of HIF-1a sensitizes U251 glioma cells to the temozolomide (TMZ) treatment. *Exp Cell Res* 2016;343:148–58
33. Wang P, Lan C, Xiong S, et al. HIF1alpha regulates single differentiated glioma cell dedifferentiation to stem-like cell phenotypes with high tumorigenic potential under hypoxia. *Oncotarget* 2017;8:28074–92
34. Chahal M, Xu Y, Lesniak D, et al. MGMT modulates glioblastoma angiogenesis and response to the tyrosine kinase inhibitor sunitinib. *Neuro-Oncology* 2010;12:822–33
35. Hardee ME, Zagzag D. Mechanisms of glioma-associated neovascularization. *Am J Pathol* 2012;181:1126–41
36. Shen Y, Grisdale CJ, Islam SA, et al. Comprehensive genomic profiling of glioblastoma tumors, BTICs, and xenografts reveals stability and adaptation to growth environments. *Proc Natl Acad Sci USA* 2019;116:19098–108
37. Eoli M, Menghi F, Bruzzone MG, et al. Methylation of O⁶-methylguanine DNA methyltransferase and loss of heterozygosity on 19q and/or 17p are overlapping features of secondary glioblastomas with prolonged survival. *Clin Cancer Res* 2007;13:2606–13
38. Drabycz S, Roldan G, de Robles P, et al. An analysis of image texture, tumor location, and MGMT promoter methylation in glioblastoma using magnetic resonance imaging. *Neuroimage* 2010;49:1398–405
39. Ryoo I, Choi SH, Kim JH, et al. Cerebral blood volume calculated by dynamic susceptibility contrast-enhanced perfusion MR imaging: Preliminary correlation study with glioblastoma genetic profiles. *PLoS ONE* 2013;8:e71704
40. Ellingson BM, Cloughesy TF, Pope WB, et al. Anatomic localization of O⁶-methylguanine DNA methyltransferase (MGMT) promoter methylated and unmethylated tumors: A radiographic study in 358 de novo human glioblastomas. *Neuroimage* 2012;59:908–16
41. Romano A, Calabria LF, Tavanti F, et al. Apparent diffusion coefficient obtained by magnetic resonance imaging as a prognostic marker in glioblastomas: Correlation with MGMT promoter methylation status. *Eur Radiol* 2013;23:513–20
42. Pope WB, Lai A, Mehta R, et al. Apparent diffusion coefficient histogram analysis stratifies progression-free survival in newly diagnosed bevacizumab-treated glioblastoma. *AJNR Am J Neuroradiol* 2011;32:882–9
43. Hempel JM, Schittenhelm J, Klose U, et al. In vivo molecular profiling of human glioma: Cross-sectional observational study using dynamic susceptibility contrast magnetic resonance perfusion imaging. *Clin Neuro-radiol* 2019;29:479–91
44. Ahn SS, Shin NY, Chang JH, et al. Prediction of methylguanine methyltransferase promoter methylation in glioblastoma using dynamic contrast-enhanced magnetic resonance and diffusion tensor imaging. *J Neurosurg* 2014;121:367–73
45. Kickingereder P, Bonekamp D, Nowosielski M, et al. Radiogenomics of glioblastoma: Machine learning-based classification of molecular characteristics by using multiparametric and multiregional MR imaging features. *Radiology* 2016;281:907–18
46. Gupta A, Omuro AM, Shah AD, et al. Continuing the search for MR imaging biomarkers for MGMT promoter methylation status: Conventional and perfusion MRI revisited. *Neuroradiology* 2012;54:641–3
47. Korfiatis P, Kline TL, Coufalova L, et al. MRI texture features as biomarkers to predict MGMT methylation status in glioblastomas. *Med Phys* 2016;43:2835–44
48. Li ZC, Bai H, Sun Q, et al. Multiregional radiomics features from multiparametric MRI for prediction of MGMT methylation status in glioblastoma multiforme: A multicentre study. *Eur Radiol* 2018;28:3640–50
49. Xi YB, Guo F, Xu ZL, et al. Radiomics signature: A potential biomarker for the prediction of MGMT promoter methylation in glioblastoma. *J Magn Reson Imaging* 2018;47:1380–7
50. Hajianfar G, Shiri I, Maleki H, et al. Noninvasive O⁶-methylguanine-DNA methyltransferase status prediction in glioblastoma multiforme cancer using magnetic resonance imaging radiomics features: Univariate and multivariate radiogenomics analysis. *World Neurosurg* 2019;132:e140–e61
51. Clark GM. Prognostic factors versus predictive factors: Examples from a clinical trial of erlotinib. *Mol Oncol* 2008;1:406–12
52. Gorlia T, van den Bent MJ, Hegi ME, et al. Nomograms for predicting survival of patients with newly diagnosed glioblastoma: Prognostic factor analysis of EORTC and NCIC trial 26981-22981/CE.3. *Lancet Oncol* 2008;9:29–38
53. Mansouri A, Hachem LD, Mansouri S, et al. MGMT promoter methylation status testing to guide therapy for glioblastoma: Refining the approach based on emerging evidence and current challenges. *Neuro-Oncology* 2019;21:167–78
54. Malmstr  m A, Lysiak M, Kristensen BW, et al. Do we really know who has an MGMT methylated glioma? Results of an international survey regarding use of MGMT analyses for glioma. *Neuro-Oncol Pract* 2020;7:68–76
55. Wenger A, Ferreyra Vega S, Kling T, et al. Intratumor DNA methylation heterogeneity in glioblastoma: Implications for DNA methylation-based classification. *Neuro-Oncology* 2019;21:616–27
56. Parker NR, Hudson AL, Khong P, et al. Intratumoral heterogeneity identified at the epigenetic, genetic and transcriptional level in glioblastoma. *Sci Rep* 2016;6:22477
57. Dullea A, Marignol L. MGMT testing allows for personalised therapy in the temozolomide era. *Tumor Biol* 2016;37:87–96
58. Bady P, Sciuscio D, Diserens AC, et al. MGMT methylation analysis of glioblastoma on the Infinium methylation BeadChip identifies two distinct CpG regions associated with gene silencing and outcome, yielding a prediction model for comparisons across datasets, tumor grades, and CIMP-status. *Acta Neuropathol* 2012;124:547–60
59. Malley DS, Hamoudi RA, Kocalkowski S, et al. A distinct region of the MGMT CpG island critical for transcriptional regulation is preferentially methylated in glioblastoma cells and xenografts. *Acta Neuropathol* 2011;121:651–61

ISBN 978-82-471-9774-5 (printed ver.)
ISBN 978-82-471-9449-2 (electronic ver.)
ISSN 1503-8181 (printed ver.)
ISSN 2703-8084 (online ver.)



NTNU

Norwegian University of
Science and Technology